THE REDUCTION OF OXYGEN ON SEMICONDUCTING OXIDES IN ALKALINE MEDIA

A Thesis submitted for the degree of

Doctor of Philosophy

of

THE CITY UNIVERSITY

by

K. L. K. YEUNG

This work was carried out under the supervision of

Dr. A. C. C. Tseung and financed by the Science Research Council,

Grant No. GRA 02664

March 1978

-From Rabbi Ben Ezva-
-Browning-

ACKNOWLEDGEMENTS

I should like to express my sincere and grateful thanks to Dr. A. C. C. Tseung for his invaluable guidance and encouragement and to [redacted] who provided technical assistance and helpful discussion. I am also indebted to my student colleagues in the Electrochemistry Group for their advice and discussions on various topics concerned with this research project.

Thanks are due to the members of The City University Technical and Library staff for help on numerous aspects of the work, and to our Secretary, [redacted], for persisting with a difficult manuscript.

Finally, I should like to extend my deepest gratitude to [redacted] for her encouragement and partial financial support throughout my studies.

ABSTRACT

The electrochemical reduction of oxygen in alkaline solution:-

$$2H_2O + O_2 + 4e \rightarrow 4OH^-$$

presents one of the challenging problems of electrochemistry. An improvement in the kinetics and efficiency of the process would have a profound effect on power generation and on other aspects of every day life.

The reduction is generally regarded as a two stage process:-

$$H_2O + O_2 + 2e \rightarrow 2OH^- + HO_2^- \quad (1)$$

$$H_2O + HO_2^- + 2e \rightarrow 3OH^- \quad (2)$$

This results in a mixed potential and most oxygen electrocatalysts have open circuit voltages in the region of 1.0 - 1.1 volts (vs RHE), significantly lower than the theoretical value of 1.229 V vs RHE at 25°C. Stage (2) is normally the rate-determining step and significant improvement in performance and open circuit voltage can be expected if the peroxide step is eliminated. The key to the solution of the oxygen electrode problem may lie in the electrocatalyst's ability to dissociatively chemisorb oxygen. If this condition is fulfilled, no HO_2^- intermediate is formed and the oxygen will go directly to hydroxyl ion via a 4-electron process. According to the joint pseudosplitting mechanism, a necessary condition for dissociative chemisorption of oxygen is for the oxygen molecule to

to be chemisorbed 'side-on' on the electrocatalyst surface. Theoretical considerations suggest that the requirement for side-on chemisorption of oxygen can be satisfied using paramagnetic or ferromagnetic oxides. According to this consideration, perovskite oxide catalysts ($La_{1-x}Sr_xCoO_3$) enable the paramagnetic oxygen molecule to be chemisorbed side-on, since Sr doped $LaCoO_3$ is paramagnetic at room temperature. One such compound $La_{0.5}Sr_{0.5}CoO_3$ exhibits complete reversible behaviour towards oxygen reduction in 45% KOH solution at room temperature. Also, the electrochemical performance of this catalyst increases linearly with temperature, surpassing that of platinum black at 170°C. However, its performance below 100°C was too low to be of practical interest. The purpose of this investigation is to study the kinetics of oxygen reduction on semiconducting oxides with particular reference to its electronic structure and magnetic properties and to optimize the performance of a practical oxygen electrode for low temperature fuel cell application. The electrochemical reduction of oxygen on teflon-bonded $Nd_{0.5}Sr_{0.5}CoO_3$ electrode in 45% KOH was studied as a function of temperature and oxygen partial pressure. The activation energy was 10.75 kcal/mol, similar to that for dissociative oxygen chemisorption. The relationship between i and P_{O_2} is of the form $\frac{d \ln i}{d \ln P_{O_2}} = \frac{1}{2}$, suggesting that the rate of oxygen chemisorption is the rate-controlling step. Galvanostatic oxygen stripping showed that the surface coverage of oxygen was only 1% for both Sr doped and $LaCoO_3$ and $NdCoO_3$ and that the coverage was independent of temperature in the range 25°C - 80°C. This suggests that the improvement in performance with temperature is not due to the increase in the number of active sites.

Further investigation on the series $La_{1-x}Sr_xCoO_3$ showed that both the maximum performance and the maximum oxygen coverage were obtained at x = 0.5. This indicates that the improvement in steady state performance with x is due to the increase in the number of the active sites. The results also suggest that the double exchange couple Co^{3+}/Co^{IV} satisfies an important condition for the splitting of the O=O bond and is acting as an active site on the perovskite oxides. Mathematical calculation shows that only a small portion of Co ions are available for the oxygen chemisorption process. Crystallographic considerations suggest that the number of active sites on $La_{1-x}Sr_xCoO_3$ is governed by geometric factors.

In view of the higher proportion of available transition metal ions, $NiCo_2O_4$ is expected to be a more suitable oxygen electrocatalyst than the perovskite oxides. Unfortunately, its electrochemical instability below 750 mV rules out the possibility of using $NiCo_2O_4$ as a practical oxygen electrode. However, by mixing graphite with the $NiCo_2O_4$, it is possible to achieve significantly higher performance at 750 mV.

TABLE OF CONTENTS

----------oOo----------

LIST OF FIGURES

LIST OF TABLES

ABBREVIATIONS

BET	Brunauer Emmett & Teller
DHE	Dynamic Hydrogen Electrode
ESCA	Electron Spectroscopy for Chemical Analysis
LCAO	Linear Combination of Atomic Orbitals Approximation
OCV	Open-Circuit Voltage (EMF)
PSD	Particle Size Diameter ($\mathring{A}$)
RE	Reference Electrode
SE	Secondary Electrode
RE	Reference Electrode
T_N	Neel Point (^oK)
W.E.	Working Electrode

CHAPTER ONE

INTRODUCTION

1. INTRODUCTION

Fuel cells provide a way to convert chemical energy directly into electricity, a process which has been known for almost a century. Yet, due to the many difficulties encountered in the course of the development of fuel cells, its application has been limited to military and space programs. For the latter applications, usually in low temperature fuel cells, platinum group metals are used as electrodes because of their stability and high catalytic activities. However, the high cost and scarcity of these metals have precluded fuel cells from general applications. Development of new, inexpensive electrodes is an imperative task if fuel cells are to compete with other energy converting devices.

The cathodic reduction of oxygen in alkaline solution

$$O_2 + 2H_2O + 4e \rightarrow 4OH^- \qquad (1)$$

presents one of the most difficult problems in the development of low temperature fuel cells. The standard reduction potential is

$$E^o = 0.401 \text{ V vs NHE} \qquad (2)$$

resulting in a theoretical H_2/O_2 fuel cell potential of 1.229 V at 25^oC. This potential has seldom been achieved in practice and most oxygen electrocatalysts exhibit open circuit potentials between 0.1 and 0.2 V below the reversible value. Rotating ring disc measurements[1] have shown that the oxygen reduction does not go through a direct four electron process but normally takes place via a HO_2^- intermediate,

$$H_2O + O_2 + 2e \rightarrow OH^- + HO_2^- \qquad (3)$$

This results in a drastic reduction of the open circuit potential and overall efficiency. On most catalysts other than carbon, HO_2^- can be further reduced either electrochemically by:

$$HO_2^- + H_2O + 2e \rightarrow 3OH^- \quad (4)$$

or by direct chemical decomposition of HO_2^-:

$$2HO_2^- \rightarrow O_2 + 2OH^- \quad (5)$$

Thus, three possible routes are available for improving the kinetics of the oxygen reduction process:

(a) To speed up the rate of electrochemical reduction of HO_2^-. This is not likely to be fruitful since $HO_2^- \rightarrow 3OH^-$ is known to be highly reversible.

(b) To speed up the rate of chemical decomposition of HO_2^-. This approach has been tackled empirically by many industrial establishments, e.g. the use of spinel oxides and Ag supported on carbon, with some degree of success. Theoretical and experimental studies on the system cobalt iron oxide/graphite by Goldstein & Tseung[2] showed that in order to achieve reversible oxygen electrode potentials, the $[HO_2^-]$ would have to be reduced to 6×10^{-18}M; this would require the peroxide decomposition catalyst to have a rate constant of 4×10^6 sec^{-1} g^{-1}. However, the most active cobalt-iron oxide tested, $Co_{2.4}$ $Fe_{0.6}$ O_4, the rate constant for peroxide decomposition is only 0.243 sec^{-1} g^{-1}. Pt black and Ag black catalysts are only marginally better. Consequently, several orders of magnitude increase in catalyst activity is required to achieve

open circuit potential close to the reversible oxygen potential.

(c) To induce the oxygen reduction process to go directly, by passing the HO_2^- intermediate. Isotopic studies by Davies, Clark, Yeager and Hovorka[3] showed conclusively that the O=O bond of the oxygen molecule remains unbroken on conversion to peroxide. Thus, the key to the solution of the oxygen electrode problem may lie in the electrocatalyst's ability to dissociatively chemisorb oxygen. If this condition is fulfilled, no HO_2^- intermediate can be formed, and the oxygen reduction will go directly to hydroxyl ion via a 4 electron process. This approach should be far more rewarding than the first two routes.

II. THE JOINT PSEUDOSPLITTING-PEROXIDE MECHANISM

The direct splitting of the O=O bond requires 117 Kcal/mol. Evans[4] proposed that O_2 molecules are absorbed 'side-on': O-O, without dissociation, on surfaces covered by adsorbed anions, such as OH^-. The O_2 molecules enter into hydrogen-bonding with OH^- ions and this bonding spreads across the OH^- layer. At certain specific sites, e.g. "kink" sites, there will be discontinuities in the OH^- 'carpet' so that for steric reasons, the OH^- ions will be more likely to enter into hydrogen bodning with nearby H_2O molecules of the electrolyte. At this point the O=O bond is effectively broken (pseudo-split). One consequence of such proton-switching is that the activation energy for bond rupture is lowered considerably. Proton switching is a process which occurs easily, e.g. in the rapid neutralisation of acid with alkali or of the great mobility in

solution of such species as OH^- or H_3O^+. The four stages of pseudo-splitting are shown in Figure 1. Goldstein and Tseung[5] proposed that since the reduction of oxygen on most electrocatalyst goes via the peroxide intermediate, it is necessary to consider the case when the oxygen molecule is chemisorbed 'end on': $\overset{O}{\underset{O}{\}}}$. In such cases, the pseudo-splitting process will lead to the formation of HO_2^- as well as OH^- (Figure 2). They therefore suggested that a necessary condition for dissociative chemisorption of oxygen is for the oxygen molecule to be adsorbed 'side-on' on the electrocatalyst surface.

III. THE IMPORTANCE OF SEMICONDUCTING OXIDES

Apart from the exceptional cases of selected precious metals at high overpotentials, the oxygen reduction on non-noble metal alloys or compounds takes place on oxide covered surfaces. Since it is difficult to control or study the properties of oxide films, it is more convenient and practical to study oxygen reduction on specially prepared oxides. The conductivity of most transition metal oxides can be significantly improved by doping with suitable oxides whose cation is of lower valency than the cation in the host oxide.[6] If doped oxide powders are used as teflon bonded electrodes supported on metal screens, then the likely ohmic drop due to the use of semiconducting oxide is given by:[7]

$$IR = \frac{\rho i L^2}{16t}$$

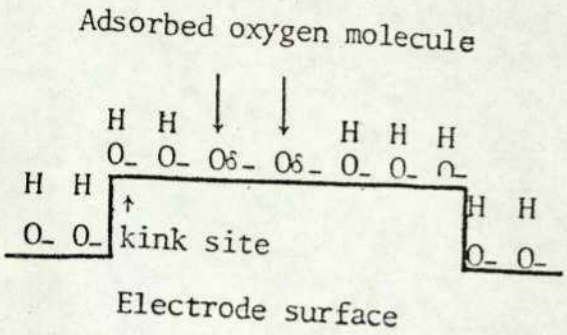

(a) Partial electron transfer

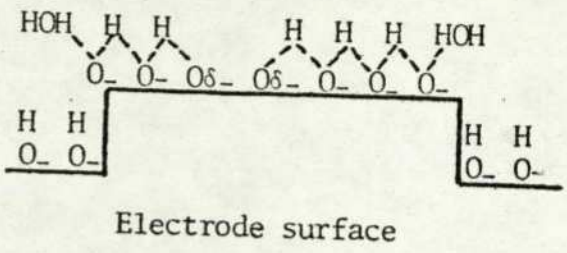

(b) Hydrogen bonding

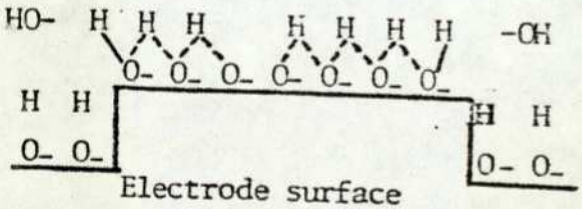

(c) Completion of electron transfer

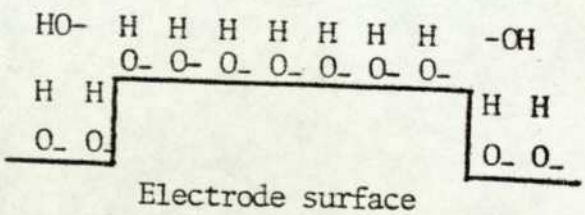

(d) Reorientation

Overall reaction:- $O_2 + 2H_2O + 4e = 4OH^-$

Figure 1 (a-d). Stages in pseudo-splitting

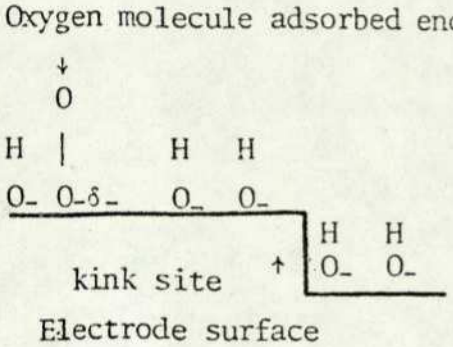

(a) Partial electron transfer

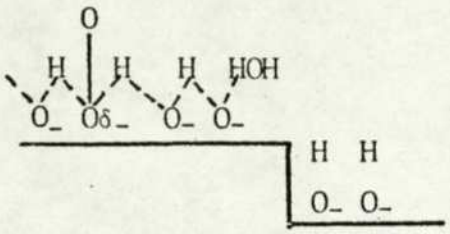

(b) Hydrogen bonding

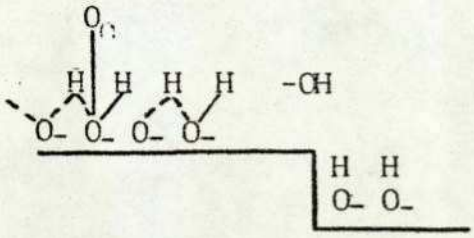

(c) Completion of electron transfer

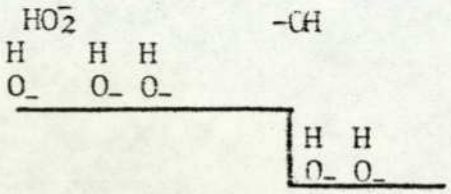

Overall reaction $O_2 + H_2O + 2e = HO_2^- + OH^-$

(d) Reorientation

Figure 2 (a-d). Stages in the peroxide mechanism

Where I is the total current, Amps; R is the total resistance of the electrode, ohm; i, current density, A/cm^2; L, length of each side of the square hole in the metal mesh, cm; ρ, resistivity of the catalyst/teflon layer, ohm-cm; t, thickness of catalyst/teflon layer, cm. Taking the typical case of teflon bonded porous electrode supported on 100 mesh metal screen, L is 0.04 cm and t is 0.025 cm. Hence, if the catalyst/teflon layer has a resistivity of 100 ohm cm and operating at $0.5A/cm^2$, the IR loss will be about 0.2 V, which is just acceptable. In actual practice, taking into account the increased resistivity due to the presence of teflon particles and contact resistance between the catalyst powder, the maximum allowable bulk resistivity of semiconducting oxide used for such applications is limited to 10-15 ohm cm.

IV. RELATIONSHIP BETWEEN THE MODE OF OXYGEN CHEMISORPTION AND MAGNETIC PROPERTIES OF SEMICONDUCTING OXIDES

The oxygen molecule is paramagnetic. It has 2 unpaired electrons with parallel spins in antibonding π orbitals. Therefore, electrons transferred at, or subsequent to, bond-rupture, from the catalyst to the adsorbed oxygen species, must similarly be of parallel spin. This immediately suggests the use of paramagnetic or ferromagnetic oxides. On the other hand, antiferromagnetic compounds, in which cations are arranged with unpaired spins aligned on alternate (111) planes, will not be able to satisfy the above requirement. Lithiated nickel oxide has been studied in far greater detail than any other oxide since it is one of the first doped semiconducting oxide

discovered by Verwey et al.[6]

Nickel oxide in its normal macroscopic state is antiferromagnetic. It becomes paramagnetic at the Neel Point, T_N at $523^{o}K$[8]. The magnetic transition is associated with a crystallographic transition from rhombohedral to cubic structure.[9] Parravano and Boudart[10] found several physical anomalies near the Neel Point of NiO. Its significance to catalytic activity was briefly mentioned by other workers[11,12,13]. Both Keier[14] and Charman, Dell and Teele[15] noticed that a definite change of mechanism of O_2 chemisorption took place near $250^{o}C$. Winter[16] however, was the first to suggest that the change in the mechanism of O_2 chemisorption was attributable to the magnetic transition. He assumed that the chemisorption took place predominently at exposed edges of magnetic domains. Below T_N, magnetostriction prevents the formation of two Ni^{+++} as adjacent nearest neighbours so that adsorption occurs as O_2^{-}. Above T_N, the restriction is removed and O_2 can be adsorbed as $2O^{-}$. Therefore, it would be interesting to observe changes in the electrochemical behaviour on passing through the Neel Point and, if the changes are favourable, to find methods of reducing the Neel Point, or prepare other compounds with lower T_N, which will hopefully exhibit reversibility to O_2 reduction at lower temperatures.

V. ELECTROCHEMICAL REDUCTION OF OXYGEN ON LITHIATED NICKEL OXIDE ELECTRODES

Tseung, Hobbs and Tantram[17] studied the electrochemical reduction of oxygen on lithiated nickel oxide at 150^{o} and $220^{o}C$ and

found that there was a six-fold improvement in performance at 220°C. The open circuit potential changed from 1.10 V to 1.16 V, very close to the theoretical open circuit potential (75% KOH, 220°C, E^{o} = 1.17 V). Doping with lithium[18] is known to lower T_N by about 20°C. (Neel Point of NiO single crystal is ∿ 250°C). They therefore suggested that oxygen is being dissociatively chemisorbed above the Neel Point, thus by-passing the formation of peroxide intermediate, leading to reversible behaviour and improved performance.

Richardson and Milligan[19] found a remarkable variation of magnetic susceptibility with specific surface area. As the mean particle size diameter decreased to below 200Å, the magnetic susceptibility curve developed a large peak, the position of which on the temperature axis was so dependent on the particle size diameter that for some powders, value of T_N below room temperature were observed. Cohen et al[20] as well as Kawada and Kawai[21] confirmed the above results and showed that NiO powders with a mean particle size diameter of 130Å exhibited paramagnetism at room temperature. Bevan and Tseung[22] investigated the properties of high surface area lithiated NiO (180 m^2/g) prepared by the Technier method[23] and found that electrodes prepared from such powders exhibited reversible behaviour at 150°C instead of 220°C found earlier for low surface area lithiated NiO samples (1-2 m^2/g). The electrode exhibits irreversibility at temperatures below 140°C, even though the Neel Point of the sample should be at room temperature (mean particle diameter 49.9Å). Though the mean particle diameter is small, electron microscopic examination confirmed the presence of particles whose diameter is greater than the critical particle diameter suggested by

Richardson and Milligan (50 m^2/g, $\sim$ 180Å particle). These large crystallites would be expected to show the normal antiferromagnetic behaviour of massive nickel oxide, i.e. Neel Point 220-250°C. These particles will not be able to dissociatively chemisorb oxygen below their Neel Point and hence the reduction of oxygen on such particles will involve the production of HO_2^-, giving rise to a mixed potential and irreversible behaviour, especially when the temperature is significantly lowered.

VI. STRONTIUM-DOPED LANTHANUM COBALT OXIDES AS OXYGEN ELECTRODES

The work on lithiated NiO has shown that it is necessary to use semiconducting oxides which are paramagnetic at room temperature, regardless of particle size; and this condition could be satisfied by the use of perovskite oxides based on Sr doped $LaCoO_3$. Work by Tseung and Bevan[24], confirmed that complete reversibility can be achieved even at room temperature and that the electrochemical performance increased linearly with temperature, surpassing that of platinum black at 170°C. Nevertheless, its performance below 100°C was too low to be of pratical interest (only 5 mA/cm^2 at 900 mV vs RHE at 80°C, 5N KOH).

VII. THE AIM OF THIS WORK

The purpose of this investigation is to study the kinetics of oxygen reduction on semiconducting oxides with particular reference to their electronic structure and magnetic properties, and to optimize the performance of a practical oxygen electrode for low temperature fuel cell application.

CHAPTER TWO

LITERATURE SURVEY

I. ELECTROCATALYSIS

Electrocatalysis is a term applied to describe processes occurring at electrode surfaces. It can be defined as the acceleration of an electrode reaction by a substance which is not consumed in the overall reaction. It may be considered as a special case of heterogeneous catalysis but with one major difference, namely that one or more of the intermediate steps in the overall reaction is a charge transfer step.

The three main processes in which the catalyst plays a role in electrochemical reactions are chemisorption, charge transfer and surface reactions. Geometric and electronic factors play a significant role in electrocatalysis as in heterogeneous catalysis. The important geometric factors are the crystal structure, the interlattice distances, the intersite distance, grain size, and the presence of point, line and plane defects in the catalyst. The electronic energy level, Fermi-level, of a semiconductor, plays an important role in electrocatalysis. The catalytic activity of a semiconductor is dependent not only on the Fermi level, but also on the position of the local levels of the adsorbed species relative to the Fermi level[25]. Surface states such as localised electronic energy levels of the surface created by adsorbed species, non-stoichiometry etc. contribute to enhanced surface activity[26,27,28]. The important electronic factors in the case of transition metals are the work function and percentage of d-band character on the d-vacancies in the metal.

Paramagnetic susceptibility, frequently discussed in terms

of apparent number of unpaired d electrons per atom, has long been recognised as a feature of many good catalysts and electrocatalysts. Based on joint pseudosplitting mechanism[5], proposed by Goldstein and Tseung, ferromagnetic electrocatalysts would be able to achieve side-on adsorption of O_2, resulting in the direct reduction of oxygen to hydroxyl ion without going through hydrogen peroxide as intermediate.

Hole conductivity of an oxide semiconductor has also been related to its activity for oxygen reduction[27]. Hole complexes, where it is defined as a hole distribution over a small group of atoms, at the surface of the electrode are proposed as reaction intermediates in the reduction of oxygen. Consequently, the rate of the reaction will be increased when the concentration of holes in the semiconductor increases.

The presence of a large density of localised electronic states of d-electrons has been qualitatively related to the catalytic properties of perovskite through molecular orbital concepts[27]. When molecules come together and react to form a product, electrons flow between the reacting molecules and redistribute themselves in the molecular orbitals of the product. As the reactants approach each other, the molecular orbitals critical to the reaction are the highest occupied and the lowest unoccupied molecular orbitals. For electron transfer to occur, the initial orbitals must be close together in energy and must have a symmetry such that they experience a net positive orbital overlap. In the case of heterogeneous catalysts, many reactions appear to be controlled by the chemisorption of one or more of the reactants. This implies the existence of occupied surface states whose symmetry permits a net positive overlap

to occur between the surface states and the anti-bonding orbitals of the gaseous reactant. Thus electronic rearrangement may occur and a new set of molecular orbitals are formed which include the wave functions of the surface state and of the chemisorbed molecule.

For the purpose of our investigation of the relation of electronic and magnetic properties on oxygen reduction, an ideal structural form is perovskite. This is because the simple structure makes it theoretically tractable and because essentially all of the electronic properties found among the transition metal oxides may be realised in perovskites by metal ion substitution.

II. PHYSICAL CHEMISTRY OF PEROVSKITE OXIDE

A large class of ionic oxides having the formula unit ABO_3 crystallize in the perovskite structure - see Figure 3.1, where A = larger cation, B = small cation.

The stability of the structure derives primarily from the Madelung energy achieved when cations, which occupy oxygen octahedral voids with shared corners. This requires that B cations have a strong preference for octahedral co-ordination. A general survey of these materials has been complied by Goodenough and Longo[30].

The properties of the perovskites are dominated by the electronic states derived from O^{2-} and the B ion. The A ion contributes strongly to the Madelung potentials but has only a minor influence on the low energy electronic and optical properties because its energy levels lie much higher than those of the B ion.

The perovskites are not completely ionic and there is some covalent sharing of charge. This has the effect of altering the formal charge on the ions. Reduction of the formal charge reduces the Madelung potentials, and changes the energy levels as illustrated in Figure 3.IIb.

Next, we consider the qualitative effects of the crystal field. The B ion surrounded by an octahedron of oxygen atoms which produce a cubic crystal field. The d-levels are split by this field into the familar t_{2g} and e_g levels as illustrated in Figure 3.IIc. The d-orbitals transforming according to the t_{2g} representation are the d_{xy}, d_{xz} and d_{yz} orbitals. The doubly degenerate e_g level includes the $d_{x^2-y^2}$ and d_{z^2} states. The t_{2g} states have their wave function lobes directed in between the repulsive oxygen-ion while the lobes of the e_g states point directly into the repulsive oxygen-ion sites. As a consequence, the t_{2g} states are lowered in energy while the e_g states are raised in energy. The "centre of gravity" of the d-level is, of course, unaffected by the higher order multipoles producing the crystal fields. The oxygen-ions experience an axial crystal field due to the cations and the p-orbitals may be classified as P_σ and P_π according to the orientation of the p-orbital lobes with respect to the cation-anion axis.

Now we proceed to a discussion of the energy band effects, as illustrated in Figure 3.IId for three points in the Brillouin zone. In terms of the simple LCAO model, the largest energies which contribute to the formation of energy bands are:

(1) The (pdσ) transfer integral which leads to mixing

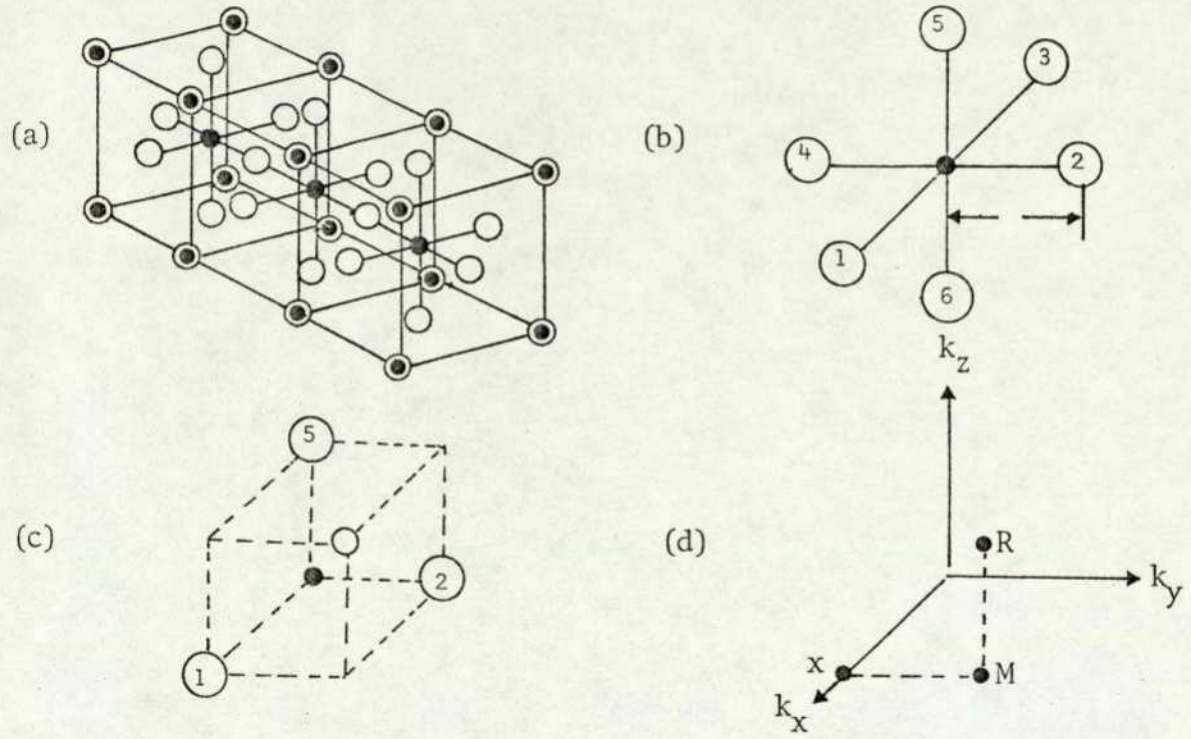

Figure 3.II. (a) Cubic perovskite structure containing octahedral clusters; (b) BO_6 octahedral cluster, B = transition metal ion, O = oxygen ion; (c) unit cell for the perovskite structure; (d) symmetry points in the Brillouin zone for the cubic perovskite structure.

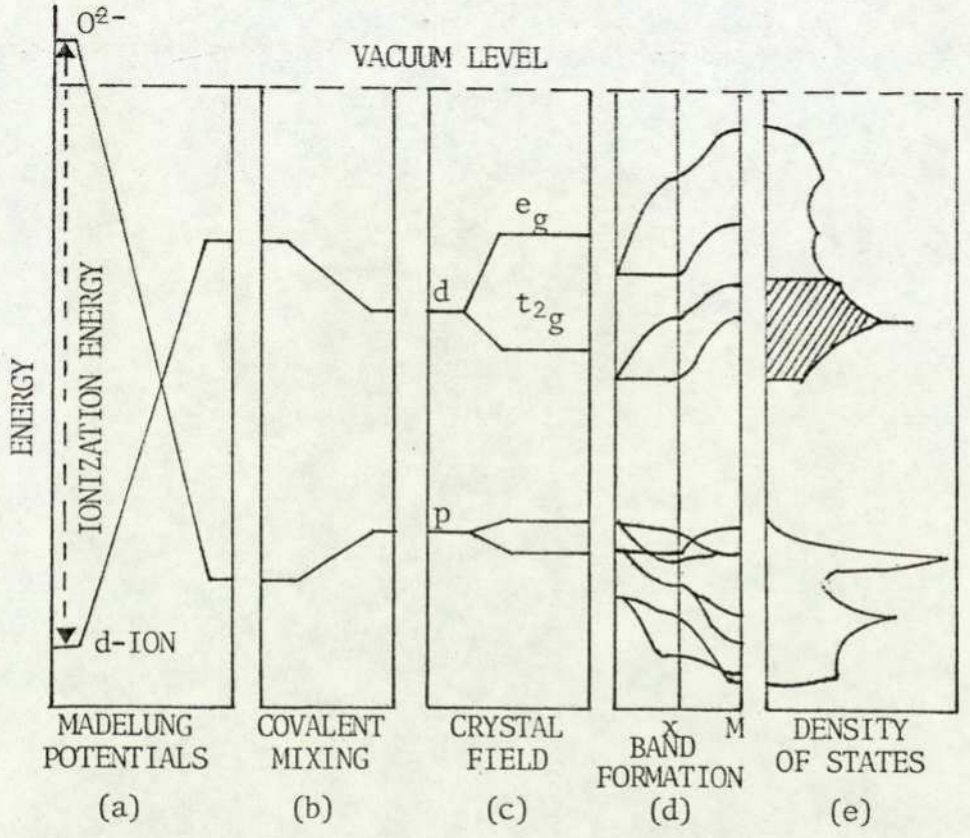

Figure 3.II. Schematic of the major energies involved in the electronic structure of a perovskite

of the e_g states with p-orbitals (2-4 eV).

(2) The ($pd\pi$) transfer integral which leads to mixing of the t_{2g} states with the p-orbitals (1-2 eV).

(3) The ($pp\sigma$) and ($pp\pi$) transfer integrals which couple p-orbitals on different oxygen sites (four tenths of an eV).

We shall be mainly interested in the lower n t_{2g} conduction band. The surface states which derive from this band and exist in the energy gap between the valence and conduction band have been shown to possess the t_{2g} symmetry important in catalytic activity.

Figure 3.IIe illustrates the density of electronic states expected for d-band perovskites. The shaded portion is the density of states associated with the three t_{2g} bands. The abrupt jump in the density at the band edges and approximate logarithmic singularity in the centre of the band are a result of the two dimensional characters of the t_{2g} conduction bands[31].

Where d-electron localisation occurs, as in $LaCoO_3$, conduction occurs by a "hopping" process. In $LaCoO_3$ the B ion configuration at low temperature is thought to be $t_{2g}^6 \; e_g^0$, but the small energy separation between the filled t_{2g} and empty e_g levels results in a room temperature mixture of "low spin" ($t_{2g}^6 \; e_g^0$) and "high spin" ($t_{2g}^4 \; e_g^2$) cobalt ions (designated Co^{III} and Co^{3+} in the literature). Electron transport involves hopping of electron between B ions creating Co^{2+} and Co^{4+} electron-hole pairs. p- or n-type conduction occurs in doped materials.

III. PEROVSKITE OXIDES AS OXYGEN ELECTRODES

Meadowcroft discovered that $La_{0.8}Sr_{0.2}CoO_3$ had catalytic activity comparable to those produced by platinum for the cathodic reduction of oxygen in alkaline solution[32]. Almost at the same time, Bevan and Tseung[33] obtained reversible behaviour for oxygen reduction with $La_{0.5}Sr_{0.5}CoO_{3-y}$. Their encouraging results have led others to try a series of perovskite compounds for oxygen reduction[34-36].

Work by Bevan and Tseung[24] suggested that the performance of oxygen reduction on $La_{0.5}Sr_{0.5}CoO_3$ is controlled by the number of Co^{3+}/Co^{4+} couples free to interact with the oxygen molecule and that the numbers of such couples are low at 25°C, but increase in number as the temperature rises.

Studies by Kudo et al[35] proposed a mechanism for oxygen reduction on $La_{1-x}Sr_xCoO_3$ in which oxygen enters into the oxide bulk, diffuses to the surface in contact with the electrolyte and is then reduced to OH^-, analogous to diffusion step limiting mechanisms which prevail in oxides having high ionic conductivity. This mechanism can be ruled out, because a limiting current of the order of 10^{-7} A cm^{-2} has been calculated[36] using a diffusion coefficient of oxygen ion in oxides of $10^{-11} cm^2 s^{-1}$[41].

Matsumoto et al[36-39,42] studied the electrochemical reduction of oxygen on Lanthanum nickel oxide and related oxides. They suggested that the oxygen adsorption on the electrode is most probably the limiting step, based on an assumption that the oxygen molecule can only be chemisorbed end-on. They also suggested that the

possibility of σ^* band formation between the e_g orbital of the transition metal ion and a molecular orbital of oxygen of the surface is an important factor in determining the electrocatalytic activity.

More recently, studies on the homomolecular oxygen exchange and the electrochemical reduction of oxygen on semiconducting oxides by Hibbert and Tseung[40], suggest that the rate determining step in reversible oxygen reduction is likely to be the dissociative chemisorption of molecular oxygen in agreement with the "joint pseudosplitting/dissociative mechanism"[5].

Even though it has evoked much controversy, the types of chemisorption of molecular oxygen and the electronic properties of the electrocatalyst are both important to the mechanism of oxygen reduction. More fundamental studies are necessary for clarifying the situation.

IV. PRESENT WORK

The purpose of our present work is to study the rate-limiting factors of cathodic oxygen reduction on perovskite oxide with particular reference to its electronic properties. The activity of the perovskite catalyst can be related to its ferromagnetism, to the hole conductivity of the doped p-type oxides and to the highly localised perovskite d-band surface states. By extending the studies of oxygen reduction on these catalysts into a wider range of doping levels, more information could be obtained which might lead to a better understanding of the reaction mechanism and the rate-limiting steps.

CHAPTER THREE

EXPERIMENTAL

I. PREPARATION OF CATALYSIS

If a solution containing two different metal salts is frozen rapidly enough to prevent the precipitation and segregation of the solutes, and if there is no melting of the ice during the subsequent vacuum drying, the resulting dried product should retain the state of sub-division and degree of homogeneity of the original solution, since the solutes are effectively immobilised by the ice crystal during the freeze-drying process[43,44].

In the present studies, all the catalysts were prepared by freeze-drying of the appropriate nitrate mixture, followed by vacuum decomposition and sintering in air at various temperatures.

The apparatus for freeze-drying is presented in Figure 4. The conditions for the preparation of the catalysts are presented in Table 1.

II. CHARACTERISATION OF CATALYSIS

(i) Chemical Composition Analysis

Several methods of analysis were considered to determine the chemical composition of the sample. Spectroscopy seemed the most appropriate method in view of the limited quantity of catalyst.

The sample was accurately weighed, dissolved in aqua regia and diluted to the appropriate concentration. The Co, Ni and Sr concentration in the sample was then determined by atomic absorption spectroscopy. La ions were separated from Sr ion by precipitation of the La ions as the hydroxide and from Co and Ni by precipitation as the oxalate.

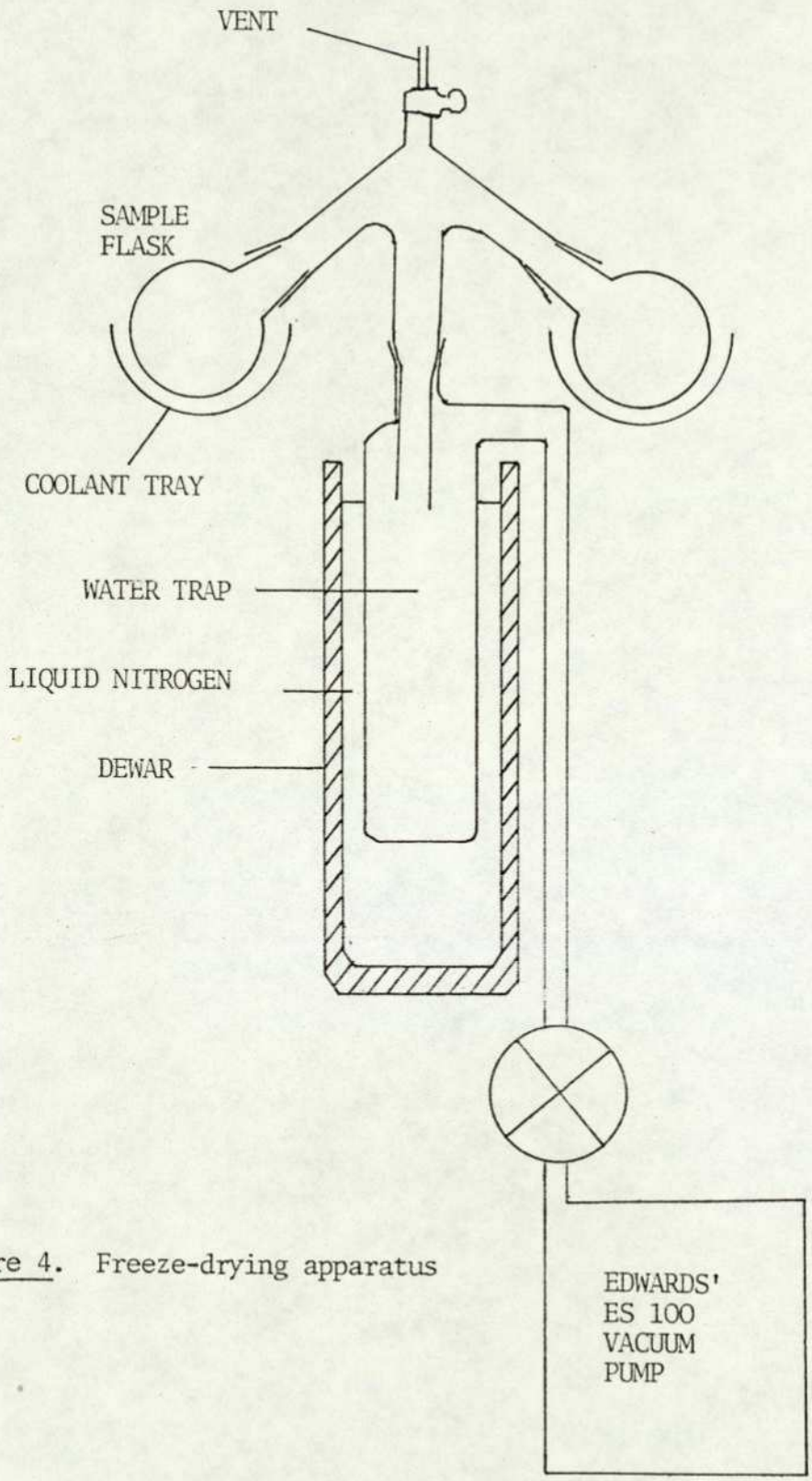

Figure 4. Freeze-drying apparatus

TABLE 1. Condition for the Catalyst Preparation

Sample No.	Compounds	Starting Materials	Preparation Method	Sintering		Phases Present
				Temp. ^{o}C	Time (hr.)	
N1	$Sr_{0.5}La_{0.5}NiO_3$	$Sr(NO_3)_2$ + $La(NO_3)_2$ + $Ni(NO_3)_2$	Freeze drying	600	3.5	Perovskite
NC1	$Sr_{0.5}La_{0.5}Ni_{0.3}Co_{0.7}O_3$	$Sr(NO_3)_2$ + $La(NO_3)_3$ $Ni(NO_3)_2.6H_2O$ + $Co(NO_3)_2.6H_2O$	Freeze drying	550	3.5	Perovskite
NC2	$Sr_{0.5}La_{0.5}Ni_{0.5}Co_{0.5}O_3$	DITTO	DITTO	600	12	Perovskite
NC3	$Sr_{0.5}La_{0.5}Ni_{0.1}Co_{0.9}O_3$	DITTO	DITTO	600	6	Perovskite
S1	$Sr_{0.5}La_{0.5}CoO_3$	$Sr(NO_3)_2$ + $La(NO_3)_3$ + $Co(NO_3)_2$	DITTO	700	6	Perovskite
S2	$Sr_{0.3}La_{0.7}CoO_3$	DITTO	DITTO	700	6	Perovskite
S3	$Sr_{0.1}La_{0.9}CoO_3$	DITTO	DITTO	700	6	Perovskite
S4	$Sr_{0.6}La_{0.4}CoO_3$	DITTO	DITTO	700	6	Perovskite

Table 1 (cont.).

S5	$LaCoO_3$	$La(NO_3)_2$ + $Co(NO_3)_2.6H_2O$	DITTO	700	6	Perovskite
C1	$NiCo_2O_4$	$Ni(NO_3)_2.6H_2O$ + $Co(NO_3)_2.6H_2O$	DITTO	400	10	Spinel
C2	$NiCo_2O_4$	DITTO	Thermal decomposition	400	10	Spinel
Nd1	$Nd_{0.5}Sr_{0.5}CoO_3$	$Co(NO_3)_2.6H_2O$ + $Sr(NO_3)_2$ + $Nd(NO_3)_3$	Freeze drying	700	10	Perovskite

(ii) X-ray Diffraction Analysis

The oxide samples were subjected to x-ray analysis by the powder technique in order to ascertain that the perovskite phase had indeed been formed. It was possible to identify and estimate other minor phases (> 5%) present and this served as a check on the chemical analysis. Also, by investigating the variation of the perovskite oxide lattice parameter as a function of composition, it was possible to demonstrate a possible geometric factor in the catalyst.

A Phillips x-ray power source and window system and a Phillips Traumanis Camera were used. Each sample was mounted in a Lindsmann glass capillary of 0.2 mm internal diameter. A molybdenum target was normally used, operated at 40 KV and 16 mA.

In the powder technique for x-ray analysis, developed by Debye and Scherrer, a monochromatic x-ray beam is allowed to fall on a quantity of the specimen in fine powder form. Since the orientation of the minute crystal fragments is totally random, many crystal planes will have exactly the correct angle with the incident beam for reflection to occur. The specimen is mounted along the central axis of a cylindrical camera, which contains a film along its inner cylindrical wall. X-rays, suitably orientated, enter via an entry port and are diffracted by the specimen, producing a series of diffraction cones which are recorded as a series of sharp lines on the photograph, symmetrically placed on each side of the entry port. The position of these lines is related to the angle θ, governed by the "Bragg's scattering condition", and is illustrated in Figure 5.

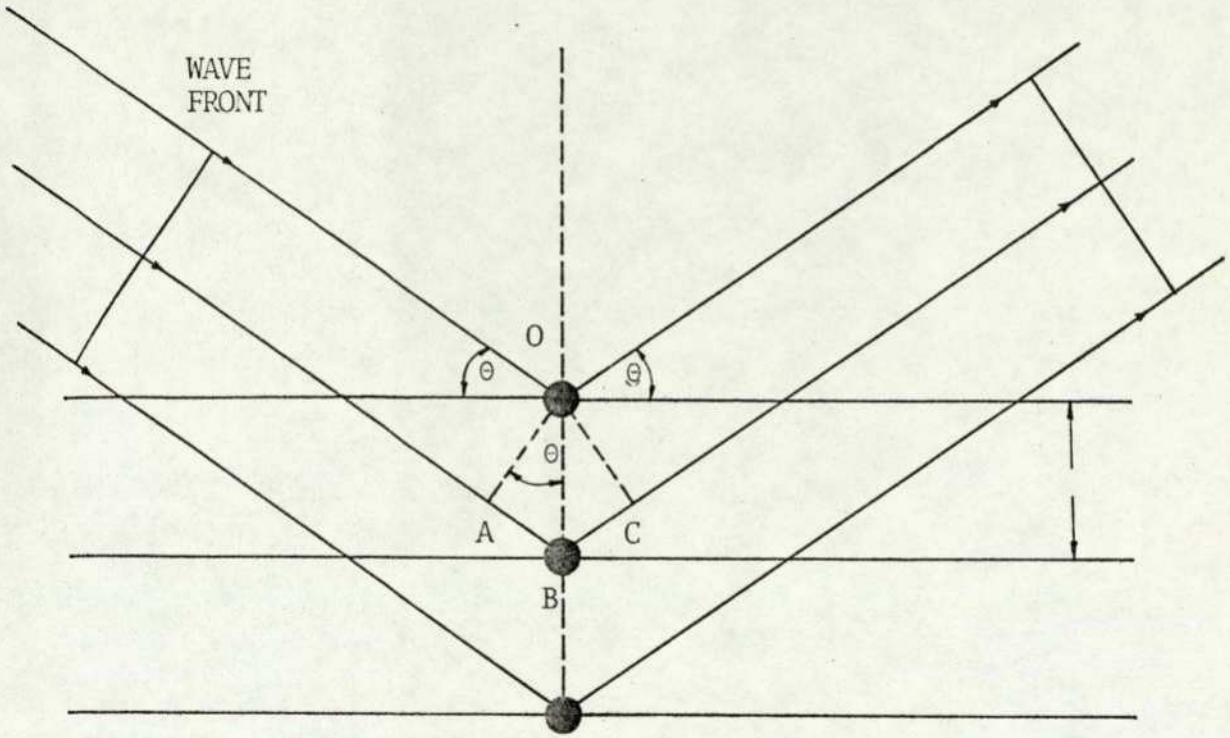

Consider the "reflected" waves at point P,

the path difference for the first two planes is $\underline{D}$,

where $\underline{D} = AB + BC$

$\underline{D} = 2(AB)$

since triangles AOB and COB are congruent

$$\underline{D} = 2d\sin\theta$$

The condition for Bragg scattering is therefore

$$\underline{n\,\lambda = 2d\sin\theta}$$

where n is an integer, and λ is the wavelength of x-rays, and d is the inter-atomic distance between planes.

Figure 5. Bragg scattering condition

The results of the lattice constants (a_o) are presented in Table 2. The d-spacings of each sample were calculated for the crystal phase determination.

(iii) Surface Area Measurement

The B.E.T. method was used. This is based on the physical adsorption of gas onto the surface of the sample at low temperatures near the boiling point of the gas. In this study nitrogen (-195^{o}C) was used. The method assumes that the adsorbate molecules are held in two-dimensional close packing on the surface.

The topic of surface area measurements of solid catalysts has been comprehensively covered by Emmett[45].

A detailed account of the experimental procedure and apparatus was given by Bevan[46] and is only briefly mentioned here.

A small amount of the powdered sample was weighed out into a small preweighed aluminium foil 'cup' which was suspended from a microbalance. The system was enclosed with the sample hanging in a glass flask, as shown in Figure 6. The apparatus was evacuated, and the glass flask immersed in liquid nitrogen. The flask was than isolated from the vacuum pump, and a small amount of gaseous nitrogen introduced. The change in weight of the sample was indicated by the microbalance, and recorded. The pressure inside the system was indicated by a manometer. This procedure was repeated for further introductions of nitrogen.

An increase in weight indicated that nitrogen had been adsorbed into the surface of the sample. The number of molecules

TABLE 2. Lattice Parameter of $La_{1-x}Sr_xNiyCo_{1-y}O_3$ from the x-ray diffraction analysis.

Compounds	Lattice Parameter (Å)
$La_{0.5}Sr_{0.5}CoO_3$	5.380
$La_{0.7}Sr_{0.3}CoO_3$	5.395
$La_{0.9}Sr_{0.1}CoO_3$	5.385
$LaCoO_3$	5.375
$La_{0.5}Sr_{0.5}NiO_3$	6.354
$NiCo_2O_4$	8.136

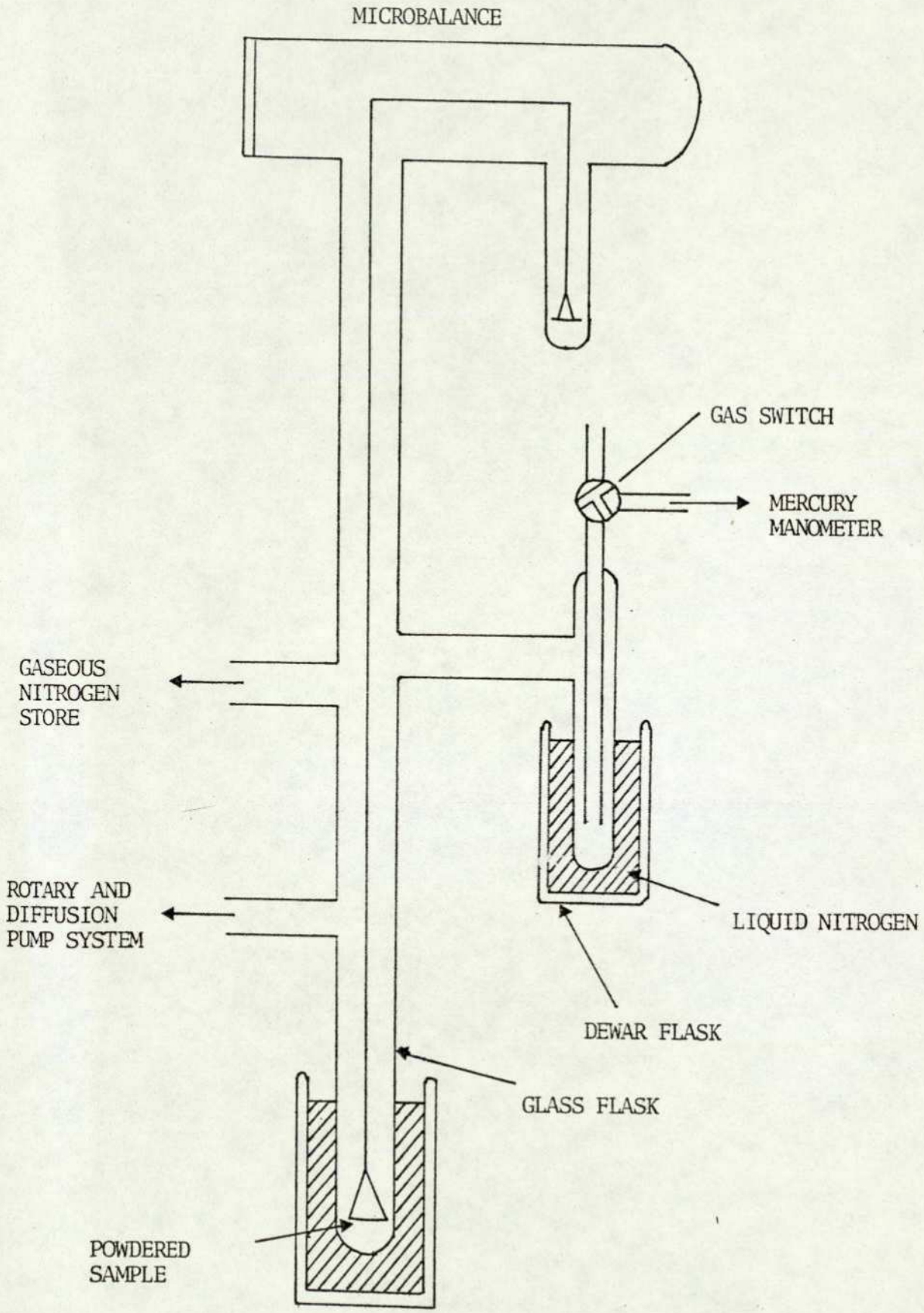

Figure 6. Section of BET apparatus

adsorbed was calculated from the weight changes and, in simple terms, the surface area was calculated by multiplying the area each nitrogen molecule covers (16.2Å^2) by the total number of adsorbed nitrogen molecules.

A decrease in weight of sample prepared by solid state sintering was observed on the initial introduction of nitrogen gas, since the surface area of the sample was relatively small ($5\ m^2/g^{-1}$) and only a little nitrogen was adsorbed. The major protion stayed in the free gaseous phase and so increased the density of the environment of the sample, which increased the buoyancy resulting in apparent loss in weight.

(iv) Electrical Conductivity Measurement

A Wayne-Kerr A.C. bridge was used (1592 Hz) for all conductivity measurements. A weighed amount of the powdered sample was loaded into a specially-designed cylindrical steel die, which had a 1 cm. diameter inner teflon sleeve. The height of the pressed powder bed was noted and the conductivity was measured. Specific conductivities were then computed and plotted against pellet density. For comparative purposes, the specific conductivity at 75% density was arbitrarily taken as representing the specific conductivity of the powder. All the measurements were carried out at $25^{\circ}C$.

Figure 7 shows a section through the cylindrical die. The extreme faces were held between the jaws of a tensometer, in which the pressure could be increased either manually or by programmed motor.

Figure 7. Section through cylindrical die used for conductivity measurement

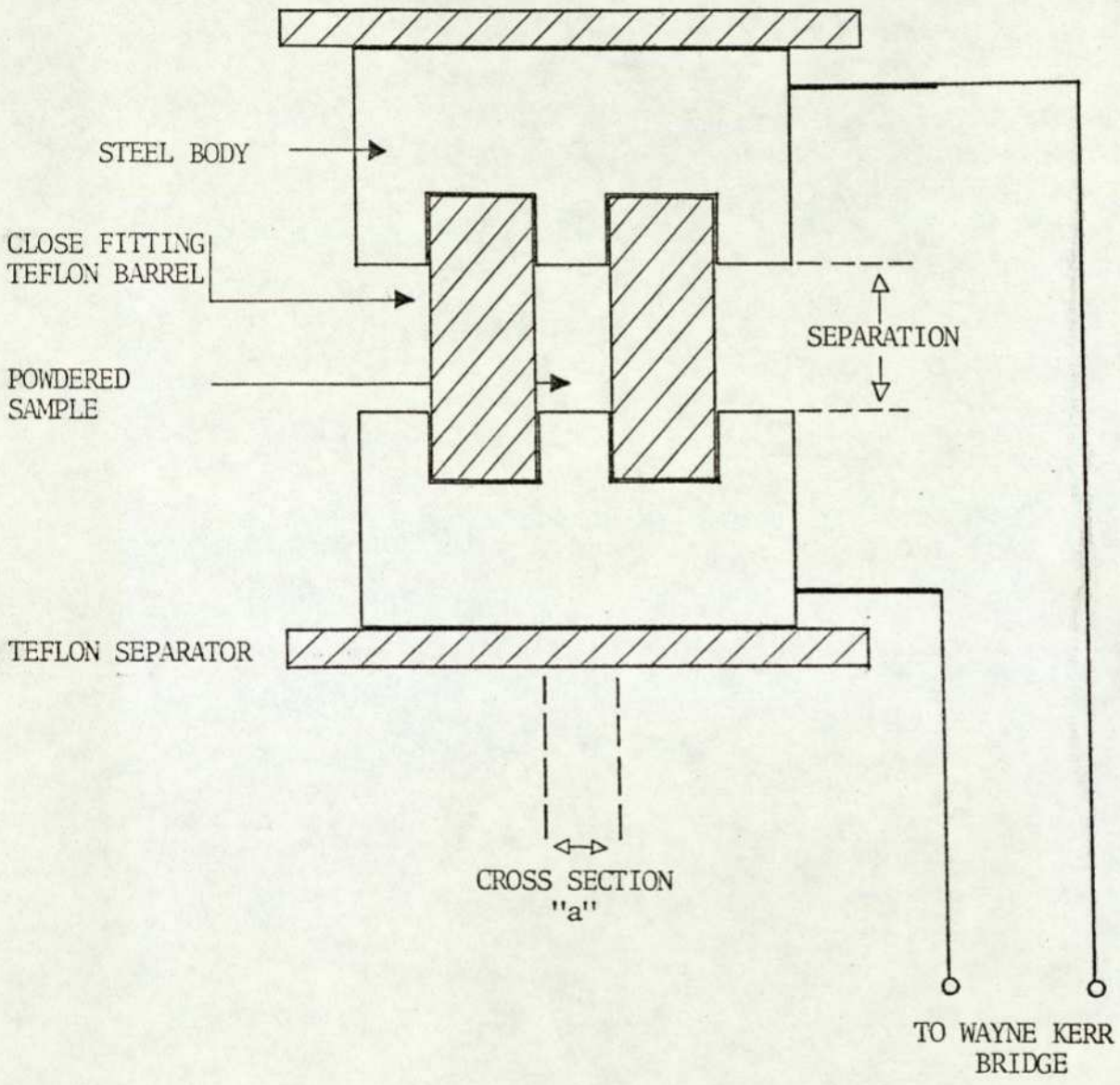

III. ELECTROCHEMICAL TESTS

(i) Instrumentation

A chemical electronics potentiostat (model TR 40/3 A) was used for most of the work. This is a solid state instrument having a built in zener diode stabilized reference potential circuit. The potentiostat is capable of imposing a maximum of three volts between the working and reference electrodes provided that the current in the cell is not in excess of 3 amp. and the potential between the working and secondary electrode is less than 40 V.

A Chemical Electronics waveform generator type WG-01 was used to generate most of the potential time waveforms required in this investigation. The instrument consists of four internal generators -01, dual attenuator -01 and a ramp generator -01.

A Data Lab. transient recorder type DL901, a Bryans X-Y-t recorder type 29000 A4, a telequipment oscilloscope type D61A and a Gould Advance digital multimeter type DMM7 were used for recording the results of the electrochemical studies.

(ii) Test Cell

Three types of test cells were used for this investigation.

Steady state performance tests in the temperature range 20°C to 80°C were conducted with a modified cell of the "Floating Electrode", the type used by Giner and Parry[47,48],(Figure 8). Teflon rings were used to clamp the working electrode to the teflon control pillar of the upper assembly inside which was

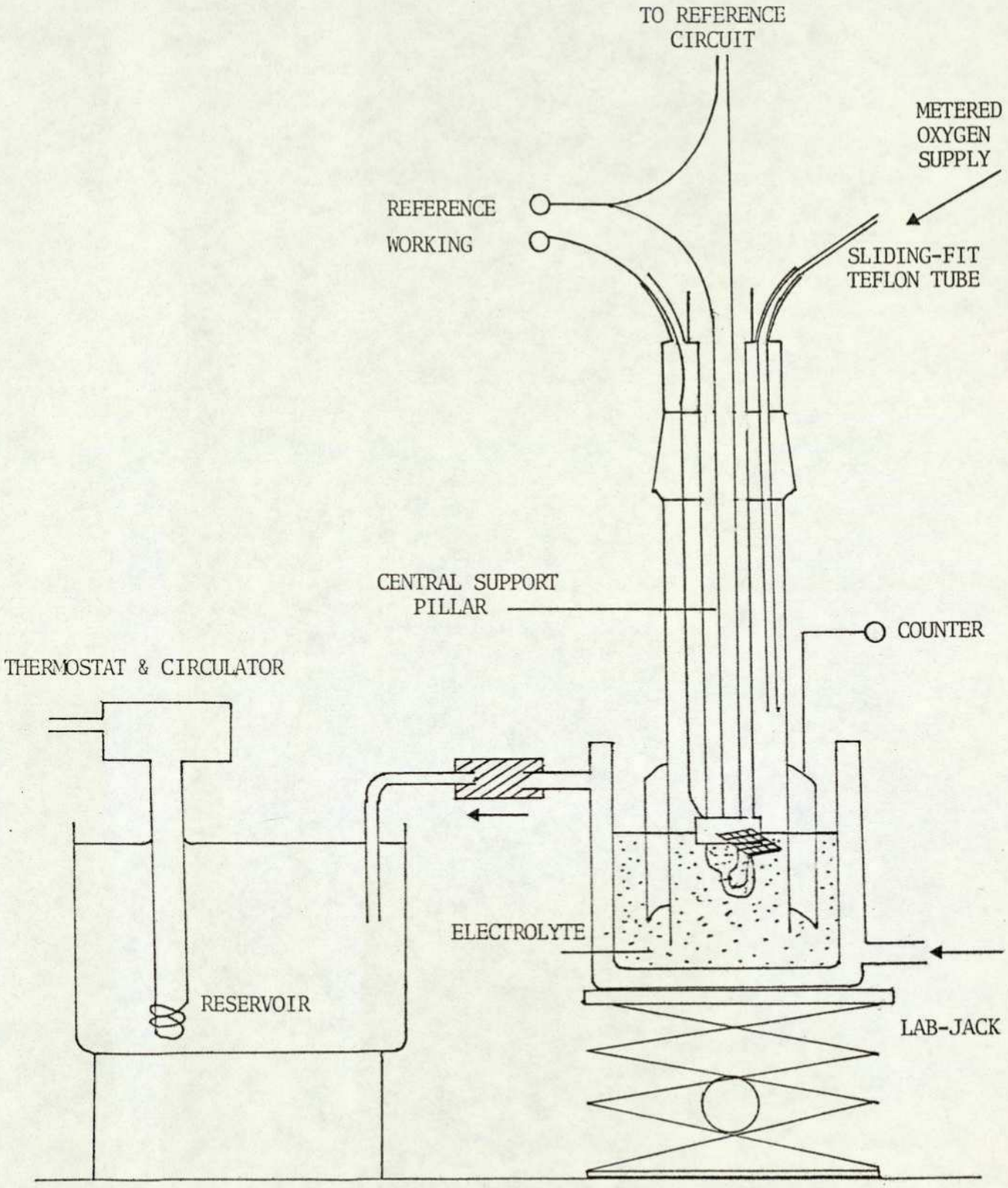

Figure 8. Floating Electrode Test Cell Assembly

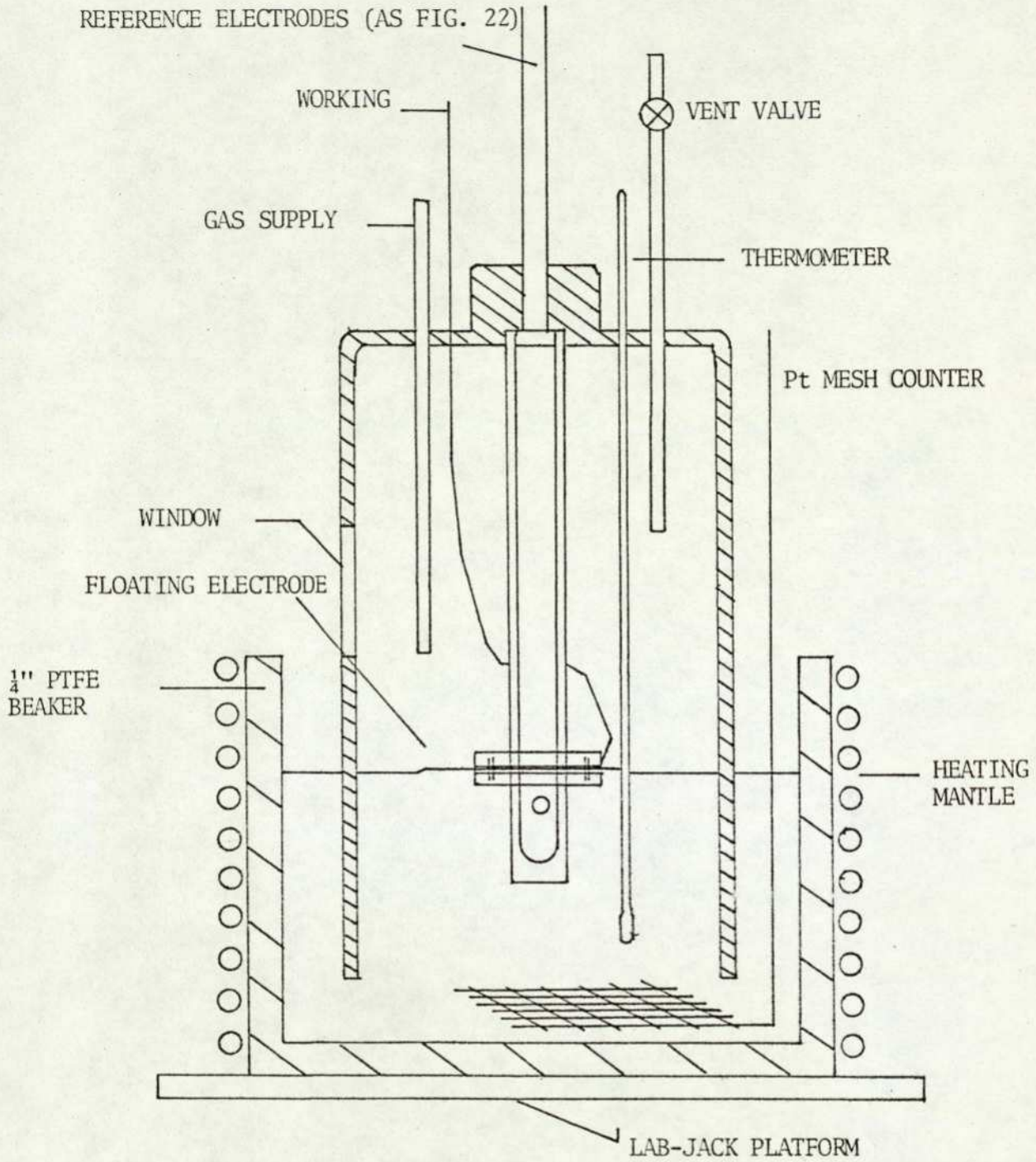

Figure 9. High Temperature Test Cell

located the reference electrode. Vertical sliding adjustment of the teflon rings enabled a constant, measured i-R drop to be reproduced for each electrode tested. Electrolyte contact was made by jacking up the lower vessel containing the KOH solution until the lower side of the electrode was in electrolytic contact with the circuit. The gas compartment, now isolated from the atmosphere, was fed with oxygen, or oxygen/nitrogen mixtures, as required, at pressures slightly above atmospheric; a small positive pressure of about 5 mm was generated by restricting the exhaust.

Figure 9 shows an "all teflon" cell which could withstand temperatures up to 250°C in 85% molten KOH. The cell wall contained a transparent window of polythene (not in contact with the KOH, hence not attacked) which enabled all the advantages of the low temperature pyrex-glass cell to the preserved. However, since it was not possible to have such a refined Luggin capillary, the latter was omitted, which resulted in higher i-R values than those obtained with the low temperature (glass-cell).

The "floating electrode" cell, as modified for the kinetic studies, is shown in Figure 10. The body of the cell consisted of a pyrex U-tube fitted with a working electrode compartment, a counterelectrode compartment and a reference electrode compartment. The working electrode was supported in an electrode holder with a Pt wire contact.

Figure 10. U-shape Cell

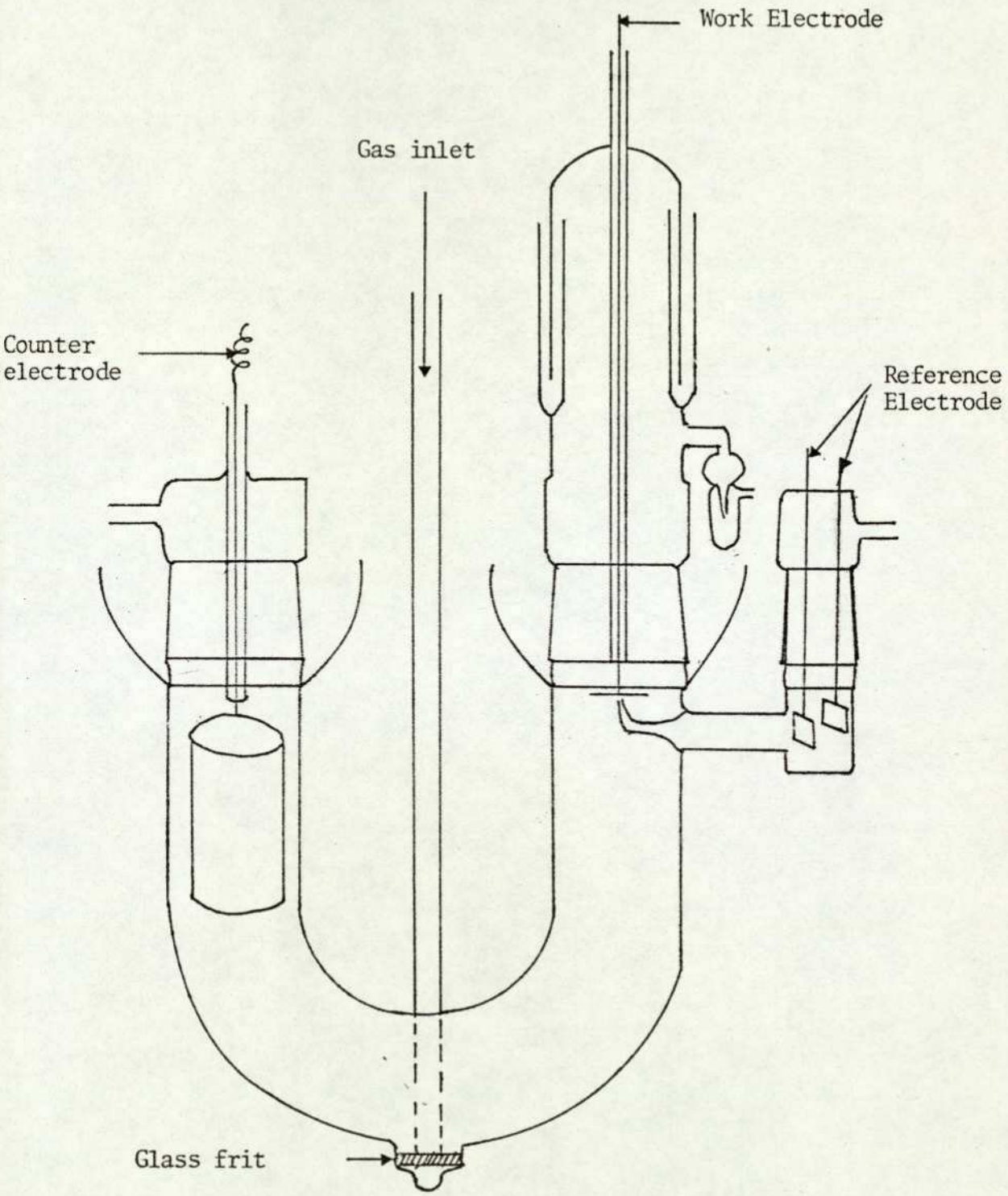

(iii) Preparation and Purification of the Electrolyte

All the work was carried out in 45 wt % KOH solutions. The solution was prepared from BDH Analar grade KOH and doubly-distilled water.

This electrolyte was then subjected to preadsorption[49] at a platinized platinum foil held at + 0.1 V (vs DHE) for 72 hours with nitrogen purging.

(iv) Reference Electrode

The dynamic hydrogen electrode (D.H.E.) was used as the reference electrode[50]. The DHE consists of a platinized platinum electrode which is cathodically polarized with the assistance of a second similar electrode. Hydrogen is evolved by passing a constant current density of 2 mA cm^{-2} between the two electrodes. The DHE was kept approximately 1 cm lower than the oxygen evolving anode to stop most of the O_2 diffusing to it. Under these conditions, the potential of the DHE should be reasonably stable.

Much of the ohmic resistance of the electrolyte can be eliminated by using a Luggin capillary[22,23]. The glass tubing which contained the DHE was drawn out into a fine capillary which ended close to the bottom side of the W.E. Seen simply, the DHE is effectively brought close to the W.E. by means of an electrolyte bridge. The distance between the capillary tip and the W.E. was made the same for each electrode tested.

(v) Electrode Fabrication

It is essential to standardise electrochemical testing. This is particularly true for the preparation of the test electrode, but difficulty arises because of certain interdependent properties.

The electrode performance for a given catalyst material will depend, apart from numerous other things, on:-

(a) Catalyst loading (mg cm^{-2})

(b) Mass ratio of catalyst to p.t.f.e. binder.

By keeping both these parameters constant, differences in performance between electrodes of a given material will be minimised. The problem arises when samples of widely-differing surface areas are compared. The degree of "hydrophobicity" of electrodes depends on the relative surface areas of catalyst and p.t.f.e. It is impossible therefore for a constant catalyst loading and constant catalyst p.t.f.e. ratio to be compatible with an optimised electrode structure. Too little binder causes the electrode to quickly "flood". Whereas too much p.t.f.e. greatly increases the ohmic drop across the electrode. In both extremes, performance is greatly impaired.

To solve this dilemma, it was decided to standardise on constant catalyst loading (normally 17 mg/cm^2) and allow the catalyst : p.t.f.e. ratio to vary freely to achieve optimum electrode performance.

The electrode fabrication technique closely followed

that of Tseung, Hobbs and Tantram[17], which is outlined below:

The weighed catalyst sample was mixed with a few drops of water and dispersed in an ultrasonic bath. The p.t.f.e. dispersion (I.C.I. Fluon GP1, containing 60% by weight solid p.t.f.e. with a mean PSD of 0.17 microns) was introduced dropwise and ultrasonic dispersion continued for a further 10 minutes. The resulting slurry was then painted onto a pre-weighed, degreased and etched 100-mesh nickel grid, until the desired catalyst loading had been attained. The electrode was then cured at 300°C for one hour (this destroys the wetting agent used to stabilise the dispersion but preserves the polycrystalline form of polymer). After curing, the electrode was spot-welded to a strip of gold foil attached to a gold wire, then mounted in a test assembly for electrochemical evaluation.

(vi) Half-Cell Testing

The current density-polarization relationship is of the utmost importance in electrocatalysis. Such characteristics of a fuel cell however give no indication of the behaviour of each electrode (anode and cathode). To do this, a third supplementary electrode, the reference electrode must be introduced, having a constant potential to which each working potential may be referred. If, as in the case of this work, only one electrode is being studied, the other can be dispensed with and replaced by a counter electrode together with an external power source so that the reaction of interest can be monitored

under a wide range of conditions.

The essential point is that although the system is being "driven" the work electrode characteristics are identical to that in a fuel cell in which the working electrode does the "driving".

This is the principle behind half-cell testing, which is shown schematically in Figure 11, and which is universally accepted as a legitimate means of evaluating fuel cell electrode activity.

(vii) The Determination of Internal Resistance

The ohmic polarization which occurs in a fuel cell due to the resistance of the electrolyte also appears as a component in a half-cell polarization curve, this time due to the working-to-reference electrolyte gap. The magnitude of this "i-R" drop will depend on electrolyte concentration and temperature. The i-R drop can be measured in two ways:-

(a) directly, using a conductivity meter (Wayne-Kerr A.C. bridge, on the low-impedence adaptor ranges)

(b) by the interruptor method. In this method, a steady D.C. polarizing current is interrupted at high frequency (50 Hz is convenient) by means of a fast-acting mercury-wetted relay, producing a train of square-waves through the cell. The components of electrode polarization can be

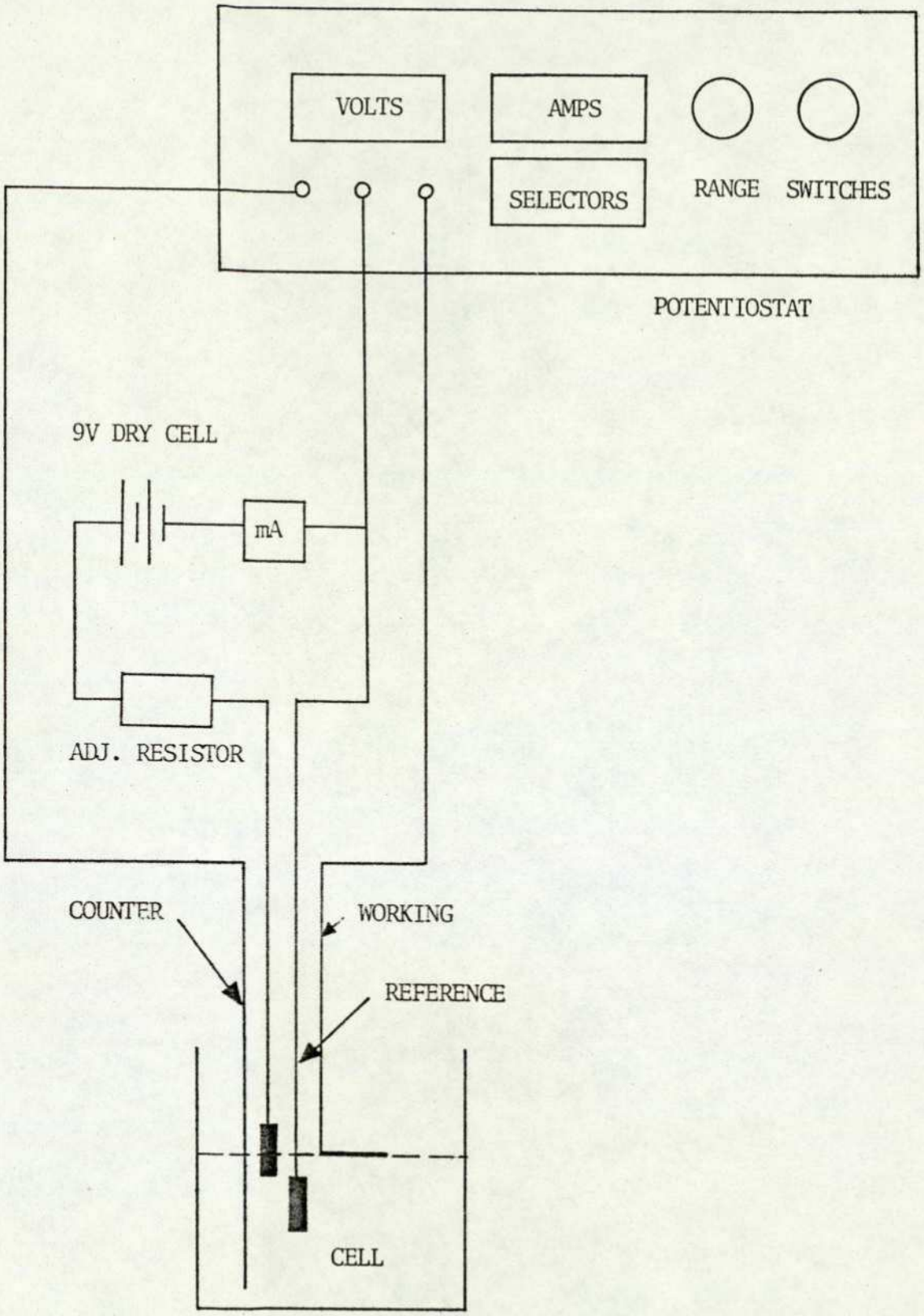

Figure 11. Half-cell test circuit

separately measured since their time-dependence of decay or growth differ. Thus ohmic polarization is instantaneous, whereas activation and mass-transfer effects require finite time intervals to react. If the potential decay trace is displayed on an oscilloscope, the magnitude of the i-R drop can be measured using Ohm's Law, for any selected current through the cell. (See Figures 12 and 13).

(viii) Cyclic Voltammetry

In this method, the potential of the electrode is controlled externally and varied linearly with time from a starting potential E_i to a final potential E_f and then the process reversed from E_f to E_i. The current is measured as a function of potential during the sweep. The potential range (E_i to E_f) is pre-selected, depending on the reaction being studied.

An advantage of using the potential sweep method to determine the kinetic parameters corresponding to the steady state conditions is that the sweep rates used could be low enough for quasi steady state behaviour, but fast enough to resolve interference effects such as oxide reduction of the electrode surface. Another advantage is that the apparatus is quite easy to set up and a plot of the current vs potential is directly obtained.

The intermediate sweep rates method was used in the

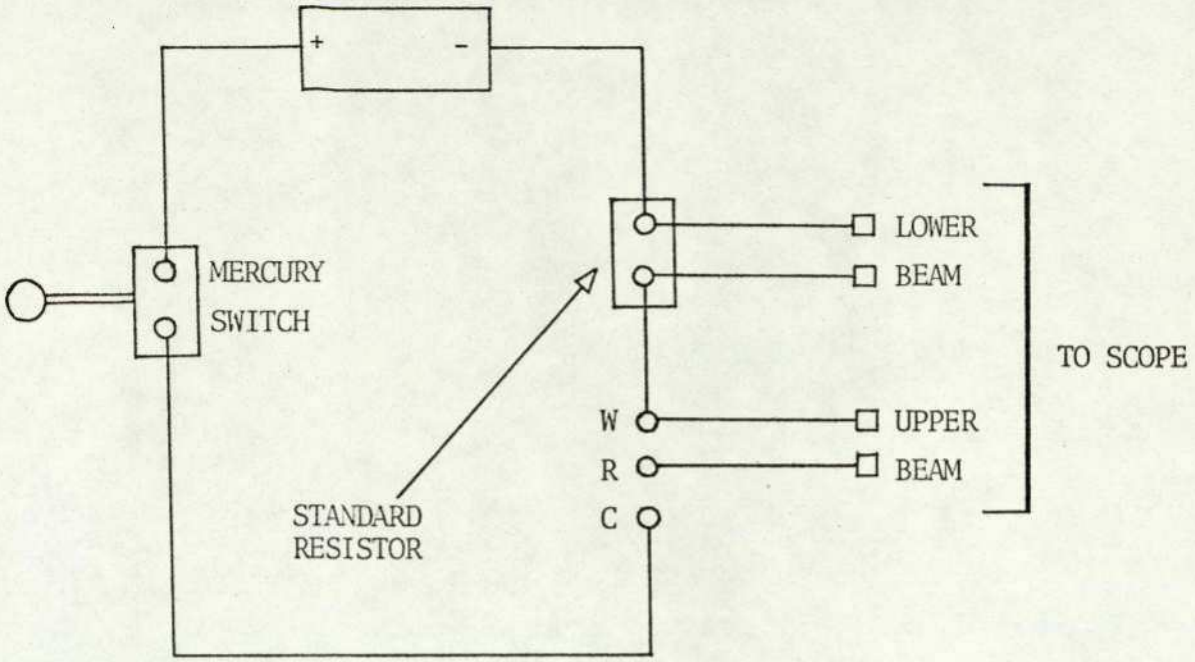

Figure 12. Interruptor Circuit

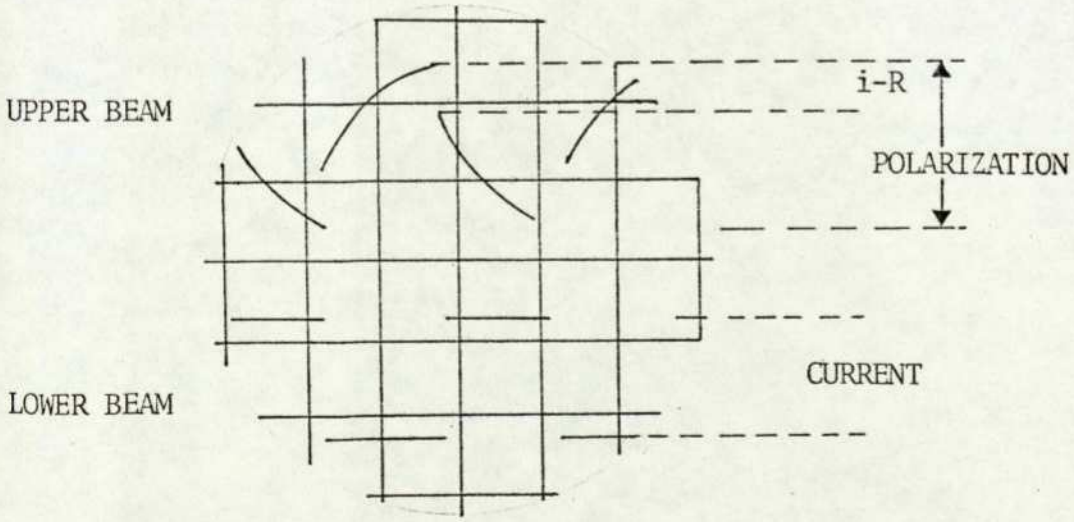

Figure 13. Oscilloscope Trace

studies of the stabilities, and also the OCV shifts after polarization of the electrodes.

The schematic circuit diagram is shown in Figure 14.

(ix) Potentiostatic Pulse Studies

In order to get more precise kinetic information on the oxygen reduction process on teflon bonded semiconducting oxide electrodes, it is necessary to reduce mass transfer effects as much as possible. In principle, the potentiostatic pulse method is ideally suited for this type of investigation[51]. The transient behaviour of an electrode under 'mass transfer free' conditions at zero time, can be displayed on an oscilloscope screen. However, it is not possible to make instantaneous measurements due to double layer charging effects. Every electrode behaves as a 'leaky' condenser solid on applying a potential, a very short but finite time is required to charge the electrode. This time interval depends on the capacity of the electrode double layer and therefore the electrode surface area.

An approximate method is to take measurements at the shortest time interval after which double layer charging is complete and accept a small amount of concentration polarization. The double layer charging time can be measured from the potential transients in the absence of reactants, as shown in Figure 15.

(x) Measurement of Oxygen Coverage

The galvanostatic "oxygen" stripping method[52] was used

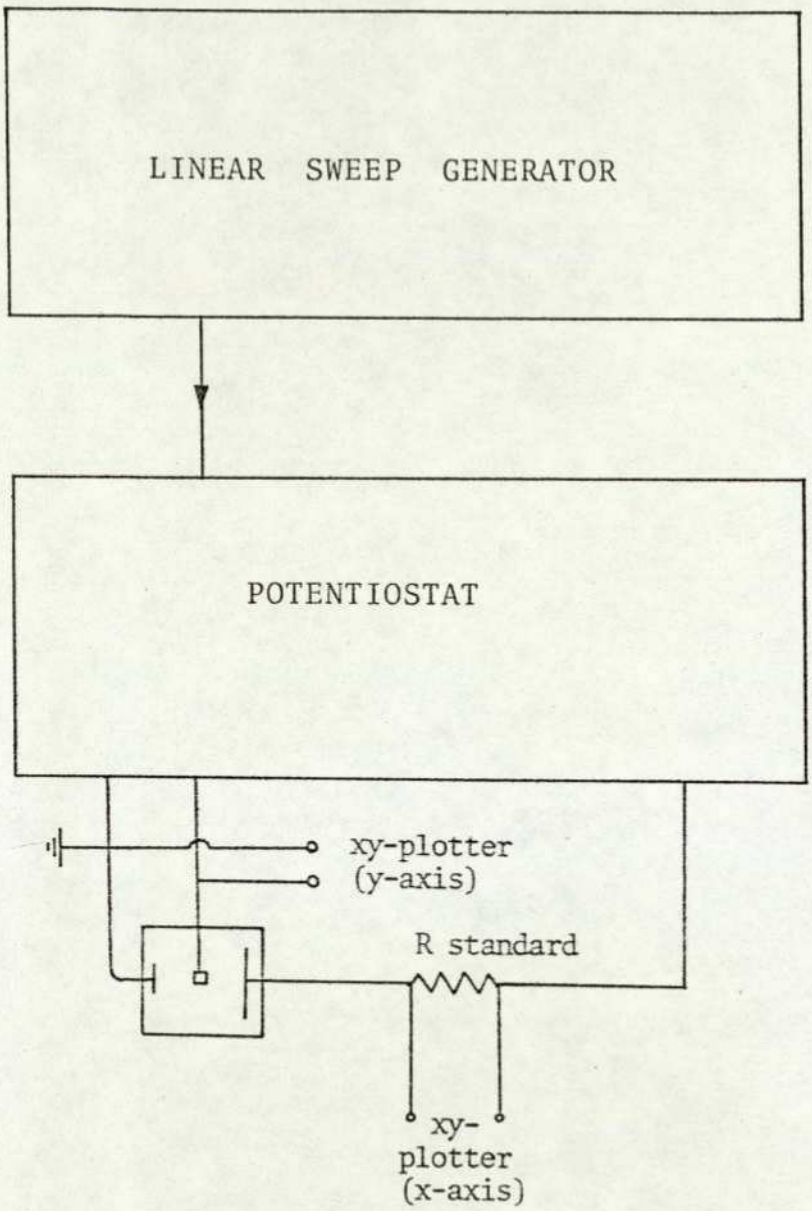

Figure 14. Schematic circuit diagram of linear sweep arrangement

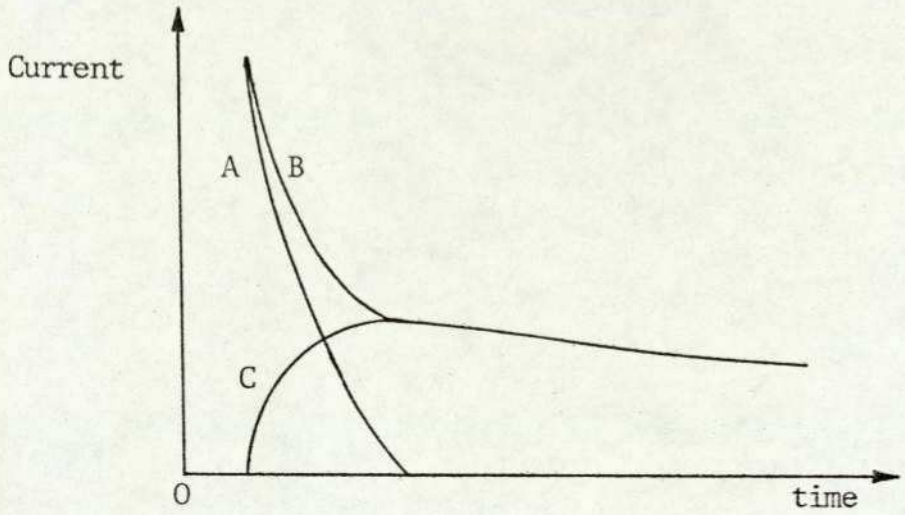

A - charging current

B - total current i.e. charging and faradaic currents

C - faradaic current

Figure 15. The effect of double layer charging

Figure 16. Schematic circuit diagram for potentiostatic pulsing

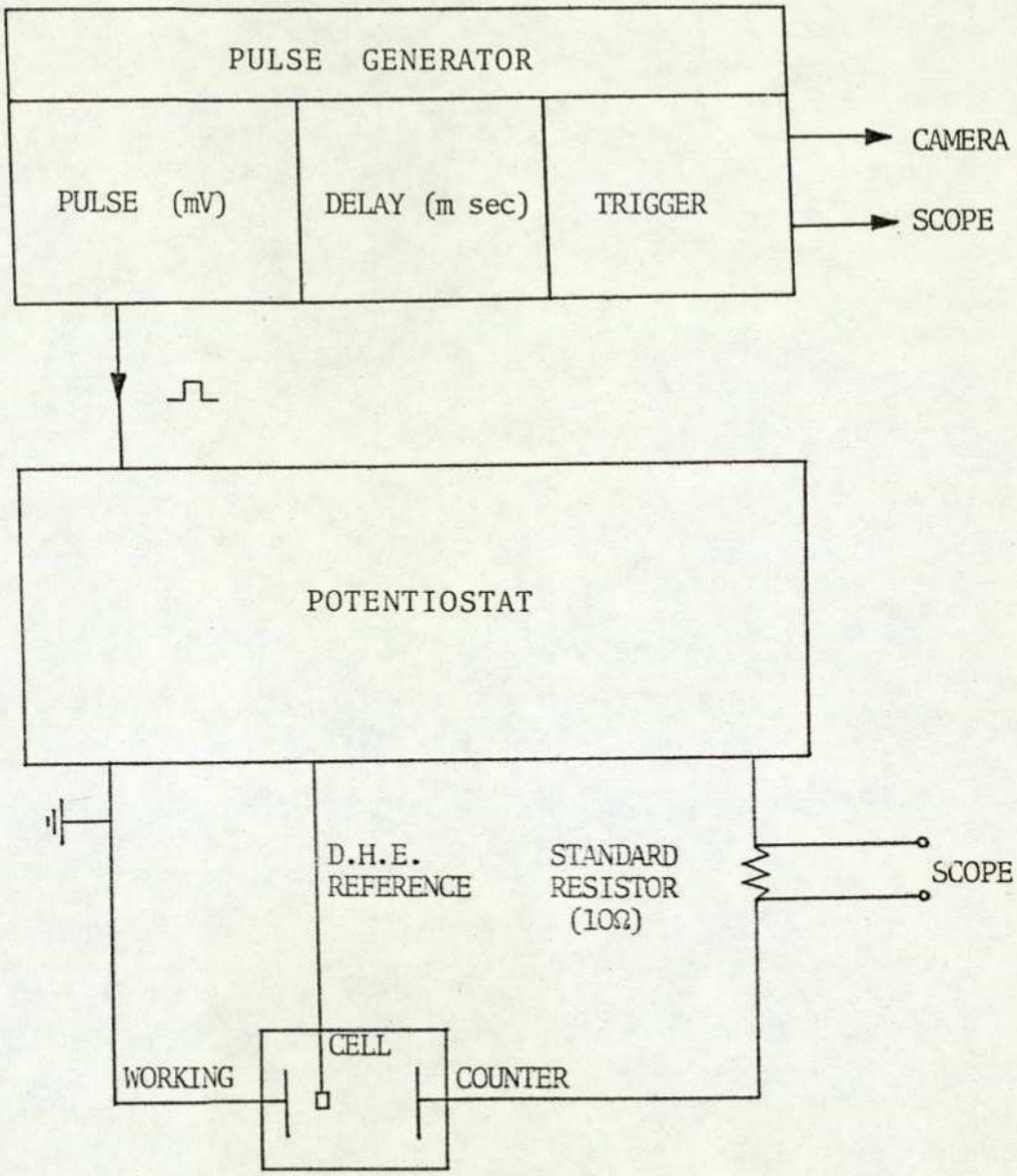

to determine the electrochemical surface area for oxygen reduction. Oxygen was bubbled through the test cell until a steady open circuit voltage was reached. The electrode was then potentiostatically held at this potential and a stream of deoxygenated white spot N_2 was used to purge dissolved oxygen in the electrolyte for 15 minutes. A cathodic, galvanostatic pulse was then used to reduce the oxygen chemisorbed on the electrode surface. The potential was recorded on a storage oscilloscope. A mercury relay switching circuit (Figure 17) was used to switch the potentiostatic circuit to the galvanostatic circuit. Figure 18 shows a typical potential time curve for a Teflon bonded $Nd_{0.5}Sr_{0.5}CoO_3$ electrode. Most of the oxygen reduction reaction was completed within 900-400 mV (vs DHE). When all the oxygen had been removed, the potential dropped sharply through a double layer region until some other process can support the current, after which a further 'potential arrestment' occurred. The product of the time taken to strip the oxygen completely, i.e. the 'transition time' and the current, yields the quantity of electricity involved. Assuming that the active site : O ratio is 1, and the area of an active site is known (discussed in the results section), the electrochemically active area of the above electrode could then be readily calculated by using Faraday's Law.

Figure 17. The mercury relay switching circuit

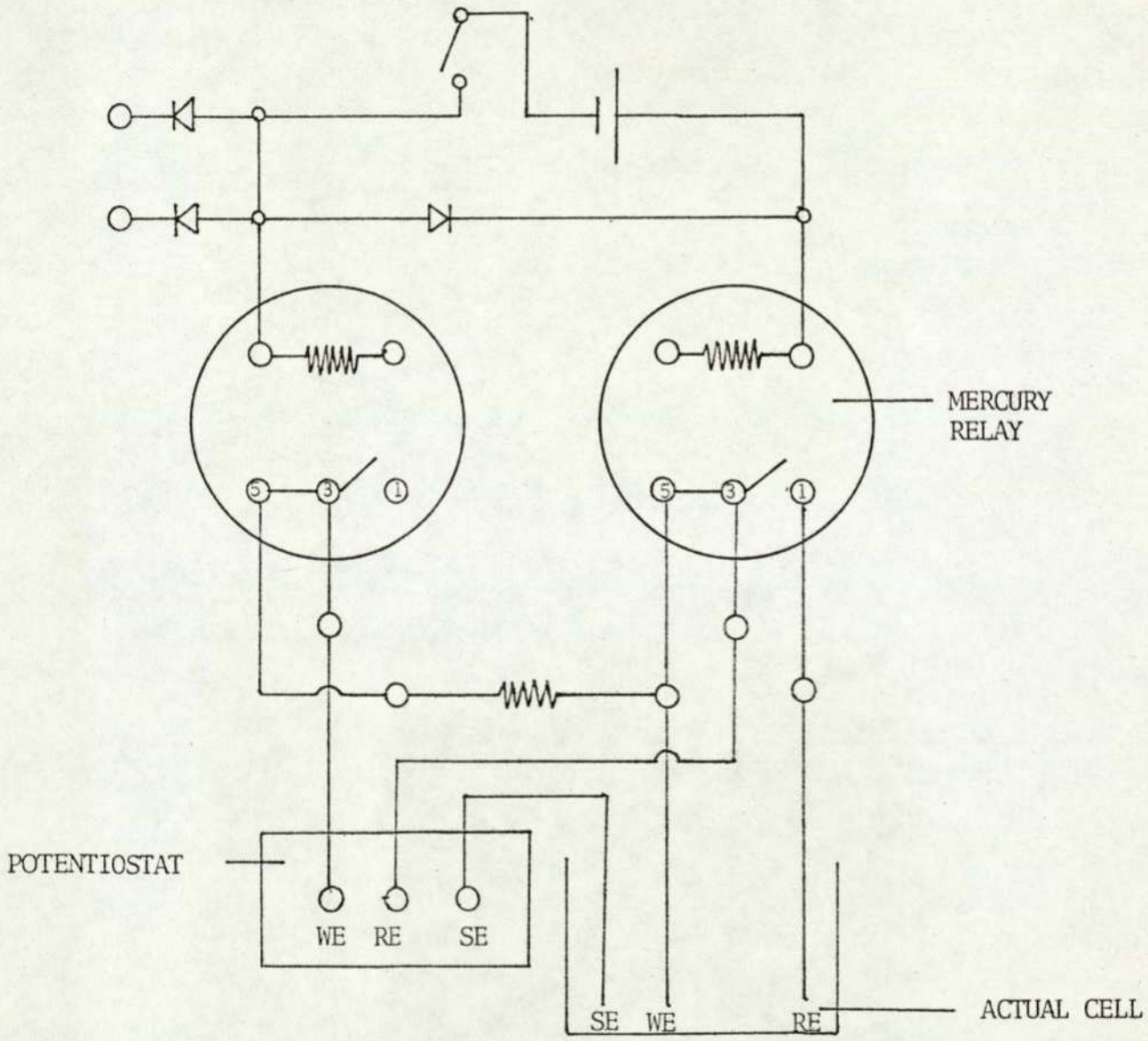

1 - 3 For Potentiostatic

3 - 5 For Galvanostatic

Figure 18. The V-t relationship for O_2 stripping of the teflon bonded $Nd_{0.5}Sr_{0.5}CoO_3$ electrode at 45°C in 45% KOH

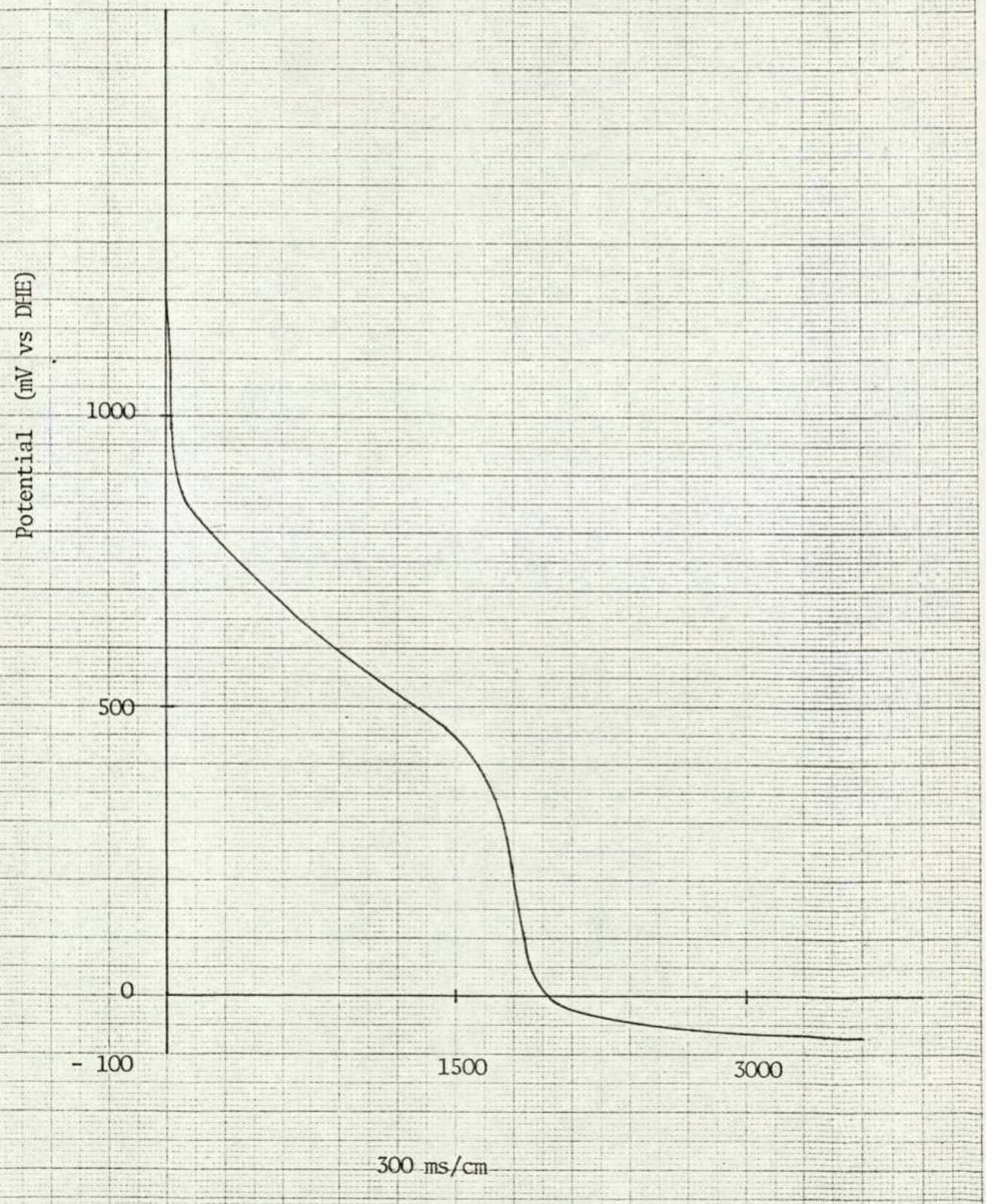

CHAPTER FOUR

THE KINETICS OF OXYGEN REDUCTION ON TEFLON BONDED PEROVSKITE OXIDES ELECTRODES

I. BASIC ELECTRODE KINETICS

Equation 4.1 represents a simple electrode reaction for which the overall reaction and the rate determining step are synonymous.

$$O^{2+} + ne \underset{k_{-1}}{\overset{k_1}{\rightleftharpoons}} R^{(2-n)+} \qquad 4.1.$$

Provided that the surface (C^o) and bulk concentration (C^b) of the ions are equal, the resultant net current can be expressed as[53],

$$i = i_o \left[\exp\left(\frac{-\beta nF\eta}{RT}\right) - \exp\frac{(1-\beta)nF\eta}{RT} \right] \qquad 4.2.$$

where η = the overpotential equals E-Er,

i_o = the apparent exchange current density equals

$$i_o = nFK\, C_o^b \exp - \frac{\beta nFEr}{RT} = nFK_{-i} C_R^b \exp\frac{(1-\beta)nFEr}{RT} \qquad 4.3.$$

For a more complex reaction where the rate-determining step and the overall reaction are not the same, but the reaction order is still unity with respect to O and R the rate expression may be formally written as[54,55].

$$i = nFA(K_1 C_o^b \exp(\frac{-\vec{\alpha}FE}{RT}) - K_{-1} C_R^b \exp\frac{\overleftarrow{\alpha}FE}{RT}) \qquad 4.4.$$

where i is the current

A is the area of the electrode

$\vec{\alpha}$ and $\overleftarrow{\alpha}$ are the transfer coefficients for the reduction and oxidation process respectively.

The transfer coefficient is related to the symmetry factor β but may

take into account other processes not confined to Tafels law. It may also be shown[54,55] that $\vec{\alpha} + \overleftarrow{\alpha} = n/\nu$.

Where ν, the stoichiometric number, is the number of times the rate determining step must occur for the transfer of n electrons in the overall process.

Two particular ranges of potential are of interest in the analysis of the current/voltage characteristics. These are:

(a) Low Overvoltage

Equation 4.4. may be written as

$$i = i_o \left(\exp - \frac{\vec{\alpha}\eta F}{RT} - \exp \frac{\overleftarrow{\alpha}\eta F}{RT}\right) \qquad 4.5.$$

Expansion of the exponential term in this equation and the retention of those terms linear in η gives.

$$i = - \frac{i_o n F \eta}{\nu RT} \qquad 4.6.$$

from which the stoichiometric number may be found provided i_o is known.

(b) At High Overvoltages

At high overvoltages the reverse reaction may be ignored and the rate expression becomes

$$i = nFAK_1 C_o^b \exp - \vec{\alpha} FE \qquad 4.7.$$

which upon taking logarithms gives

$$\log i = \log nFAK_1 C_o^b - \frac{\vec{\alpha}\, FE}{2.303\ RT} \qquad 4.8.$$

Hence a linear relationship is predicted between the logarithm of the current and the potential. A corresponding relationship applies in the anodic region.

In order to differentiate between possible mechanisms, the predictions of the theoretical rate equation must be compared with the experimental results. Some important diagnostic criteria are the Tafel slope, the order of the reaction and the stoichiometric number. There is sometimes insufficient data for unambiguous identification of the rate determining step and information as to the degree of surface coverage may be required[54].

II. MECHANISM OF OXYGEN REDUCTION ON PEROVSKITE OXIDES

Oxygen reduction in aqueous solutions requires a strong interaction of O_2 with the electrode surface for the reaction to proceed at a reasonable rate. Three types of models for such interaction have been proposed[56,57]. These are shown in Figure 19, together with the corresponding reaction pathways for O_2 reduction.

The Griffiths model[58] involves a lateral interaction of the π orbitals of the O_2 interacting with empty d_{z2} orbitals of a transition element, ion or metal atom with back bonding from at least partially filled d_{xz} or d_{yz} orbitals of the transition element to the π^* orbitals of the O_2. This type of interaction should lead to a weakening of the O-O bond with a corresponding lengthening of this bond. The formation of a strong metal-to-oxygen interaction results in a weakening of the O-O bond and an increment in the length of this bond[60]. Sufficiently strong interaction of

Figure 19. Models for adsorbed O_2 and corresponding reaction pathway for O_2 electroreduction.

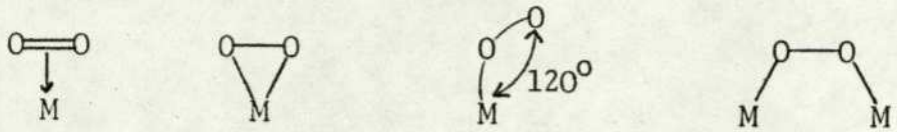

A. Griffiths Model (58) B. Pauling (59) C. Bridge Model

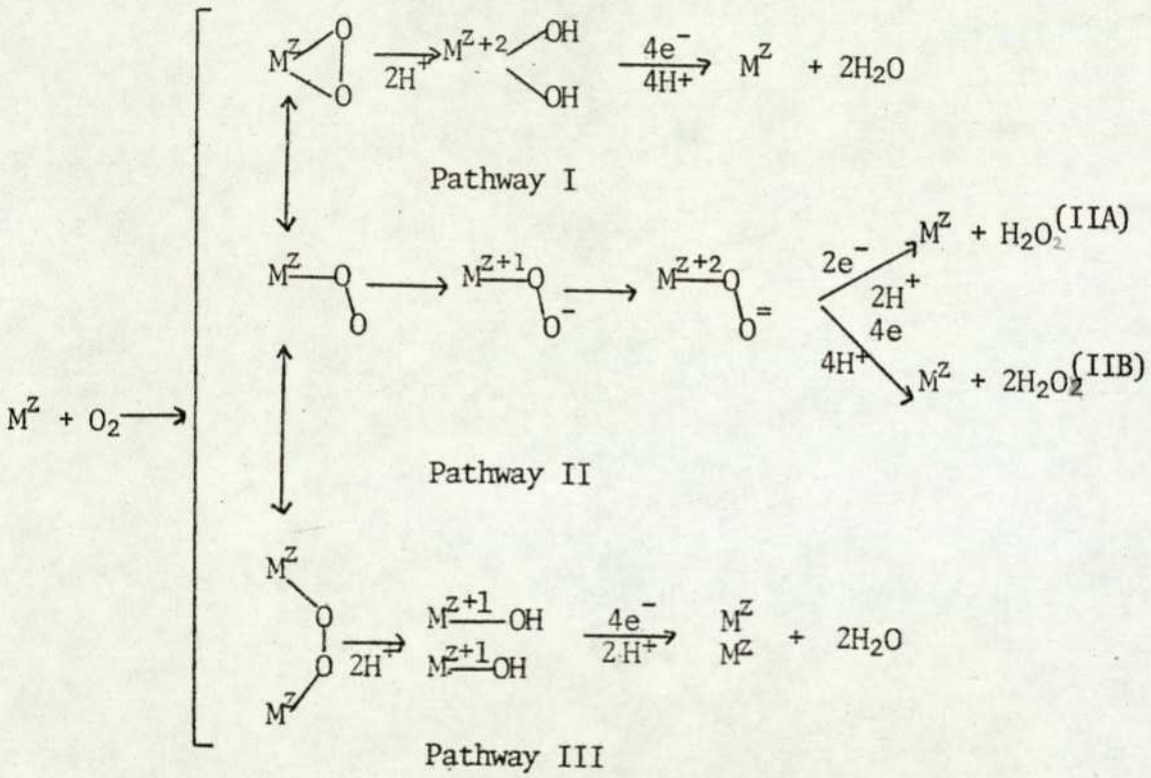

this type may lead to the dissociative adsorption of O_2 with probbaly simultaneous proton addition and valency change of the transition element in the manner represented by Pathway I in Figure 19, followed by reduction of the $M(OH)_2$ to regenerate the catalyst site. Sandstete et al[61,62], have attempted to explain oxygen reduction with square pyramidal Co(II), Fe(II) and Fe(III) complexes as well as on the thiaspinels on the basis of such π bonding, Tseung et al[17] have proposed that O_2 reduction on Li-doped NiO changes from a non-dissociative to dissociative mechanism above the Neel point (200°C for their ~10 atom % Li doped NiO) in order to explain the enhanced catalytic activity in KOH hydrate melts above the Neel temperature.

With most transition metal catalysts, the most probable structure for O_2 adsorption is the Pauling model[59] in which Sp^2 orbitals of O_2 interact with d_{z2} orbitals of the transition metal. This adsorption of O_2 is expected to be accompanied by at least a partial and probably complete charge transfer to yield a superoxide and then peroxide state, as represented in Pathway II in Figure 19. The change in valence state of the transition metal coupled with the change in O_2 oxidation state during formation of the O_2 adduct corresponds in principal to the redox electrocatalyst concept proposed by Beck et al[63,64]. The further reduction of the O_2 state requires rupture of O-O bond. This can occur in Pathway IIB through the formation of O^- or $HO^\cdot$ free radicals in solution or the simultaneous reduction-bond cleavage (electrochemical desorption) to yield H_2O or OH^-. Neither of these processes are likely to be sufficiently fast at practical operating potentials for O_2 cathodes

but the electrochemical desorption is a better candidate. The free energies of formation of O^{-} and $HO^{\cdot}$ radical in solution are just too high to achieve sufficiently high concentrations for the subsequent homogeneous reactions to proceed at rates corresponding to reasonable current densities at acceptable electrode potentials. Substantial evidence exists for Pathway IIA, yielding solution phase peroxide for various metallic and non-metallic electrode surfaces. With non-metallic electrodes such as carbon, graphite and lithiated NiO in aqueous alkaline solution, significant amounts of peroxide are found in solution and the potential under open-circuit conditions follows the Nernst equation predictions for the O_2-HO_2^{-} couple[65,66]. Eventually the peroxide is further reduced at practical O_2 cathodes.

Pathway III in Figure 19 provides an alternate means for bringing about rupture of the O-O bond through the foundation of an O-O bridge. Such a mechanism may come into play with the proper surface spacing of transition metal atoms or ions in a metal, oxide or thiospinel or in a bimetal complex such as macrocyclic. The formation of the bridge species requires proper spacing of the two metal species plus partially filled d_{xz} or d_{yz} orbitals to participate in bonding with the Sp^2 orbitals of the oxygen.

Hibbert and Tseung[40], by studying the rate of homomolecular exchange between $^{16}O_2$ and $^{18}O_2$, proved conclusively that oxygen can be dissociatively chemisorbed above the Neel point of lithiated nickel oxide and $La_{0.5}Sr_{0.5}CoO_3$. In addition there is close correlation between the activation energy for the dissociative oxygen chemisorption and electrochemical oxygen reduction, suggesting a similar mechanism is involved in each case, i.e. the Pathway I in Figure 19.

III. THE POSSIBLE RATE LIMITING FACTORS

The cathodic oxygen reduction on Teflon bonded perovskite oxide electrode are believed to be governed by one of the following factors.

(1) diffusion of oxygen ion in the oxide solid phase[35].

(2) diffusion of dissolved oxygen to the electrode

(3) limited adsorption of oxygen on the electrode

(4) limited numbers of active sites[24].

This Chapter presents the results of further cyclic voltammetric and potentiostatic pulse measurements on the reduction of oxygen on perovskite oxides.

IV. RESULTS AND DISCUSSION

(i) Cyclic Voltammetric Studies

Figure 20 shows one of the cyclic voltammograms of a 'floating' Teflon bonded perovskite oxides electrode purged with nitrogen. The catalysts were stable throughout the whole potential range (from OCV to 150 mV vs DHE) of the investigation.

Figure 21 shows the cyclic voltammogram of a 'floating' teflon bonded $Nd_{0.5}Sr_{0.5}CoO_3$ electrode. The electrode was swept initially from the open circuit potential to 1.5V. The subsequent cathodic current increases almost linearly with decreasing potential until 950 mV is reached. Thereafter, the cathodic current decreases and on the reverse sweep, the cathodic current is markedly lower.

Figure 20. The cyclic voltammogram of a teflon bonded $Nd_{0.5}Sr_{0.5}CoO_3$ electrode (45% KOH, N_2, 25°C) (Catalyst loading 17 mg) (scan rate 50 mV/sec)

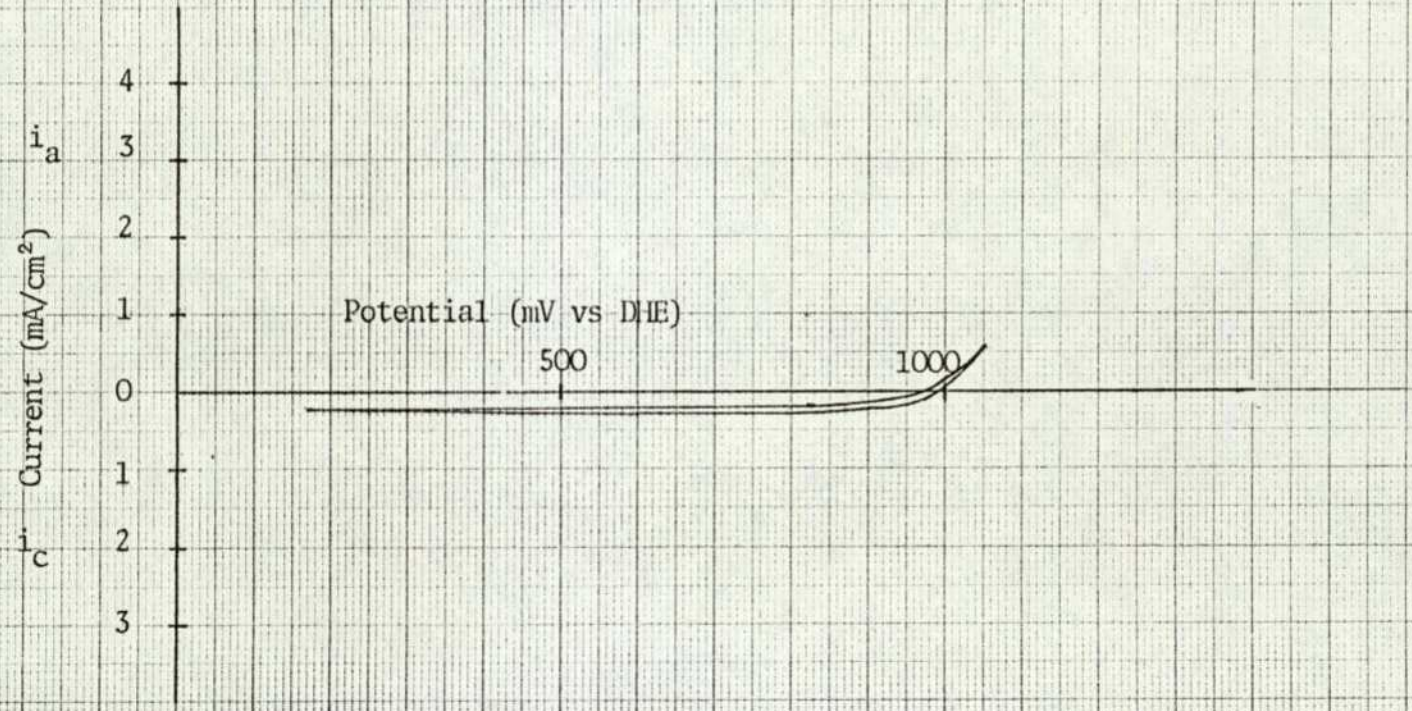

Figure 21. The cyclic voltammogram of a teflon bonded $Nd_{0.5}Sr_{0.5}$ electrode in O_2, 25°C, 45% KOH (catalyst loading 17 mg) (scan rate 50 mV/sec)

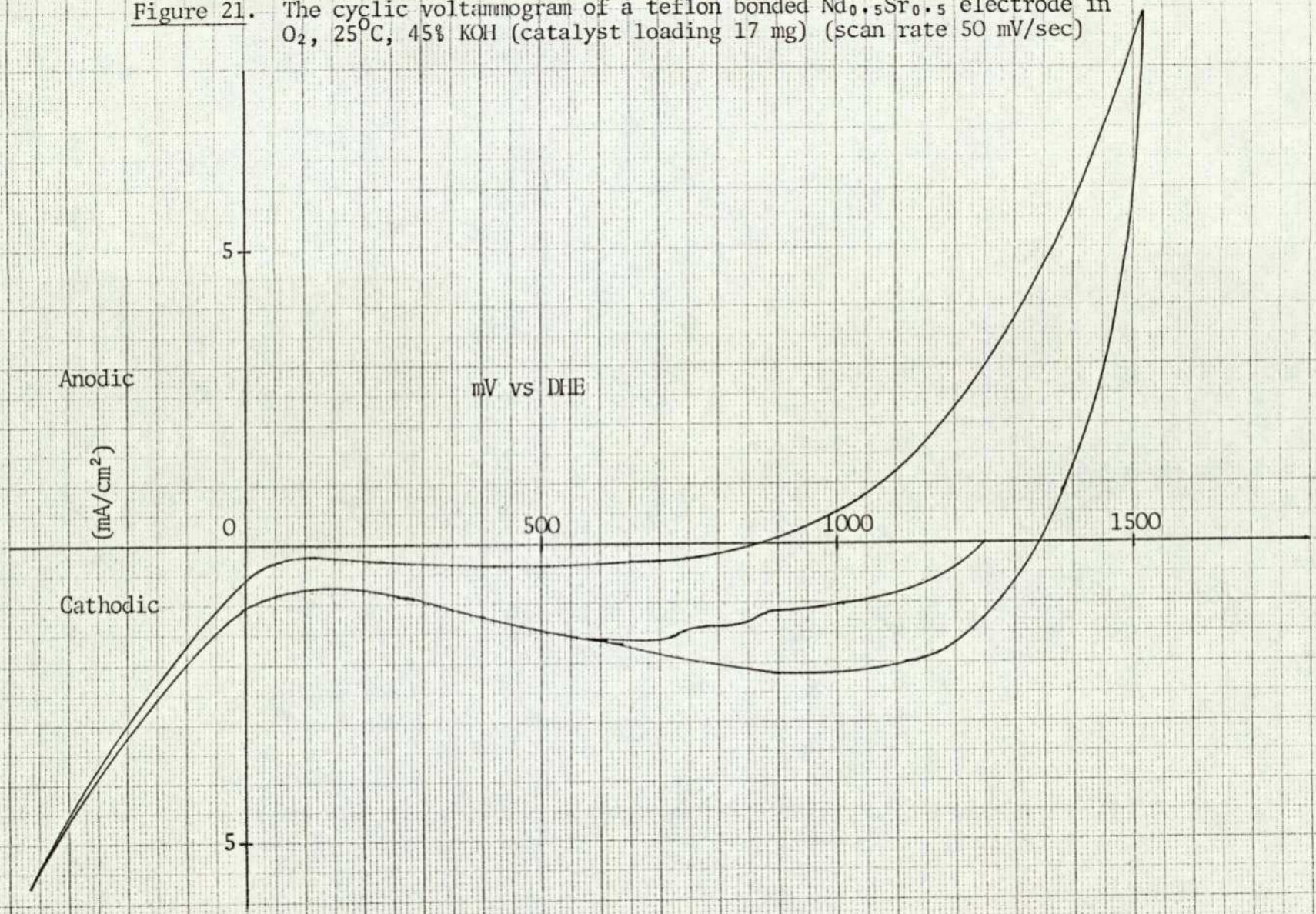

The results are similar to those obtained by Kudo et al[35]. Kudo et al suggest that this shows that the oxide ion is reduced and that the limiting step is the rate of oxygen ion diffusion in the oxide lattice.

Then anomalous results however can be better explained by taking into account the presence of high pressure oxygen generated and stored inside the pores of the electrocatalyst[67]. This would lead to higher performance.

However, if the electrode is taken to 1.5 V for 15 minutes and then purged with N_2 at the open circuit potential for different periods of time, the anomalous behaviour gradually disappears at longer purging time, as shown in Figure 22. These results indicate that the anomalous behaviour is associated with the high pressure oxygen generated inside the pores and is not due to the reduction of the oxide.

(ii) Steady State Performance of $Nd_{0.5}Sr_{0.5}CoO_3$

Figure 23 shows the performance of $Nd_{0.5}Sr_{0.5}CoO_3$ at 25, 40, 60 and 80°C. The open circuit voltage of the electrode at 25°C was 1.20 V very close to the oxygen electrode potential (1.22 V vs RHE at 25°C, 45% KOH). The attainment of reversible oxygen electrode potential suggests that oxygen is dissociatively chemisorbed[24]. Therefore, for every oxygen molecule chemisorbed "side-on", there will be two electron-transfer sites. Thus the current should be directly proportional to the square root of O_2 partial pressure, i.e.

$$I = k (P_{O_2})^{0.5}$$

Figure 22. The cathodic sweep for a teflon bonded $Nd_{0.5}Sr_{0.5}CoO_3$ electrode after holding at 1.5 V for 15 minutes and subsequently purged with N_2 for different time (scan rate 50 mV/sec)

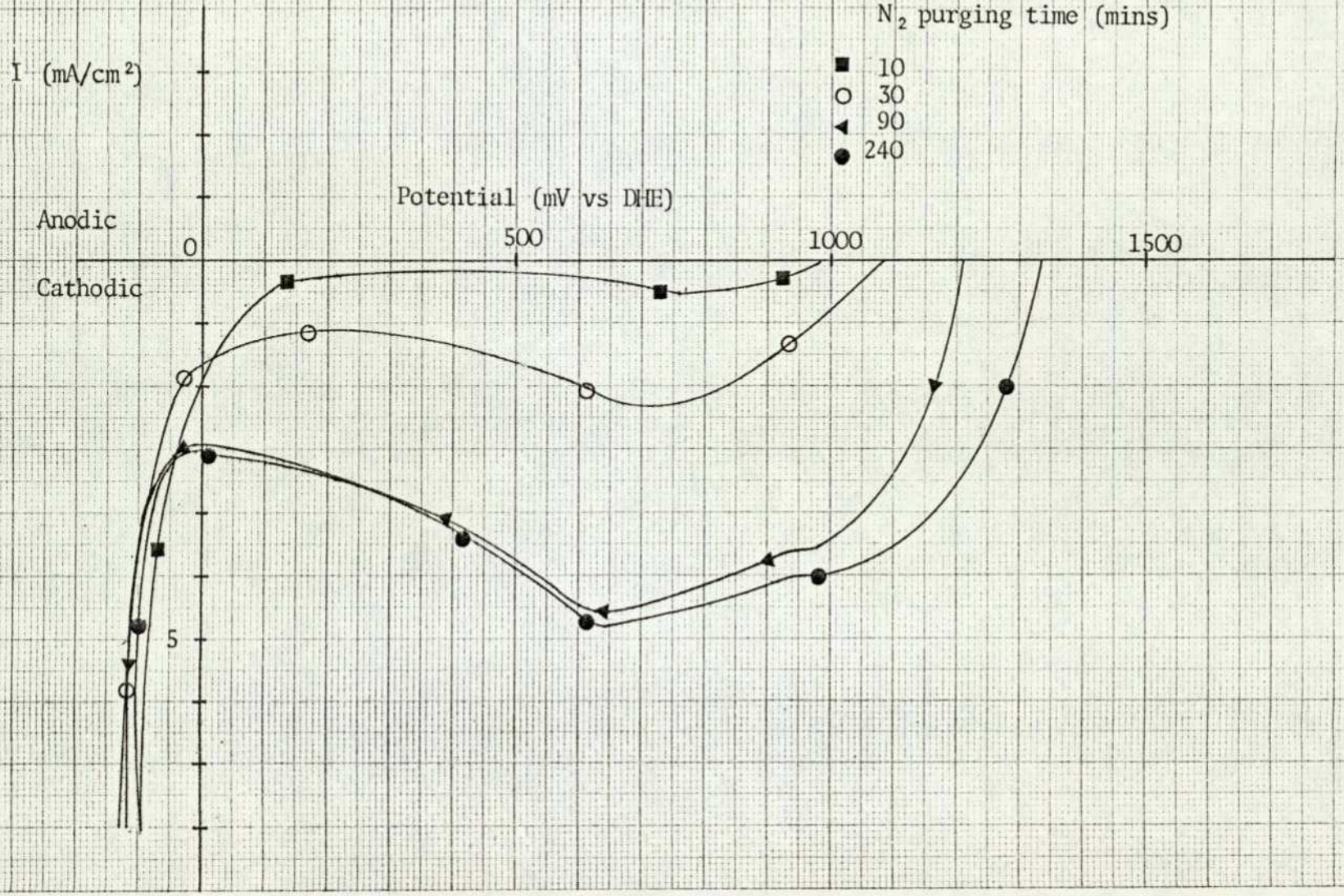

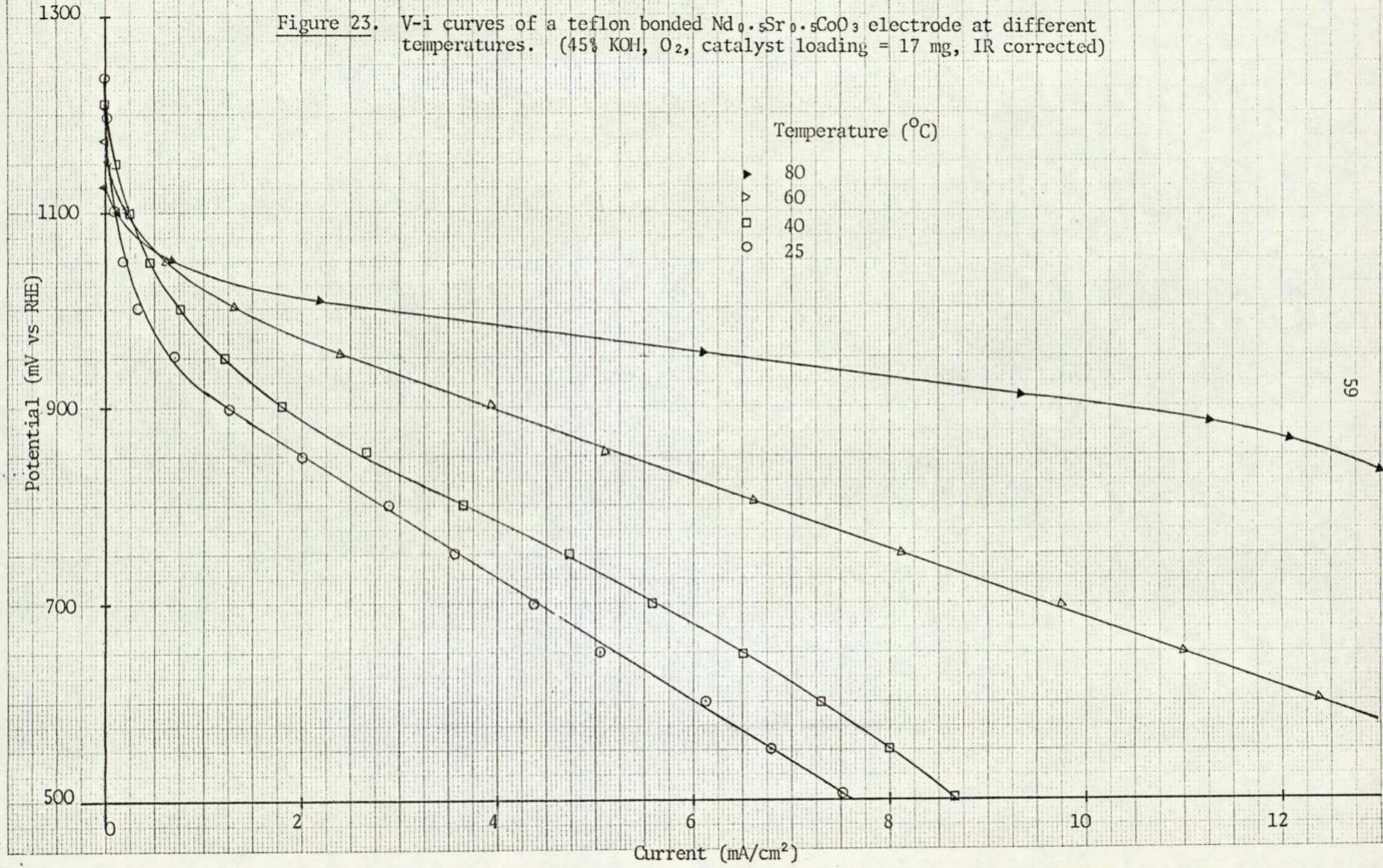

Figure 23. V-i curves of a teflon bonded $Nd_{0.5}Sr_{0.5}CoO_3$ electrode at different temperatures. (45% KOH, O_2, catalyst loading = 17 mg, IR corrected)

By plotting log I, at constant electrode voltage vs RHE, against log PO_2, the value of the index in the general relation $I = kP^n$ can be ascertained. Results for tests at different oxgyen partial pressures and temperatures show that the value of n is between 0.45 - 0.53, (Figure 24). A plot of $\frac{1}{T}$ vs ln i (Figure 25) shows that the performance increases linearly with temperature and the activation energy for the oxygen reduction is 10.75 kcal/mol.

(iii) Potentiostatic Pulse Studies

Figure 26 compares the steady state performance of a $Nd_{0.5}Sr_{0.5}CoO_3$ with its potentiostatic pulse performance at 25°C, 45% KOH. At 500 mV, the steady state performance was only 7.5 mA/cm^2, whereas over 85 mA/cm^2 was obtained by potentiostatic pulse measurements. Since teflon bonded electrodes do not show appreciable mass transfer limitations except at very high current densities, the differences in performance could not be attributed to mass transfer limitations alone. Figure 27 shows that there is only a small difference between the steady state and potentiostatic pulse performance for a teflon bonded Pt electrode operating under similar conditions.

As shown in Figure 28 a plot of ln i (i, current density at 200 mV overpotential) against $\frac{1}{T}$ for the potentiostatic pulse results gave a linear plot but the calculated activation energy was only 2.26 kcal/mol significantly lower than the results obtained earlier from the steady state results (10.75 kcal/mol). The very low activation energy for results obtained by potentiostatic pulse suggest that under transient conditions the rate of reaction is not

Figure 24. Evaluation of index n for $Nd_{0.5}Sr_{0.5}CoO_3$ at different temperatures

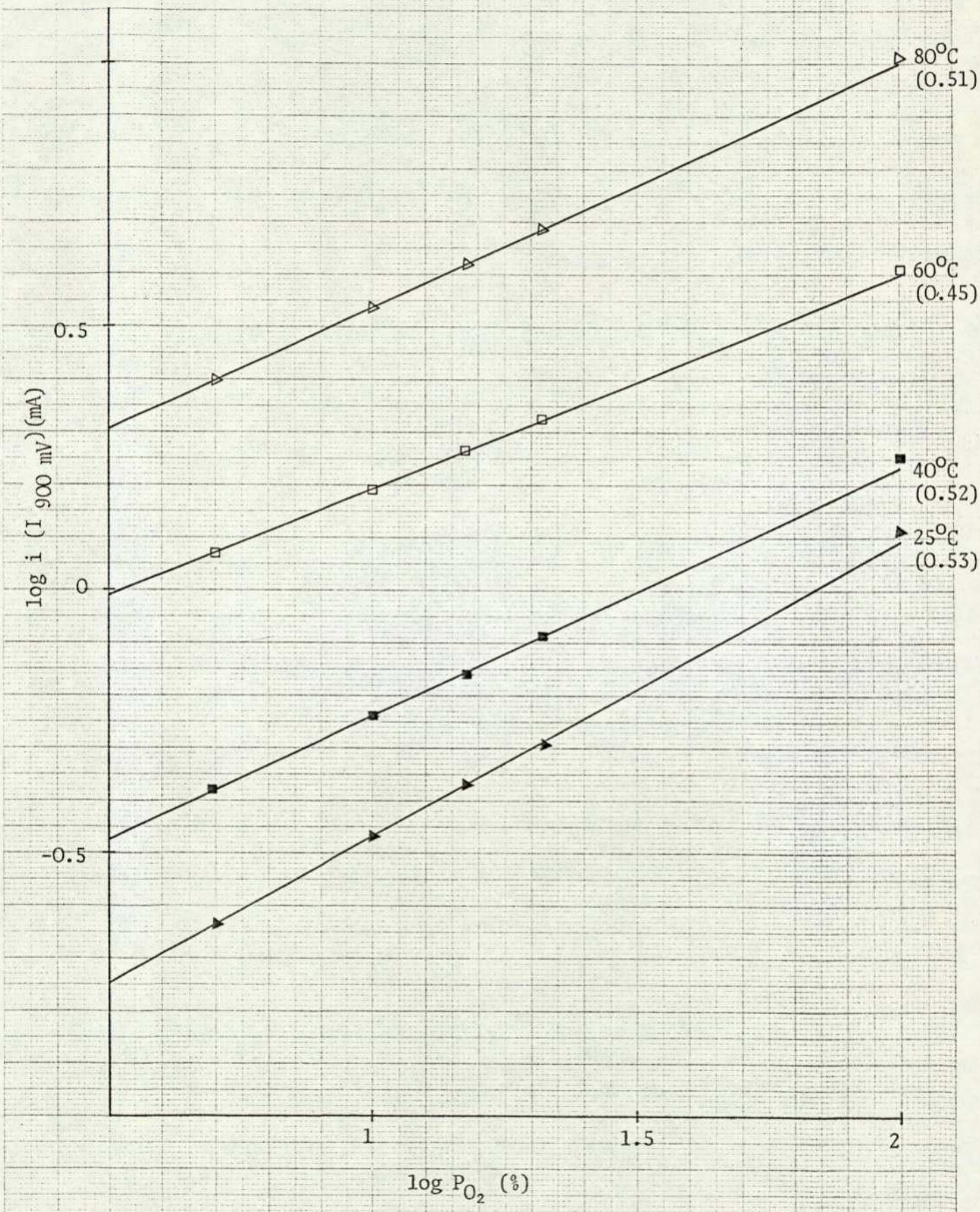

Figure 25. ln i vs $\frac{1}{T}$ plot for a teflon bonded $Nd_{0.5}Sr_{0.5}CoO_3$ electrode. (Steady state measurement).

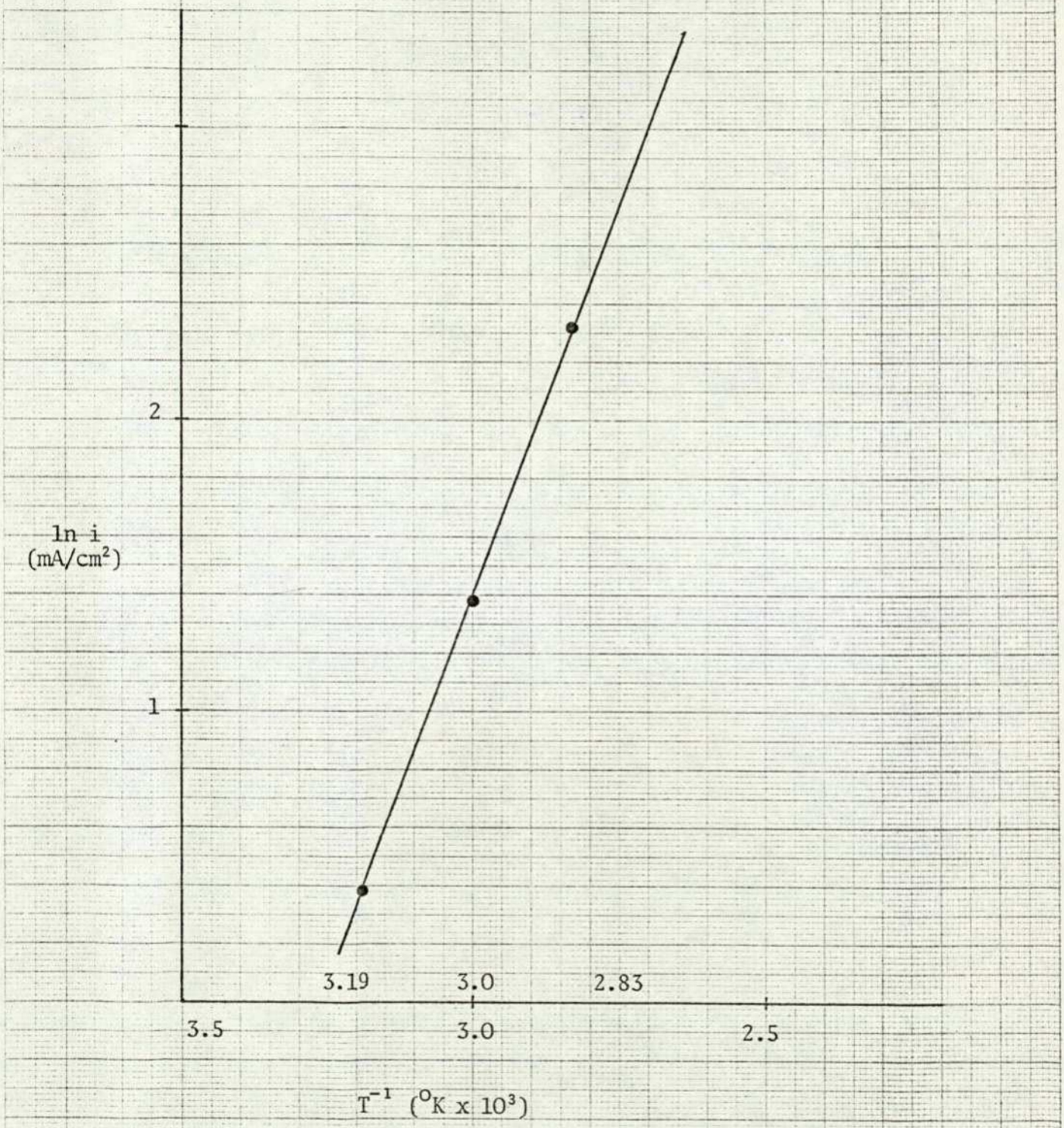

Figure 26. The polarization curve of a teflon bonded $Nd_{0.5}Sr_{0.5}CoO_3$ electrode.

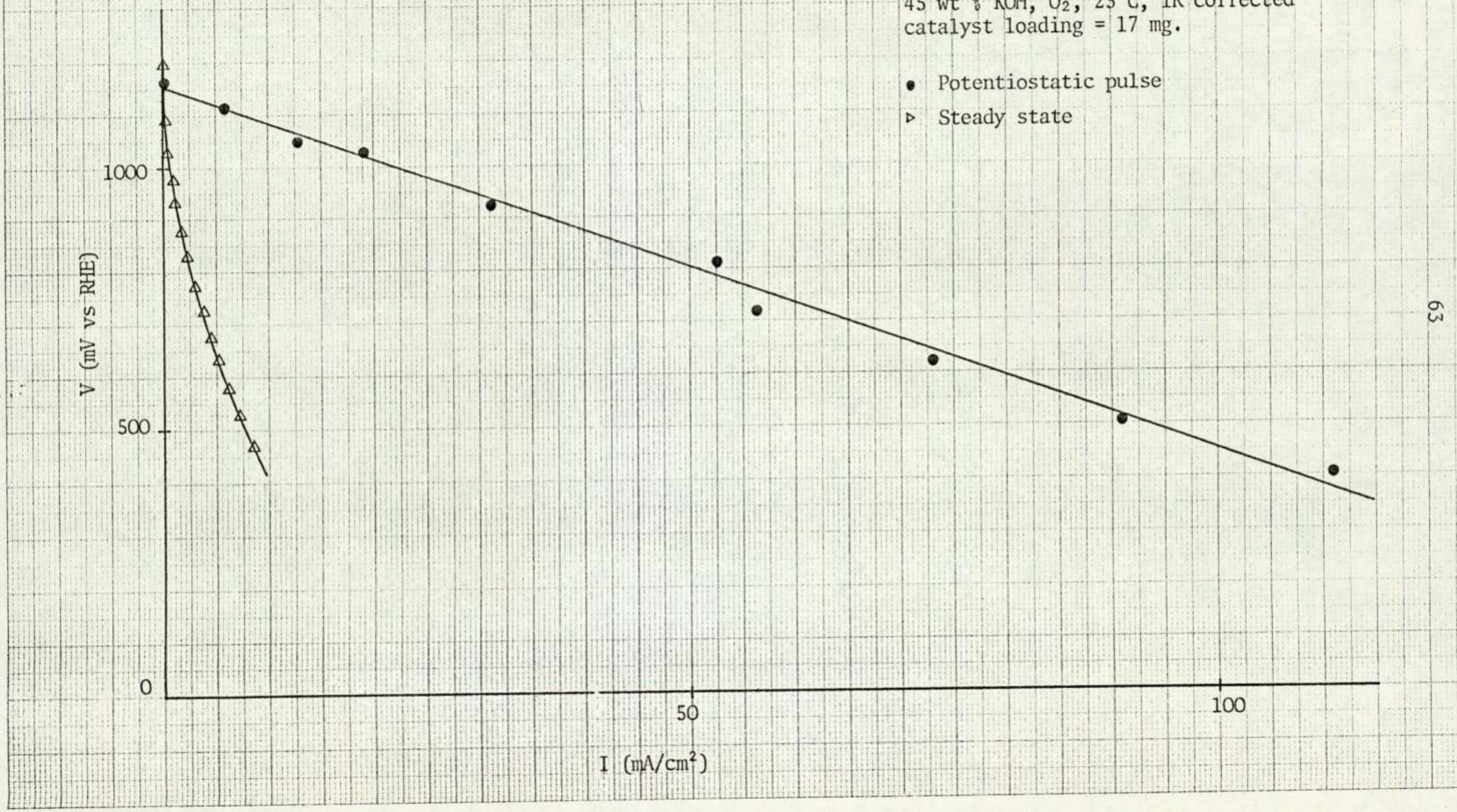

Figure 27. The polarization curve of a teflon bonded Pt black electrode.

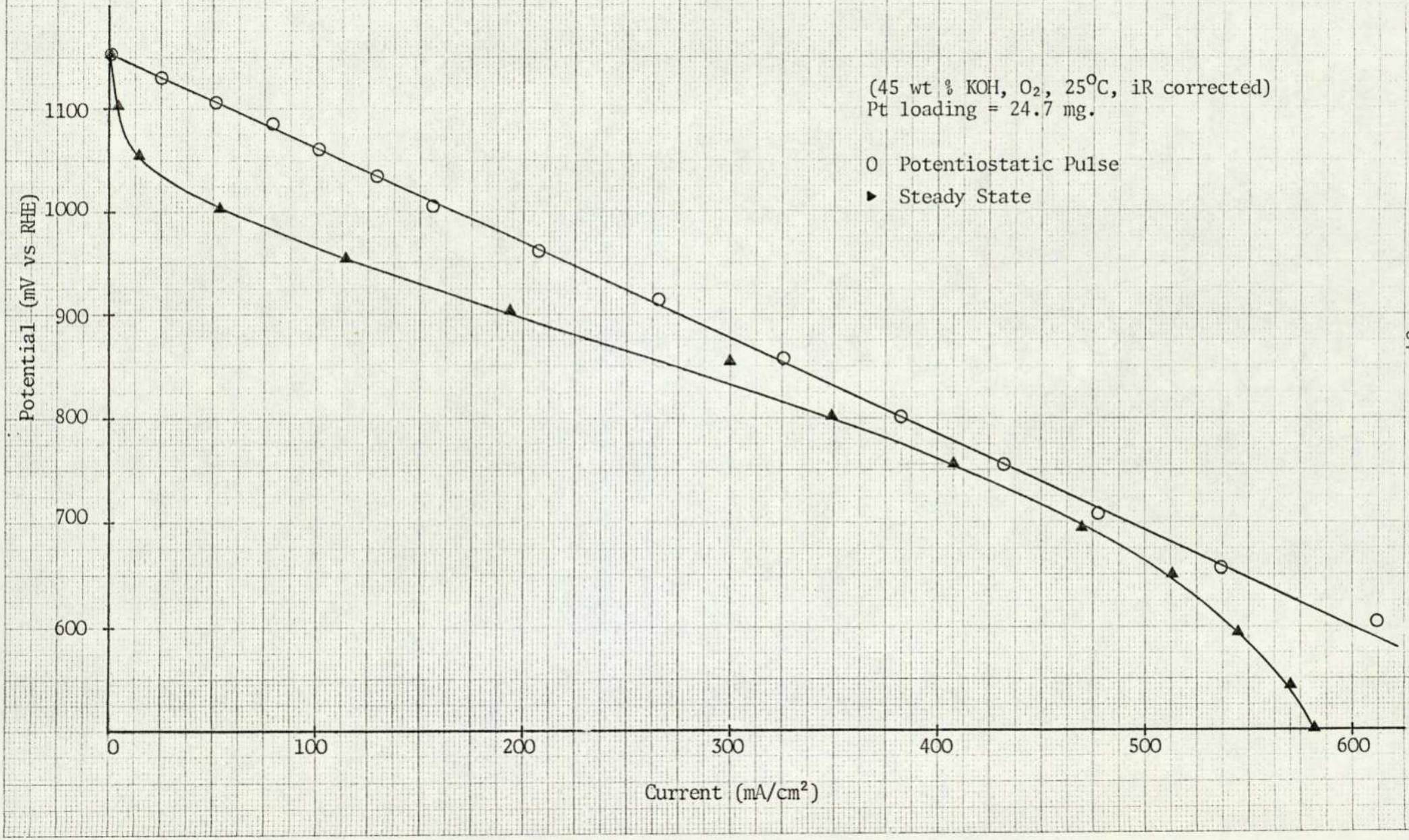

Figure 28. ln i vs $\frac{1}{T}$ for a teflon bonded $Nd_{0.5}Sr_{0.5}CoO_3$ electrode. (Potentiostatic pulse measurement)

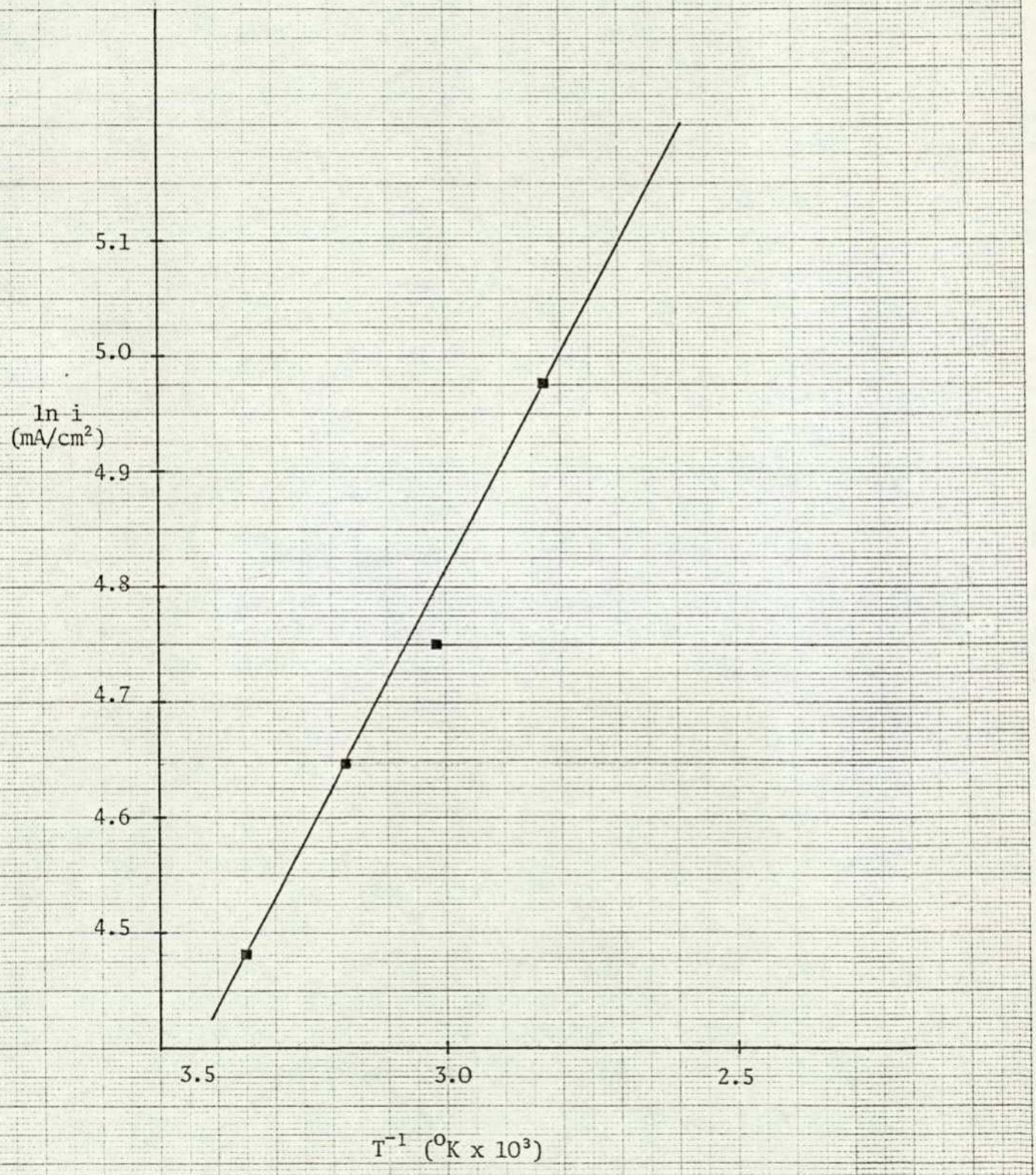

controlled by the rate of oxygen chemisorption, since before each pulse, the oxygen molecules have already been adsorbed on the electrode surface.

(iv) Measurement of Oxygen Coverage

The galvanostatic "oxygen" stripping method[52] was used to determine the electrochemical surface area for oxygen reduction. Table 3 gives the oxygen coverage on $Nd_{0.5}Sr_{0.5}CoO_3$ and $La_{0.5}Sr_{0.5}CoO_3$ as a function of temperature. The electrochemically active surface area was based on the galvanostatic results for oxygen reduction, assuming that the oxygen molecule to be chemisorbed "side-on" (cross section area of oxygen atom 1.72$\mathring{A}^2$). The total surface area of the electrode was calculated from the catalyst loading and the BET surface area of the catalyst. The result for a Pt electrode (the area of a Pt site assumed to be 8.9 $\mathring{A}^2$) is also included for reference.

TABLE 3

	O_2 Surface Coverage $(\frac{\text{electrochemical area}}{\text{BET area}})$		
Temperature	Pt	$Nd_{0.5}Sr_{0.5}CoO_3$	$La_{0.5}Sr_{0.5}CoO_3$
25°C	100%	1.08%	1.06%
40°C	-	1.08%	1.06%
60°C	-	1.08%	1.06%
80°C	-	1.08%	1.06%

The results show that the oxygen coverage is very low in both of the Sr doped $NdCoO_3$ and $LaCoO_3$ electrode and the surface coverage is independent of temperature. The degree of surface

coverage is almost the same in both cases. This is to be expected since Sr doping levels are the same in both cases. This is to be expected since Sr doping levels are the same in both cases. The fact that there is no change in surface coverage with temperature suggests that the improvement in performance with temperature is not due to the increase in the number of active sites as suggested previously by Tseung and Bevan[24].

(v) General Discussion

Recent homomolecular studies by Hibbert and Tseung[40] have shown that the activation energy for the dissociative oxygen chemisorption on $La_{0.5}Sr_{0.5}CoO_3$ is 15 kcal/mol, similar to the activation energy for oxygen reduction under steady state conditions, 13 kcal/mol, suggesting that the rate of dissociative oxygen chemisorption is the rate limiting step. The present electrochemical studies are also in accord with the above findings.

If the rate of oxygen chemisorption is the rate determining step, then we can derive the mathematical relationship between the current density and oxygen partial pressure. When O_2 is dissociative chemisorbed, the reaction mechanism can be expressed as

$$\tfrac{1}{2}\, O = O \underset{k_{-1}}{\overset{k_1}{\rightleftharpoons}} [O]\ \text{ads} \qquad 4.9.$$

$$[O]\ \text{ads} + 2e \underset{k_{-2}}{\overset{k_2}{\rightleftharpoons}} O^{2-} \qquad 4.10.$$

$$O^{2-} + H_2O \underset{k_{-3}}{\overset{k_3}{\rightleftharpoons}} 2OH^- \qquad 4.11.$$

Let p be the partial pressure of O_2 in contact with the electrode

and O be the fraction of energetically and geometrically suitable sites covered by $[O]_{ads}$ at given current i. At steady state, this fraction remains constant. The fraction of the surface covered at p is then found by setting $d\theta/dt$ equal to zero, since the surface coverage is low (1%), the Langmuir adsorption equation can be applied to this case.

$$\frac{d\theta}{dt} = k_1 p^{\frac{1}{2}} (1-\theta) - k_{-1}\theta - k_2 \theta = 0 \qquad 4.12.$$

$$\therefore \quad \theta = \frac{k_1 p^{\frac{1}{2}}}{k_{-1} + k_2 + k_1 p^{\frac{1}{2}}} \qquad 4.13.$$

If the chemisorption is the rds, then the current i is given by $2F k_2\theta$, thus

$$i = \frac{2F k_1 k_2 p^{\frac{1}{2}}}{k_{-1} + k_2 + k_1 p^{\frac{1}{2}}} \qquad 4.14.$$

However, the rate constant (k_2) for the ionization of [O] ads is dependent on the electrode potential

$$k_2 = k \exp\left[(1-\alpha)F\eta/RT\right] \qquad 4.15.$$

Sub. 4.15 into 4.14.

$$i = \frac{2F k_1 k p^{\frac{1}{2}} \exp\left[(1-\alpha)F\eta/RT\right]}{k_{-1} + k \exp\left[(1-\alpha)F\eta/RT\right] + k_1 p^{\frac{1}{2}}} \qquad 4.16.$$

If the reaction is controlled by the rate of chemisorption, k_1 and $k_1 p^{\frac{1}{2}}$ should be small. Under heavy cathodic polarization, the denominator of 4.16. is determined mainly by the exponential term. Hence the current is given approximately by

$$i = \frac{k\, p^{\frac{1}{2}} \exp\left[(1-\alpha)F\eta/RT\right]}{k_{-1} + k \exp\left[(1-\alpha)F\eta/RT\right]} \qquad 4.17.$$

where $k = 2F\, k_1\, k$.

Taking logarithms on both sides, we have

$$\ln i = \ln A + \tfrac{1}{2} \ln P \qquad 4.18.$$

where $$A = \frac{k_2 \exp\left[(1-\alpha)F\eta/RT\right]}{k_{-1} + k \exp\left[(1-\alpha)F\eta/RT\right]}$$

therefore $$\frac{d \ln i}{d \ln p} = \tfrac{1}{2} \qquad 4.19.$$

Since both $La_{0.5}Sr_{0.5}CoO_3$[24] and $Nd_{0.5}Sr_{0.5}CoO_3$ (Figure 24) obey equation 4.19, it is suggested that the rate limiting process is the rate of dissociative oxygen chemisorption on the electrode surface.

CHAPTER FIVE

THE ACTIVE SITES ON PEROVSKITE OXIDES

I. INTRODUCTION

The galvanostatic "oxygen" stripping studies (Chapter 4, Section III(iv) showed that the oxygen coverage was very low in both Sr doped $NdCoO_3$ and $LaCoO_3$, although the calculation was based on the area covered with the oxygen atoms (cross section area of oxygen atom 1.72Å). This implies that only a small portion of sites on the surface are available. Since both $Nd_{1-x}Sr_xCoO_3$ and $La_{1-x}Sr_xCoO_3$ are complex oxides, they are composed of Sr, Co, Nd (or La) and $O^=$ ions; the low oxygen coverage may be due to the fact that only one or two of the constituent ions are involved in the cathodic oxygen reduction process. Therefore, further investigation to clarify the situation is necessary.

II. THEORETICAL CONSIDERATION

Since the rate of oxygen chemisorption is the rate determining step in the cathodic oxygen reduction in the perovskite oxides (see Chapter 4), it is necessary to consider the contribution from each of the constituent ions and their availability for oxygen chemisorption.

In recent years, it has become customary to treat chemisorption on transition metal oxides in terms of the boundary layer theory[68,69], according to which electron exchange between the solid and the adsorbed gas changes the concentration of charge carriers in the appropriate conduction or valence band of the oxide. This theory predicts that for "enrichment chemisorption", where there is an increase in the number of charge carriers (e.g. oxygen on p-type

oxides, hydrogen on n-type oxides) a large excess of available centres for electron transfer is present and chemisorption should proceed to high surface coverage. Studies by Charman et al[15], suggest that strict application of the band theory of solid to explain surface phenomena in transition metal oxide is an over-simplification and some modification is necessary. The collective electron approach, according to which chemisorption is a delocalised or co-operative phenomenon, requires modifying in the light of the activation energy necessary for the movement of positive holes between the conduction band of adjacent metal ions. This, then leads to a picture of chemisorption as essentially a localised phenomenon, with co-operative interactions becoming more important the lower the activation energy of the conduction process.

In case of perovskite oxides, the A ion (La, or Nd) has only a minor influence on the low energy electronic and optical properties because its energy levels lie much higher than those of Co ion. Even Sr ions, due to a lack of available d electrons, has no direct effect on the catalytic activity toward oxygen chemisorption. It seems reasonable to assume that exposed Co ions in the perovskite oxides serve as centres for oxygen chemisorption.

In fact, three types of cobalt ions have been reported in Sr doped $LaCoO_3$[70]. They are the trivalent ion in the high spin state (denoted as Co^{3+}). Trivalent ion in the low spin state (denoted as Co^{III}) and the tetravalent ion which is assumed to be in the low spin state (denoted as Co^{IV}). Since the concentration of these Co ions is dependent on the Sr ion doping level, the information about their effects toward the cathodic oxygen reduction

may be obtained indirectly from the studies of $La_{1-x}Sr_xCoO_3$.

III. RESULTS AND DISCUSSION

(i) Stabilities of the Catalyst

The stabilities of the oxides were tested by cyclic voltammetry over the entire potential range of interest in purified N_2. The catalysts ($La_{1-x}Sr_xCoO_3$) were stable throughout the whole potential range. Maximum corrosion currents were less than 0.5 mA/cm^2 (B.E.T. area = 17 m^2/gm) (Figure 20), equivalent to 2.94 μA/cm^2 of the actual catalyst area.

(ii) Steady State Performance of $La_{1-x}Sr_xCoO_3$

Figure 29 shows the effect of Sr doping level on the cathodic oxygen reduction by comparing their steady state performance at 900 mV vs DHE. It is observed that at $0 < x < 0.5$ the electrochemical performance increase as a function of x. The maximum performance occurs when $x = 0.5$. It is also observed that there is a sharp increase in performance at $x > 0.3$.

The plots of T^{-1} vs ln i (Figure 30) show that the performance increases linearly with temperature and the activation energies for the oxygen reduction are independent of x (Table 4). The results suggest that the mechanism of oxygen reduction on $La_{1-x}Sr_xCoO_3$ are the same in all cases.

(iii) Measurement of Oxygen Coverage

Figure 31 gives the oxygen coverages on $La_{1-x}Sr_xCoO_3$

TABLE 4. The Activation Energies on $La_{1-x}Sr_xCoO_3$ (45 wt % KOH, O_2 900 mV vs DHE

Value of x	E_a (kcal/mol)
0	7.21
0.1	7.18
0.3	7.19
0.5	7.18
0.6	7.18

Figure 29. Effects of variation of x value in $La_{1-x}Sr_xCoO_3$ (25°C, 900 mV vs DHE. Air).

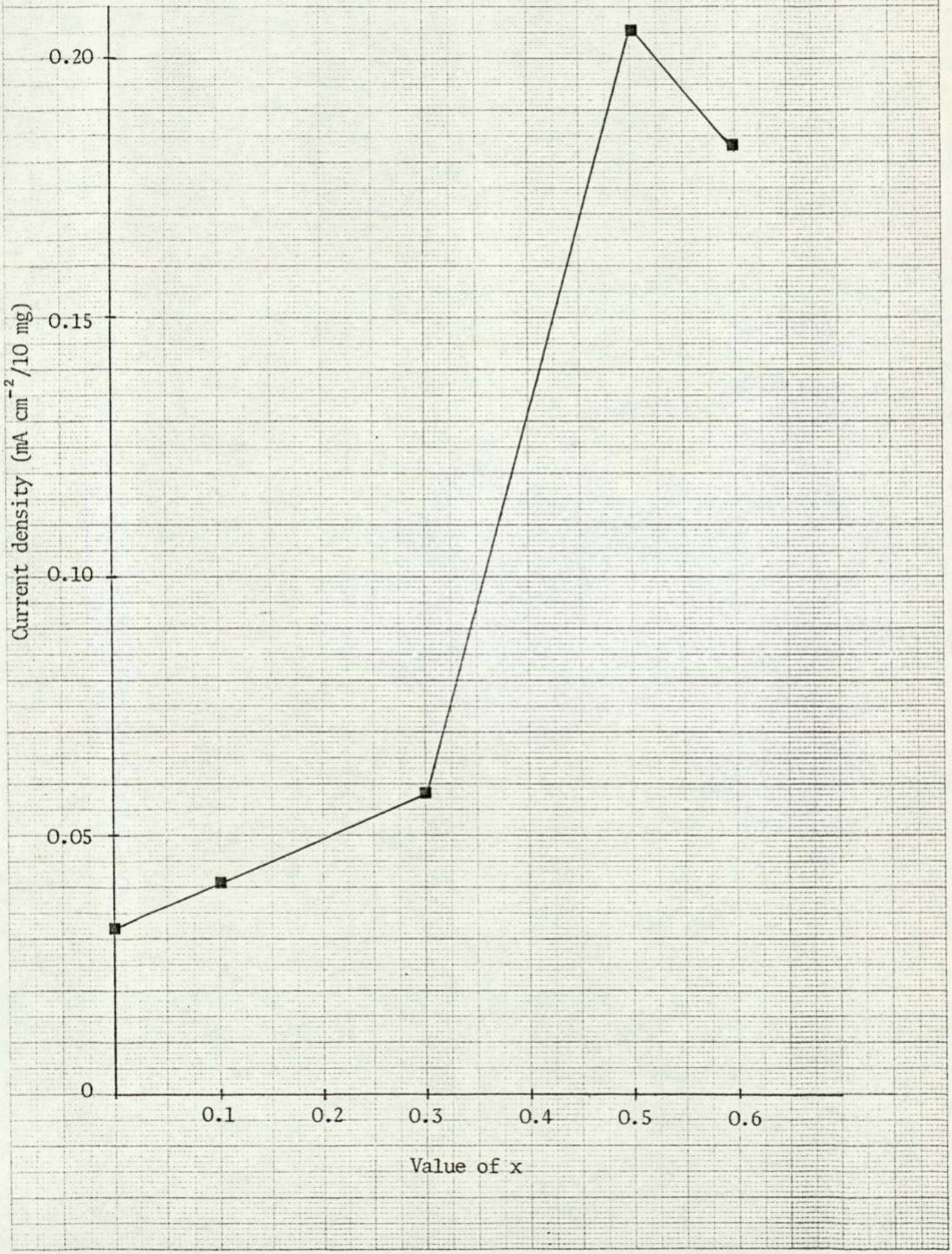

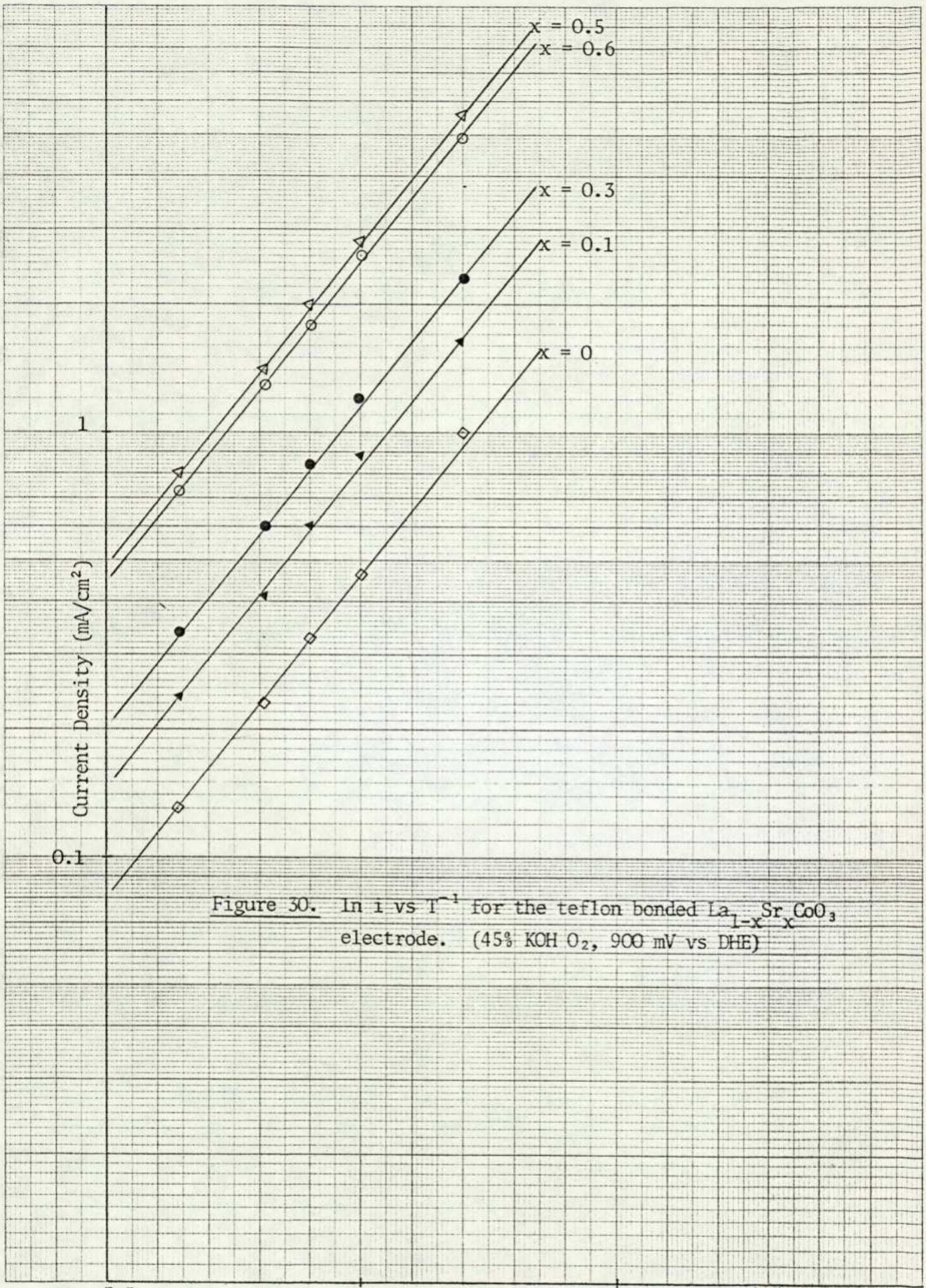

Figure 30. In i vs T^{-1} for the teflon bonded $La_{1-x}Sr_xCoO_3$ electrode. (45% KOH O_2, 900 mV vs DHE)

Figure 31. The oxygen coverage on $La_{1-x}Sr_xCoO_3$ (45% KOH, O_2, 25°C).

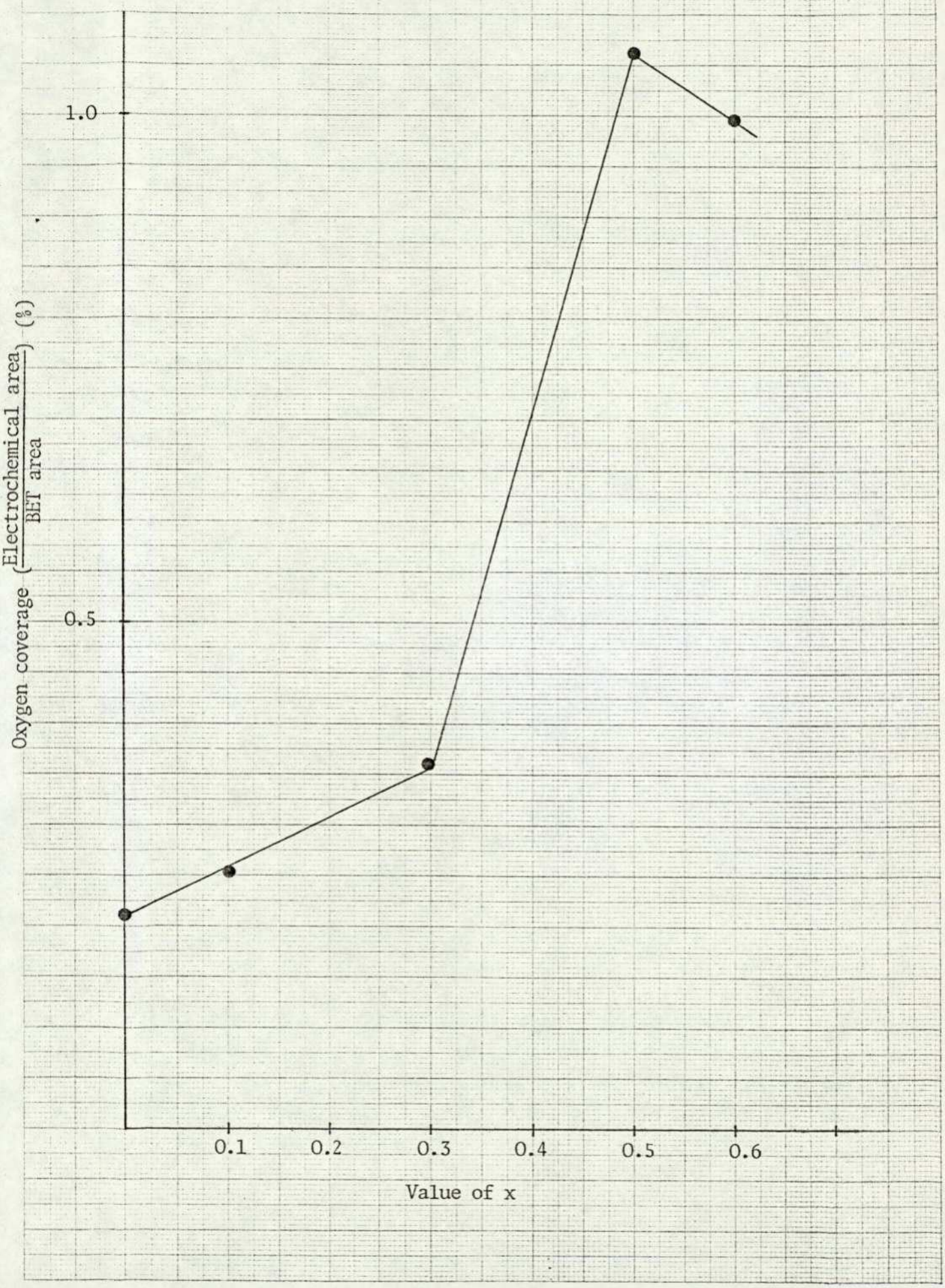

as a function of x. It behaves similarly to those of steady state performance. Between $0 < x < 0.5$, the oxygen coverage increases as a function of x. Maximum coverage occurs at $x = 0.5$. It implies that the improvement in steady state performance with x is due to the increase in number of the active sites.

The results confirm the suggestions by Tseung and Bevan[24] that the double exchange couples Co^{3+}/Co^{IV} can be considered as the active centres for oxygen reduction. Since the concentration of the Co^{IV} ion is dependent on the degree of Sr doping, the number of the Co^{3+}/Co^{IV} couples should theoretically reach the maximum for x approximately 0.5, depending on the non-stoichiometry of the perovskite oxide. Hence, the steady state performance of $La_{1-x}Sr_xCoO_3$ for O_2 reduction should peak at $x = 0.5$; this is indeed the case.

It is observed (Figure 31) that there is a sharp increase in performance beyond $x = 0.3$. This effect can be correlated to the lattice change at $x = 0.3$ and will be discussed later.

(iv) Crystallographic Properties

The x-ray data was obtained from literature[71,72]. X-ray diffraction patterns of $La_{1-x}Sr_xCoO_3$ compounds were indexed on a hexagonal as well as on a rhombohedral basis. The resulting data are shown in Figure 32. All the compositions except $x = 0.5$ show a slight rhombohedral distortion. The hexagonal C-axis (CH) as well as the rhombohedral angle α_R show, as a function of x, discontinuities around $x = 0.125$. The hexagonal a_H and the rhombohedral a_R do not show any discontinuity, although a definite

Figure 32. Hexagonal and rhombohedral parameters for $La_{1-x}Sr_xCoO_3$. Also shown is the unit cell volume.

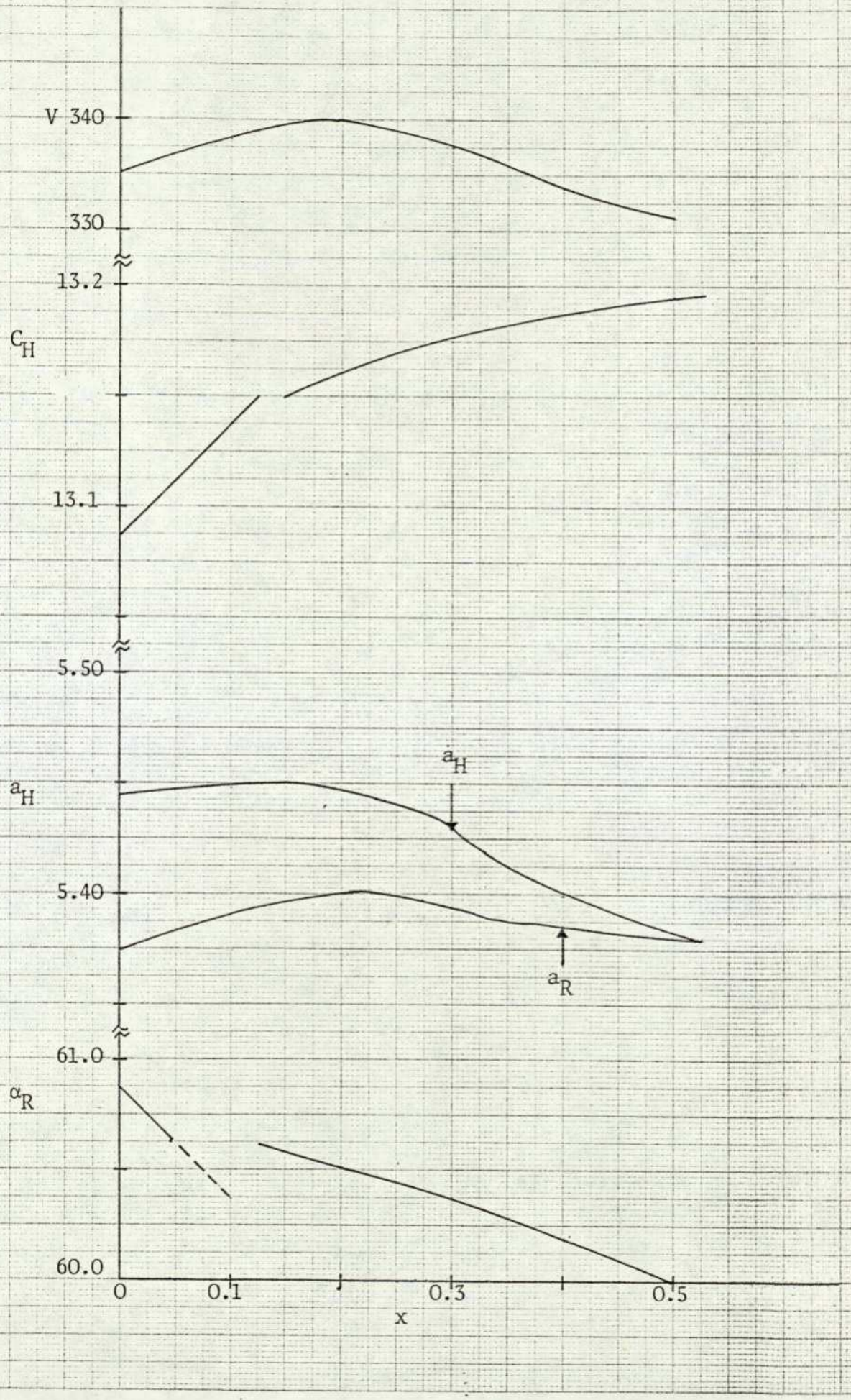

decrease is seen beyond x = 0.2. All these results are consistent with a change at x ≃ 0.125 from isolated magnetic islands in a paramagnetic host to paramagnetic islands in a ferromagnetic host. Moreover, the rhombohedral distortion decreases with increasing Sr content, and $La_{0.5}Sr_{0.5}CoO_3$ appears to be perfectly cubic.

Comparing the behaviour of the oxygen coverage and steady state performance, as a function of x, the definite decrease of a_H and a_R beyond x = 0, suggests that the geometric factor of the catalyst is important for oxygen reduction.

(v) The Magnetic Properties

Due to lack of facilities and time, the results were obtained from the literature[71]. The ferromagnetic compositions with $0.125 < x < 0.5$ exhibit a paramagnetic peak as well as a magnetically split spectrum below Tc. The area under the paramagnetic peak relative to that under the ferromagnetic peak increases with decreasing x and with increasing temperature. Figure 33 shows the ratio of the ferromagnetic to paramagnetic areas at 78K as a function of x. A Mössbauer study on $La_{1-x}Sr_xCoO_3$ by Rao et al[71] shows that the ferromagnetism observed in the system can be explained on the basis of itinerant-electron ferromagnetism[72,73].

The itinerant-electron model proposed by Goodenough[72,73] is represented in Figures 34 and 35, which show schematically the cobalt 3d bands for small and large x. At T = 0 K° and small x, a narrow π^* band (formed from the crystal-field d-orbitals of t_{2g} symmetry) is filled. The cobalt atoms nearest neighbour to a Sr^{++}

Figure 33. Ferromagnetic to paramagnetic ratio in $La_{1-x}Sr_xCoO_3$ for various values of x.

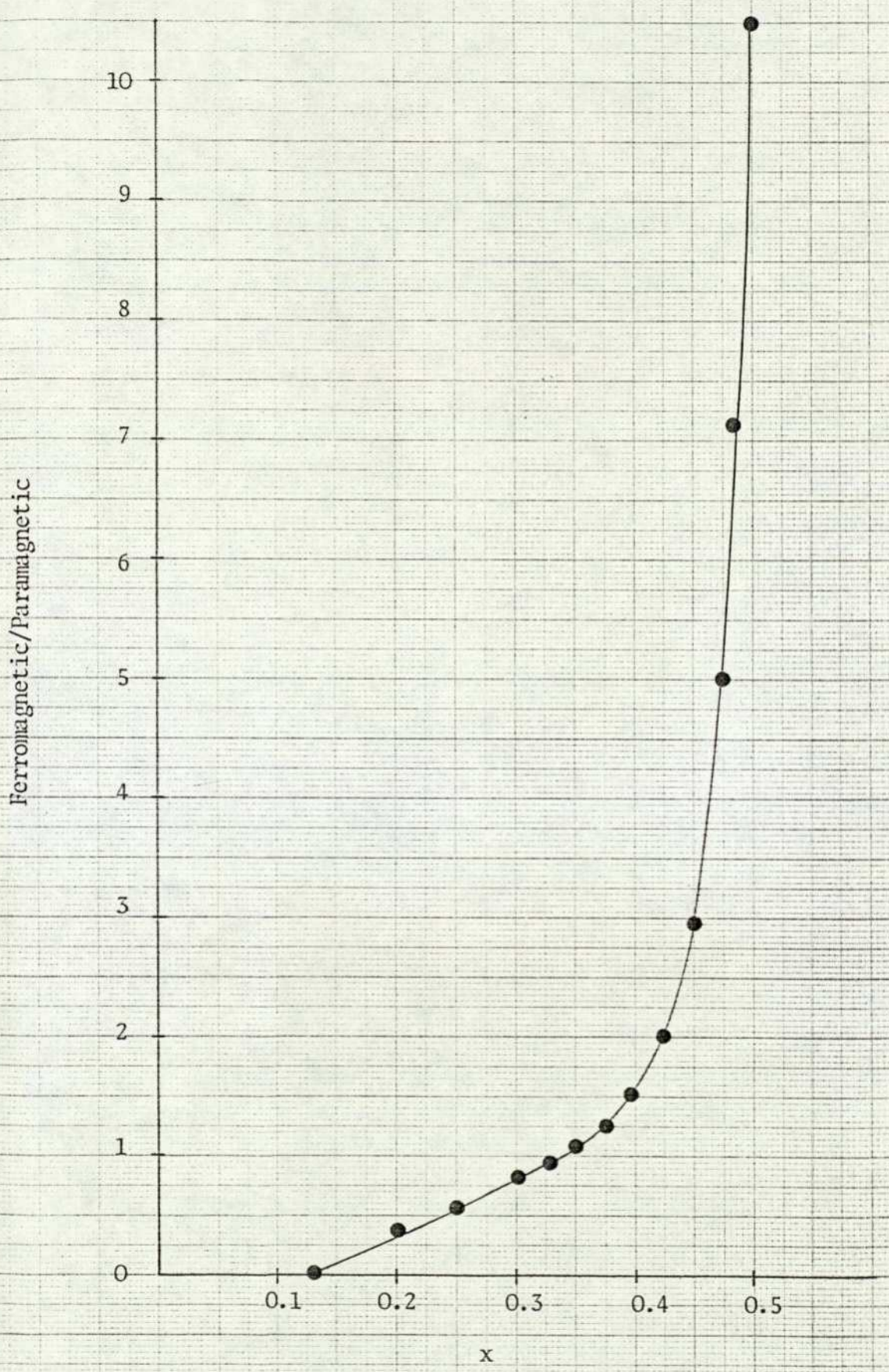

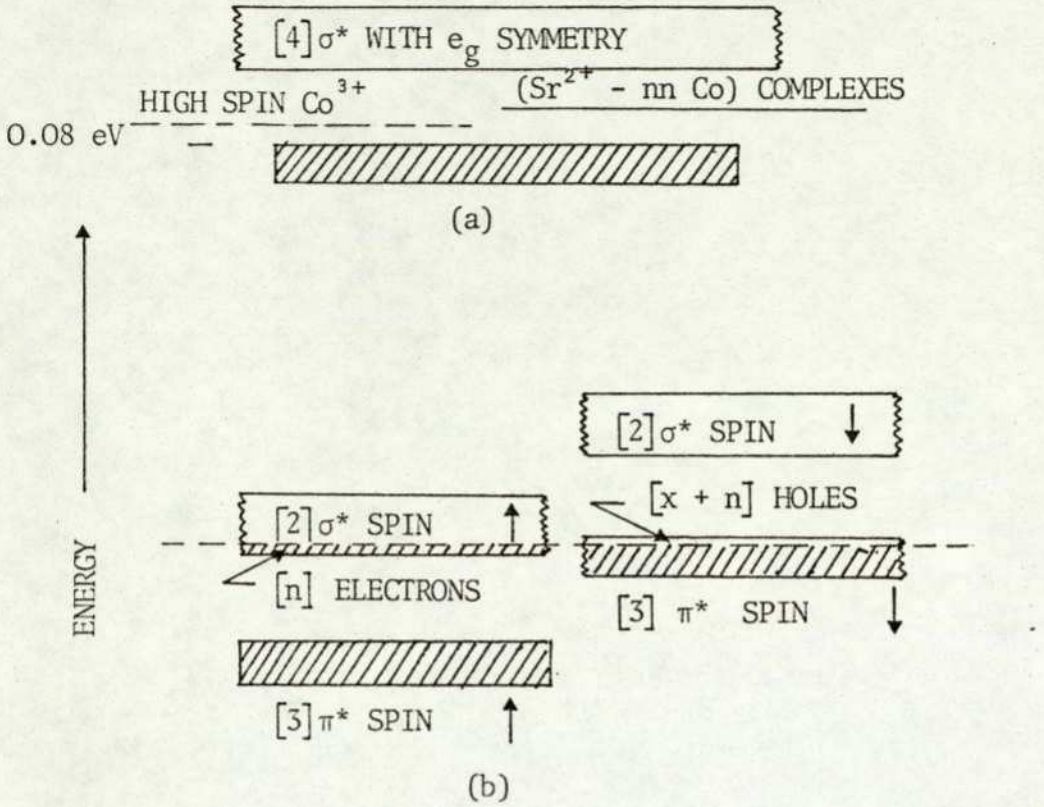

Figure 34. (a) Cobalt 3d bands for La rich region showing the Sr^{2+} impurity level; (b) Cobalt 3d bands for ferromagnetic $La_{0.5}Sr_{0.5}CoO_3$ if no correlating splitting of π* bands (Ref. 72).

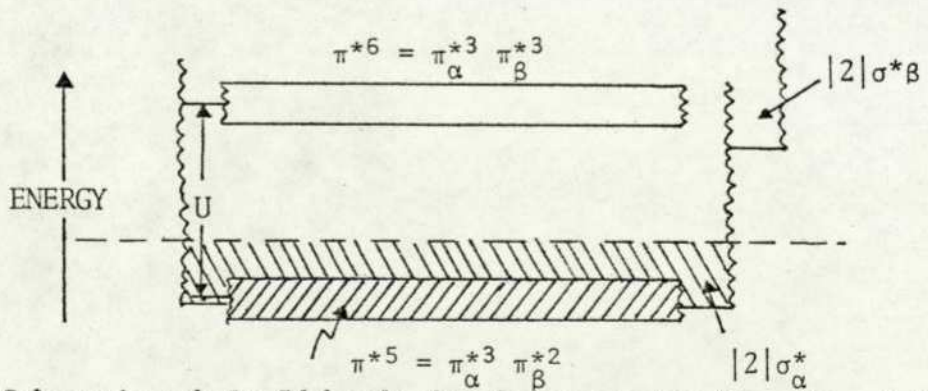

Figure 35. Schematic cobalt 3d bands for ferromagnetic $La_{0.5}Sr_{0.5}CoO_3$ if the π* bands are split by electron correlations. (Ref. 73).

ion provide molecular d-orbitals, those found from atomic t_{2g} or e_g orbitals having about the same deep acceptor energy level. Thermal excitation to the high-spin Co^{3+} (t_{2g}^4 e_g^2) configuration creates a magnetic ion, but it does not produce a mobile hole. Mobile holes are created by excitation of an electron from the π^* band to an acceptor level. At higher Sr^{2+} ion concentration x, the acceptor orbitals interact to form an impurity band. Because the high-spin (Co^{3+}) and low spin (Co^{III}) configurations have comparable energies, the formation of impurity bands generates a spontaneous ferromagnetism having the σ^* band of up spin overlapping the π^* bands of down spin. Because there is a critical Sr^{2+} ion concentration for impurity band formation, which from experiment is $x_c \approx 0.125$, chemical imhomogeneities can produce interpenetrating ferromagnetic and paramagnetic domains. The co-existence of two magnetic phases within the same crystallographic phase would be most pronounced in the vicinity of the critical concentration x_c. On this model, the paramegnatic component is expected to decrease with increasing x and decreasing T, and this has indeed been observed.

The results (Figure 33) indicate that the possibility of relating the magnetic properties and the cathodic oxygen reduction, since both of them have a sharp change beyond x = 0.3.

(vi) General Discussion

As the rate of oxygen chemisorption is the rate determining step, the Co ion can be considered as an active centre for oxygen chemisorption. If each chemisorbed oxygen molecule occupies 2 Co ions (Co^{3+}/Co^{IV}) then we can calibrate the fraction of Co ions on

the surface available. The best one in the series, $La_{0.5}Sr_{0.5}CoO_3$, is used as a model.

Assuming that the catalyst is perfectly cubic[71] and that the Co^{3+}/Co^{IV} couples are homogeneously distributed, the area as well as the distance between 2 Co ions in each basic plane (100, 110, 111, 200) are as follows.

(a) 100 plane.

Assume the radius of Co^{3+}, La^{3+} (Sr^{++} are very similar to La^{3+}) and $O^{=}$ to be 0.63Å, 1.15Å and 1.40Å respectively.

The area of 100 planes.

$= 4 \times \frac{1}{8} \times (4\pi \times 0.63^2) + 4 \times \frac{1}{4} \times (4\pi \times 1.4^2)$

$+ [4.06^2 - 4 \times \frac{1}{4} \times (\pi \times 0.63^2) - 4 \times \frac{1}{2} \times (\pi \times 1.4^2)]$

$= 30.045541 Å^2$

The distance between 2 Co ion

= Diameter of oxide ion

= 2.80Å

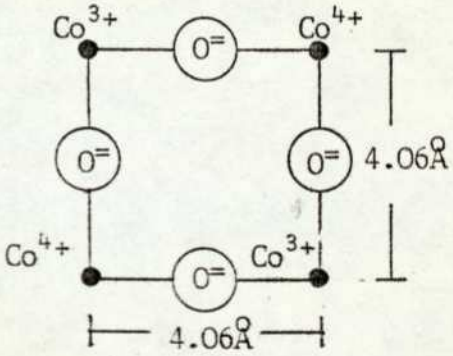

(b) 110 plane.

The area of 110 plane

$= 4 \times \frac{1}{8} \times (4\pi 0.63^2) + \frac{1}{2} \times (4\pi \times 1.15^2)$

$+ [5.7417 \times 4.06 - (\pi \times 1.15^2) - 4 \times \frac{1}{4} (\pi \times 0.63^2)]$

$= 28.71 Å^2$

The distance between 2 Co ion.

= 2.8Å, 4.48Å or 5.77Å.

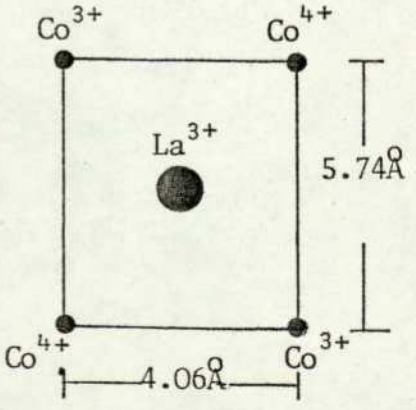

(c) 111 plane.

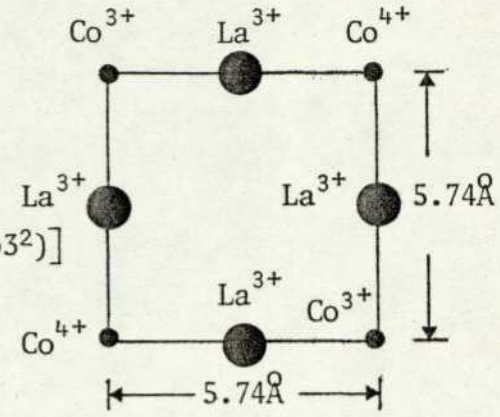

The area of 111 plane

$= 4 \times \frac{1}{8} \times (4\pi 0.63^2) + 4 \times \frac{1}{2} (4\pi \times 1.15^2)$

$+ [5.7417^2 - 4 \times \frac{1}{2} (\pi\ 1.15^2) - 4 \times \frac{1}{4} (\pi \times 0.63^2)]$

$= 42.523529 \text{Å}^2$

The distance between 2 Co ion

$d = 4.48\text{Å}$ or 6.86Å

(d) 200 plane.

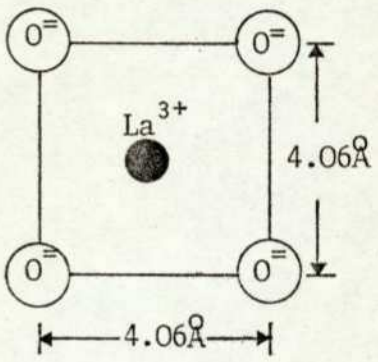

The area of the 200 plane

$= 4 \times \frac{1}{8} (4\pi \times 1.4^2) + \frac{1}{2} (4\pi \times 1.15^2)$

$+ [4.06^2 - 4 \times \frac{1}{4} \pi.1.4^2 - \pi \times 1.15^2]$

$= 26.80 \text{Å}^2$

There is no cobalt ions in this plane.

The average area of the four basic planes

$= 32.02.$

From the experimental data.

(1) The charge for O_2 stripping is 110000 μConl.

i.e. $0.1716398964 \times 10^{18}$ molecules of oxygen.

(2) Catalyst loading is 31.84615 mg.

(3) S.S.A. is 17 m^2/gm (170 cm^2/mg).

Hence, the total number of the sites on the surface

$$= \frac{31.84615 \times 170 \times 10^{15}}{32.018737}$$

$= 1.690837 \times 10^{18}$

Thus, the fraction of the active sites (out of the total)

$$= \frac{2 \times 0.1716398964 \times 10^{18}}{1.690837 \times 10^{18}}$$

$= 0.203023$

$= 20.3\%$.

Thus, the fraction of the active sites in terms of the total sites with cobalt ion containing

$$= \frac{2 \times 0.1716398964 \times 10^{18}}{1.690837 \times 0.75 \times 10^{18}}$$

$= 0.270698$

$= 27.1\%$.

This rough calculation shows that the fraction of the active sites compared to the total sites with cobalt ion containing 100, 110 and 111 planes is only 27%. This is probably due to two factors:

Firstly, there is only a limited number of sites available, due to geometric factors. Since the length of the oxygen molecule is only about 3Å (depending upon intramolecular motion), it is reasonable to assume that only those Co^{3+}/Co^{IV} couples within a suitable range of distance are available for dissociative chemisorption. As the distance between two ions in $La_{0.5}Sr_{0.5}CoO_3$ is varied from 2.8Å on 100 plane to6.86Å on 111 plane, it is obvious that not all the sites can be used for oxygen chemisorption. The dependence of the steady state performance on the lattice parameter (Section III(iv)) also support this suggestion.

Secondly, there is only a small amount of Co ions on the surface, as its size and weight favour it to diffuse inside the lattice during the formation of the perovskite structure by sintering of the mixed oxides. In this case, there should not be any increase in steady state performance for the series $La_{1-x}Sr_xCoO_3$ with increasing x. Also, since the sintering temperature for the

for the mixed oxides was only 600°C, migration of the Co ions to the lattice might have been incomplete.

It is therefore suggested that the number of the active sites on $La_{0.5}Sr_{0.5}CoO_3$ is governed by the geometric factor of the catalyst. This also plays an important role in the cathodic oxygen reduction on $La_{1-x}Sr_xCoO_3$, apart from magnetic and electronic properties.

CHAPTER SIX

THE OPTIMIZATION OF AN OXYGEN ELECTRODE

I. INTRODUCTION

It seems clear that the rate of oxygen reduction on perovskite oxides is controlled by both the rate of oxygen chemisorption and by the small proportion of sites available for reaction. Thus, two possible routes are available for improving the performance of the oxygen electrode:

(a) To speed up the rate of oxygen chemisorption by mixing in some other material with a higher rate of dissociative oxygen chemisorption. This would enable the gaseous O_2 to dissociatively chemisorb on the added materials and migrate across the interface and be reduced on the perovskite oxide surface. However, this is an unlikely alternative, since it is difficult to find a material which can fulfil this requirement.

(b) To increase the number of sites by using semiconducting oxides such as $NiCo_2O_4$, which possesses a higher proportion of transition metal ions.

II. $NiCo_2O_4$

For $La_{0.5}Sr_{0.5}CoO_3$, there is a maximum of 20% of ions available for catalytic reaction, since only the Co ion is considered to be active. Therefore, it is possible to increase the number of active sites by using material with a higher proportion of active ions. Thus, $NiCo_2O_4$ spinel oxide seems to fulfil the requirement as 42.5% of the ions (Ni, Co) are active.

King and Tseung[75,76,77] studied the reduction of O_2 on freeze dried $NiCo_2O_4$ and found that it possesses high activity for the reduction of oxygen, about 250 mA/cm^2 at 0.65 V vs DHE was obtained in 45 wt % KOH, 100% O_2 at room temperature. However, the performance decreased to less than 2 mA/cm^2 within 2-3 hours. X-ray and thermogravimetric measurement and solid state consideration suggests that the spinel $NiCo_2O_4$ phase, prepared by freeze drying of the mixed nitrates, followed by thermal treatment at 400°C for 10 hours has the following electronic structure:

$$Co^{2+}_{0.9}Co^{3+}_{0.1}[Ni^{2+}_{0.9}Ni^{3+}_{0.1}Co^{3+}]O^{2-}_{3.2}O^{-}_{0.8}$$

where cations outside the brackets occupy tetrahedral sites and those inside the brackets occupy octahedral sites. The existence of loosely bound O^- on the surface is most probably responsible for the high activity of $NiCo_2O_4$ at room temperature.

Figure 36 shows the i-t curve of the teflon bonded $NiCo_2O_4$ electrodes operated in the floating mode in air, 5N KOH, room temperature. There is a rapid decay on the electrode held at 500 mV vs DHE, (from 120 mA to 50 mA within 3 hours), whereas the one held at 750 mV gave steady performance over a test period of 120 hours.

As it is difficult to get clear x-ray powder diffraction patterns of the catalyst in a teflon bonded $NiCo_2O_4$ electrode, the electrodes prepared by direct decomposition of the mixed nitrates in nickel screens were used in the x-ray studies.

Figure 36. I-t relationship of teflon bonded $NiCo_2O_4$ electrode for oxygen reduction (45% KOH, 25°C, Air)

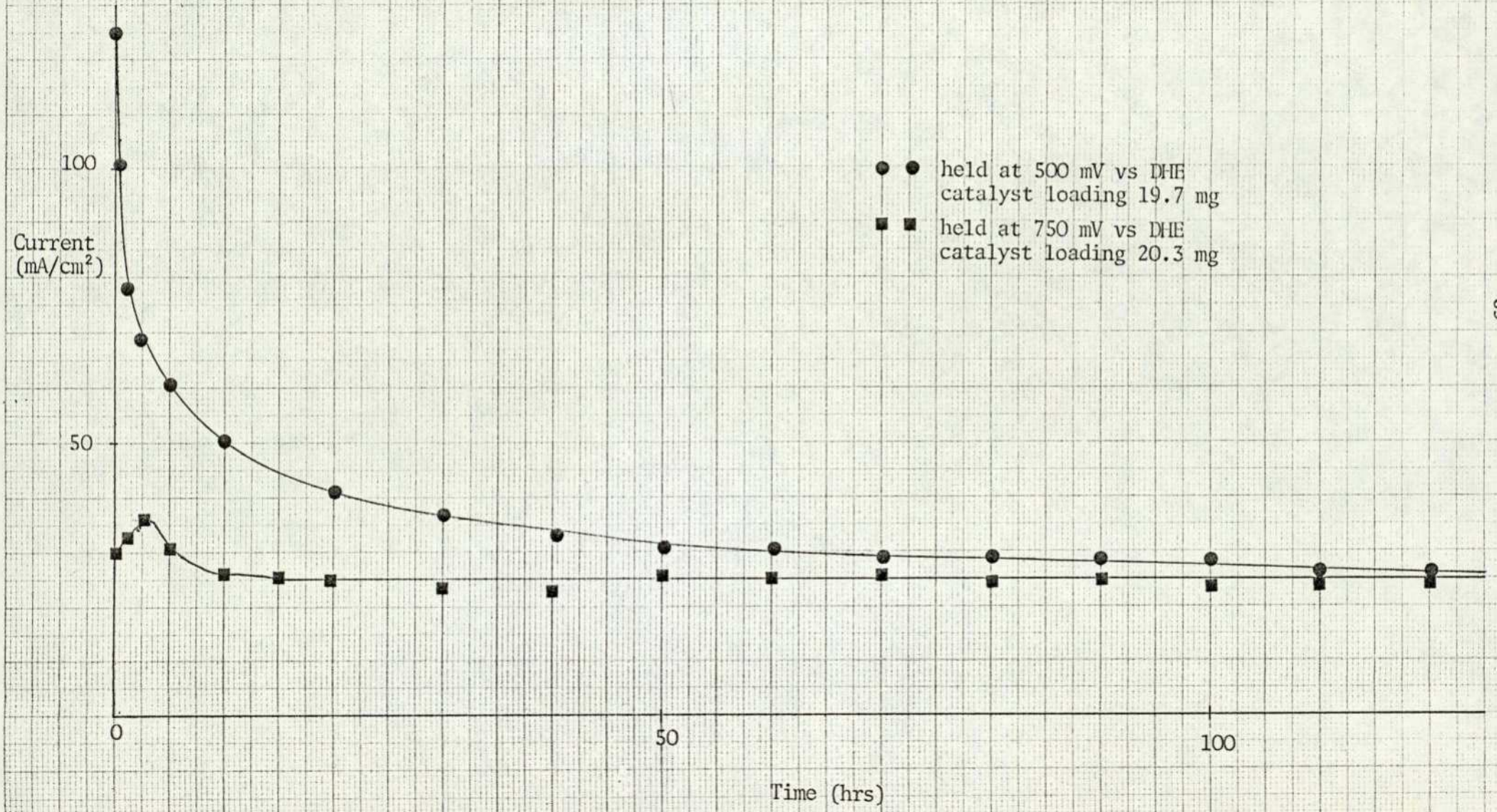

TABLE 5

X-ray Powder Diffraction Analysis of the $NiCo_2O_4$ Electrode in 5N KOH at Room Temperature

Electrode	Potential (mV) (vs DHE)	Atmosphere	Time	Phases Present
1	500	air	1 week	Co_2O_3, NiO, CoO NiOOH, $CoO.H_2O$.
2	750	air	1 week	$NiCo_2O_4$ spinel
3	open circuit	air	1 week	$NiCo_2O_4$ spinel
4	500	N	3 days	Co_2O_3, NiO, CoO NiOOH, $CoOH_2O$
5	750	N	3 days	$NiCo_2O_4$ spinel

The results clearly show that the $NiCo_2O_4$ spinel is stable at potentials above 750 mV vs DHE. At 500 mV vs DHE, the $NiCo_2O_4$ spinel structure is destroyed completely and the resultant product is a mixture of Co_2O_3, NiO, CoO, $CoO.H_2O$, NiOOH, none of which are active for O_2 reduction. Therefore, it is reasonable to assume that if a teflon-bonded electrode is operated at or above 750 mV vs DHE, the performance should be stable. This is indeed the case - the performance of a teflon-bonded $NiCo_2O_4$ electrode remained unchanged at 25 mA/cm^2, 750 mV, 5N KOH, air over a test period of 120 hours.

Controlled-potential coulometric studies at 500 mV in a stream of N_2 showed that the reduction current is over 4 times greater than the amount required to reduce the loosely bound oxygen, thus giving additional evidence that the bulk of $NiCo_2O_4$ is reduced.

III. PERFORMANCE OF TEFLON BONDED $NiCo_2O_4$/GRAPHITE ELECTRODES

Since the current density of $NiCo_2O_4$ electrodes at or above 750 mV vs DHE is only of the order of 30 mA/cm^2 at room temperature, it is necessary to improve the performance by mixing $NiCo_2O_4$ with high surface area graphite (500 m^2/g). Previous work by Goldstein and Tseung[2] on the cobalt-iron oxide/graphite system showed that the reduction of oxygen can be treated as a two step process:

(1) $O_2 + H_2O + 2e = HO_2^- + OH^-$

(2) $2HO_2^- = O_2 + 2OH^-$ (catalytic decomposition)

The evolved O_2 is then recycled for a further reduction in (1). The maximum possible enhancement for a cobalt-iron oxide/graphite electrode is a doubling of a graphite electrode's i_o. Cobalt-iron oxide is a non-conductor which has good H_2O_2 decomposition activity but it cannot reduce oxygen. On the other hand, since $NiCo_2O_4$ is a good peroxide decomposition catalyst, as well as a relatively active oxygen reduction catalyst, we expect such combinations to be more active. The performance of teflon-bonded $NiCo_2O_4$/graphite, and graphite electrodes at 20°C shows (Figure 37) that 10 wt % $NiCo_2O_4$/graphite electrodes give 170 mA/cm^2 at 750 mV, significantly better than graphite electrodes. Further optimization should lead to more significant improvements.

Figure 37. V-i curve for teflon bonded 10% $NiCo_2O_4$/C electrode (45% KOH, 20°C, Air).

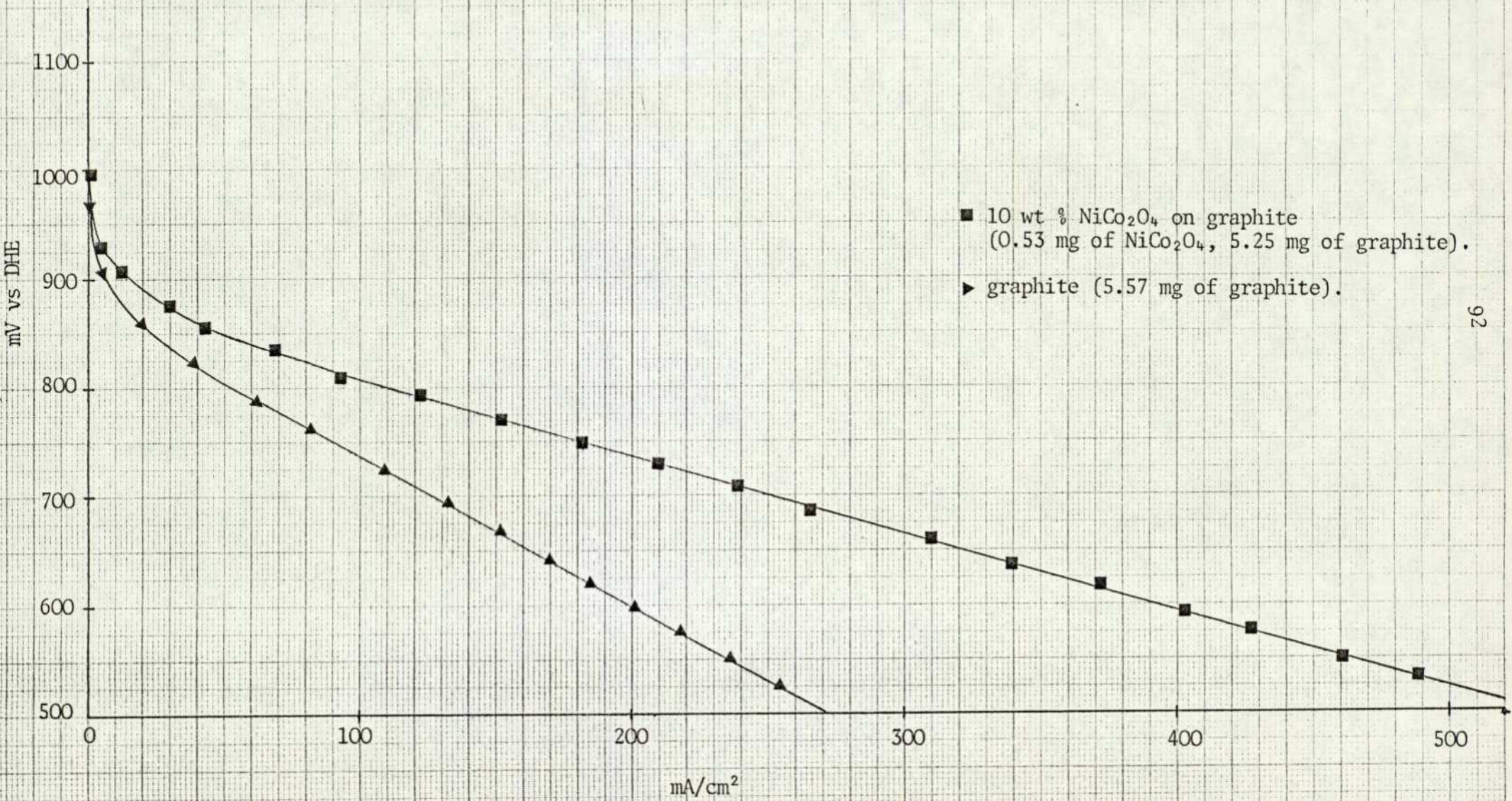

CHAPTER SEVEN

CONCLUSION AND SUGGESTION FOR FURTHER WORK

I. CONCLUSION

The Joint Pseudo-splitting/Peroxide mechanism for oxygen reduction in alkaline electrolyte provides a useful standpoint from which to evaluate possible approaches to the oxygen electrode problem. According to this theory, oxygen reduction can only occur at favourable sites on the electrode surface and the reaction pathway is largely determined by the mode of oxygen chemisorption. The direct 4-electron reduction process can occur if and only if oxygen molecules absorb in a side-on configuration. Solid state considerations suggest that requirement for side-on chemisorption of oxygen can be satisfied by the use of paramagnetic or ferromagnetic oxides. The attainment of reversible oxygen electrode potential on $Nd_{0.5}Sr_{0.5}CoO_3$ suggest that oxygen molecule is dissociatively chemisorbed, a point which has been proved by Hibbert and Tseung[40]. This confirms that paramagnetic electrocatalysis would favour side-on chemisorption, resulting in the direct reduction of oxygen to hydroxyl ion without going through the hydrogen peroxide intermediate.

The results on $Nd_{0.5}Sr_{0.5}CoO_3$ also suggest that the rate limiting process is the rate of dissociative oxygen chemisorption. Since this is a highly activated process, it is quite likely to be the main reason for the low performance at ambient temperature. Oxygen coverage measurements show that the surface coverage of oxygen was only 1% for both Sr doped $LaCoO_3$ and $NdCoO_3$ and that the coverage was independent of temperature in the range 25°C - 80°C. This suggests that the improvement in performance with temperature is not due to the increase in the number of active sites.

Studies on the series $La_{1-x}Sr_xCoO_3$ showed that both the maximum performance and the maximum oxygen coverage were obtained at x = 0.5. It indicates that the improvement in steady state performance with x is due to the increase in number of the active sites. It also confirms that the double exchange couple Co^{3+}/Co^{IV} are the active centres for oxygen reduction.

Mathematical calculation shows that only a small proportion of Co ions are available for the oxygen chemisorption process. Crystallographic considerations suggest that the number of active sites on $La_{1-x}Sr_xCoO_3$ is governed by geometric factors of the perovskite structure.

In view of the higher proportion of available transition metal ions, $NiCo_2O_4$ is expected to be a better oxygen electrocatalyst than perovskite oxides. Unfortunately, the electrochemical instability below 750 mV rules out $NiCo_2O_4$ as a practical oxygen electrode. However, by mixing high surface area graphite powder (7500 m^2/gm) with $NiCo_2O_4$, it is possible to achieve significantly high performance at 750 mV (170 mA, 45 at % KOH, 25°C, air, iR corrected). In this case, the oxygen reduction can be treated as a catalytic regenerative process; in alkaline solution, oxygen is initially reduced to give hydrogen peroxide

$$O_2 + H_2O + 2e \rightarrow HO_2^- + OH^-$$

which is then catalytically decomposed

$$2HO_2^- \rightarrow O_2 + 2OH^-$$

yielding oxygen for recycling. Since $NiCo_2O_4$ is a good H_2O_2 decomposer

as well as a relatively active oxygen reduction catalyst, an improvement in the performance of the graphite electrode could be expected.

II. SUGGESTION FOR FURTHER WORK

(i) Fundamental Studies

The author has been constantly aware of the need to correlate physical properties with electrochemical behaviour. Further work should concentrate more on the former aspects and the acquisition of facilities for the determination of magnetic susceptibility over a suitable temperature range would be a significant advance.

The general suitability of mass spectrometry for adsorption studies means that much more fundamental work on chemisorption kinetics can be carried out in future, again with the aim of relating the results to the electrochemical mechanism.

For a clear understanding of oxygen chemisorption on perovskite oxides, it is necessary to possess a detailed appreciation of the environment of surface, hence, the use of ESCA and LEED to study the nature of the Catalyst surface would be useful.

Ultimately of course, the aim remains to establish a General Theory of Catalysis which will also embrace the field of electrocatalysis.

(ii) The Correlation Between Electronics Properties and the Kinetics of Oxygen Reduction

According to the modified collective electron approach[15],

chemisorption is essentially a localized phenomenon with co-operative interactions becoming more important the lower the activation energy for conduction. This implies that the energy level of the impurity band in $La_{1-x}Sr_xCoO_3$, which is created by the doping of Sr ions[71], might play an important role in determining the rate of dissociative chemisorption. In order to clarify this situation, studies of the series $La_{0\cdot5}Sr_{0\cdot5}Co_{1-x}B_xO_3$ (where B = Ni or Mn) would be useful, since the doping of Ni or Mn ions into $La_{0\cdot5}Sr_{0\cdot5}CoO_3$ is expected to alter the energy level of the impurity band.

Studies of oxygen reduction on perovskite oxides with double magnetic ions[74], such as $HoFeO_3$ etc, could give some indirect information on the effect of electronic properties. An improvement in steady state performance is expected due to doubling the number of available paramagnetic ions, provided that the rate of dissociative oxygen chemisorption is not determined by the energy level of the impurity band.

(iii) The Kinetics of Oxygen Reduction on $NiCo_2O_4$/Graphite

The mathematical correlation[2] indicated that a limited improvement is possible in an oxygen electrode operating solely according to the regenerative catalytic route. Thus, even with perfect catalysis, the maximum improvement in i_o^* is to $2i_o^*$. The oxygen reduction on the graphite-based electrode catalysed with $NiCo_2O_4$ could occur by more efficient non-regenerative routes, since $NiCo_2O_4$ is a good hydrogen peroxide decomposer as well as a relatively active oxygen reduction catalyst. In order to study the

role of $NiCo_2O_4$ in the $NiCo_2O_4$/graphite system, further investigation of the kinetics of oxygen reduction must be carried out.

(iv) Optimization of the $NiCo_2O_4$/Graphite

So far, work on $NiCo_2O_4$/graphite were concentrated mainly on the stability of $NiCo_2O_4$, only a few tests on 10 wt % $NiCo_2O_4$/graphite at 20°C were carried out. Optimization of the ratio of $NiCo_2O_4$ on graphite and the catalysis/teflon ratio etc. is necessary.

Since 70°C is a more practical temperature for operating an alkaline fuel cell, studies of the stability as well as the steady state performance of $NiCo_2O_4$/graphite at this temperature would help to assess this system as a practical oxygen electrode.

REFERENCES

1. Gu Lin-in, N. A. Shumilova, V. S. Bagotsky, Electrochimiya, 3, 460 (1967).

2. J. R. Goldstein, A. C. C. Tseung, J. Phys. Chem., 76, 3646, (1972)

3. M. Davies, M. Clark, E. Yeager, F. Hovorka, J. Electrochem. Soc., 106, 56, (1959).

4. U. R. Evans, The corrosion and oxidation of metals - First supplementary volume, Pub. E. Arnold, (1968).

5. J. R. Goldstein, A. C. C. Tseung, Nature, 222, 869, (1969).

6. E. J. W. Verwey, J. H. de Boer, Rec. Trav. Chim., Pay-Bas, 115, 1156, (1959).

7. A. C. C. Tseung, unpublished results.

8. M. Foex, Comptes Rend., 227, 193, (1948).

9. H. P. Rooksby, Acta Crystallog., 1, 226, (1948).

10. G. Parravano, M. Boudart, Adv. Catal., 7, 66, (1955).

11. A. Cimino, E. Molinari, G. Romeo, Z. Physik. Chem. (Leipzig), 83, 333, (1951).

12. D. Mehandjiev, G. Bliznakov, Proc. Third Intern. Congress on Catalysts, Amsterdam, p. 781, (1965).

13. A. Bielanski, J. Haber, Z. Physik. Chem. (Leipzig), 24, 345, (1960).

14. N. P. Keier, Kinetika i Kataliz, 1, 221, (1960).

15. H. B. Charman, R. M. Dell, S. S. Teale, Trans. Faraday Soc., 59, 453, (1963).

16. E. R. S. Winter, J. Catalysis, 6, 35, (1966).

17. A. C. C. Tseung, B. S. Hobbs, A. D. S. Tantram, Electrochimica Acta, 15, 473, (1970).

18. M. Perakis, J. Wuchner, G. Parravano, Comptes Tend., 248, 2306, (1959).

19. J. T. Richardson, W. O. Milligan, Phys. Review, 102, 1289, (1956).

20. J. Cohen, K. M. Creer, R. Pauthenet, K. G. Strivastava, J. Phys. Soc., Japan, 17, (Suppl. B-1), 685, (1962).

21. T. Kawada and N. Kawai, ibid., 691.

22. H. L. Bevan, A. C. C. Tseung, Electrochimica Acta, 9, 201, (1974).

23. S. J. Teichner, Advan. Catal., 20, 167, (1969).

24. A. C. C. Tseung, H. L. Bevan, Electroanalytical Chemistry and Interfacial Electrochemistry, 45, 429, (1973).

25. F. F. Wolkenstein, "Electronic Theory of Catalysis on Semiconductors", Pergamon Press (1963).

26. H. Gerischer, Surface Sci., 18, 97, (1969).

27. F. J. Morin and T. Wolfram, Phys. Rev. Lett., 30, 1214, (1973).

28. S. R. Morrison, J. of Catalysis, 20, 110, (1971).

29. O. K. Davtyan, E. G. Misyuk et al, Zh. Fiz. Khim. 43, 321, 1467, 1475 (1969).

30. J. B. Goodenough, "Progress in solid state chemistry", 5, 149, (1971), (ed. H. Reiss).

31. L. F. Mattheiss; Phys. Rev. 181, 987, (1967), Ibid. B2, 3918, (1970), Ibid. B4, 3548, (1971).

32. D. B. Meadowcraft, Nature, 226, 167, (1969).

33. A. C. C. Tseung, H. L. Bevan, "A low temperature reversible oxygen electrode", The Electrochemical Society, Extended Abstracts, Fall Meeting, Atlantic City, N.J., Oct. 4-8, 1970, pp. 28-30.

34. Yasumiti Matumoto, Hirosi Yoneyama and Hideo Tamura, Chemistry letters, pp. 661-662, (1975). Published by the Chemical Society of Japan.

35. T. Kudo, H. Obayashi and M. Yoshida, J. of Electrochemical Society. pp. 321-325. March, (1977).

36. Y. Matsumoto, Y. Yoneyama and H. Tamura, J. Electroanal. Chem., 79, 319-326, (1977).

37. Y. Matsumoto, Y. Yoneyama and H. Tamura, J. of Electroanal. Chem., 83, 167-176, (1977).

38. Y. Matsumoto, H. Yoneyama and H. Tamura, ibid. 237-243.

39. Y. Matsumoto, Y. Yoneyama and H. Tamura, ibid., 245-249.

40. D. B. Hibbert and A. C. C. Tseung, J. Electrochem. Soc., 125, 74-78, (1978).

41. T. Kudo, H.Obayashi and T. Genjo, J. Electrochem. Soc., 122, 159, (1975).

42. Y. Matsumoto, H. Yoneyama and H. Tamura, J. Electroanal. Chem., 80, 115, (1977).

43. A. C. C. Tseung, H. L. Bevan, J. of Materials Science, 604-610, (1970).

44. R. F. Sale, The Metallurgist and Materials Technologist, 439-443, August, (1977).

45. P. H. Emmett; 'Measurement of the Surface Area of Solid Catalysis', Catalysis, 1, 31-74, Reinhold Publ. (1954).

46. H. L. Bevan, Ph.D. Thesis, The City University. p. 20, (1970).

47. J. Giner, J. M. Parry, L. Swette and R. Catabinga, NASA Contract CR-97624, Final Report, 30 June, (1968).

48. J. Giner, J. M. Parry, S. Smith and M. Turchan, J. Electrochem. Soc. 116, 1692, (1969).

49. J. Giner, G. Holleck and P. A. Malachasky, Report on Contract NA 5313234, NASA CR-7299, p. 8, June, (1971).

50. J. Giner, J. Electrochem. Soc., 111, 376, (1964).

51. B. S. Hobbs, P. R. Vassie, A. C. C. Tseung, Electrochemical Engineering Symposium, Newcastle, Ed. J. D. Thornton, 1, 123, (1972).

52. A. C. C. Tseung and S. C. Dhara. Electrochimica Acta., 19, pp. 845-848, (1974).

53. J. O. M. Bockris, A. K. N. Reddy, in "Modern Electrochemistry", (Vol. 2), p. 862, Macdonald Technical and Scientific, (1970).

54. J. O. M. Bockris, A. K. N. Reddy, ibid., p. 1007.

55. J. Horiuti, Physical Chemistry. An Advance Treatise (Ed. H. Eyring), Academic Press, (1970).

56. J. A. McGinnety, in MTP International Reviews of Science, Inorganic Chemistry Series I, Vol. 5, D. Shapp, ed., Butterworths, London, (1972), p. 229.

57. J. S. Valentine, Chem. Revs., 73, 235, (1973).

58. J. S. Griffiths, Proc. Roy. Soc., (A), 235, 23, (1956).

59. L. Pauling, Nature, 203, 182, (1964).

60. J. McGinnety, N. Payne and J. Ibers, J. Amer. Chem. Soc., 91, 6301, (1969).

61. H. Behret, H. Binder and G. Sandstede in Proc. of the Symposium on Electrocatalysis, M. Breiter, ed. The Electrochemical Society, Princeton, N.J. pp. 319-338, (1974).

62. H. Behret, H. Binder and G. Sandstede, Electrochim. Acta. 20, 111, (1975).

63. F. Beck, W. Dammert, J. Heiss, H. Hiller and R. Polster, Z. Naturforsh, 28A, 1009, (1973).

64. F. Beck, Ber. Bunsenges, Physik. Chem., 77, 353, (1973).

65. E. Yeager, P. Krouse and K. Rao, Electrochim. Acta, 9, 1057, (1964).

66. E. Yeager and A. Kozawa, Kinetic Factors in Fuel Cell Systems: The Oyxgen Electrode Proc. 6th AGARD Meeting Cannes, 1964, Pergamon Press, Oxford, pp. 769-793, (1965).

67. K. L. K. Yeung, M.Sc. Dissertation, The City University, (1975).

68. Engell and Hauffe, Z. Electrochem., 57, 762, 773, (1953).

69. Stone in Chemistry of the Solid State (ed. Garner), (Butterworths), Chap. 15, (1955).

70. J. B. Goodenough, J. Appl. Phys. 37, 1415, (1966).

71. V. G. Bhide, D. S. Rajoria, C. N. R. Rao, G. Rama Rao and V. G. Jadhav. Physical Review, B12, 2832, (1975).

72. P. M. Raccah and J. B. Goodenough, J. of Applied Physics. 39, 1209, (1968).

73. J. B. Goodenough, Mat. Res. Bull, 6, 967, (1971).

74. H. Makram and M. Vichr, "Magnetic Oxides", Part 1, 134, (1975), (ed. D. J. C. Craik).

75. W. J. King, A. C. C. Tseung, Electrochimica Acta, 19, 485, (1974).

76. W. J. King, A. C. C. Tseung, ibid., 493, (1974).

77. W. J. King, A. C. C. Tseung, Brit. Pat. 1461764, 19 Jan. (1977).